Boundary layer flashback prediction for high hydrogen flames at gas turbine burner geometry and operating conditions

C.K. Sarakatsanis

TU Delft

Boundary layer flashback prediction for high hydrogen flames at gas turbine burner geometry and operating conditions

By

Christos K. Sarakatsanis

to obtain the degree of

Master of Science

in Mechanical Engineering

at the Delft University of Technology,

to be defended publicly on Friday, December 4, 2020, at 1:00 PM.

Student number: 4816633

Project duration: December 2019 – December 2020

Thesis committee: Prof. dr. ir. S.A. Klein, TU Delft, Supervisor &Chairman

Thesis committee: Prof. dr. D.J.E.M. Roekaerts, TU Delft

Thesis committee: Dr. ir. M.J. Tummers, TU Delft

Thesis committee: Ir. L. Altenburg, TU Delft

TU Delft

Abstract

The idea of using hydrogen as a medium for storing excess renewable energy is gathering momentum but to deliver, several technological advances are required. One of the main challenges is boundary layer flame flashback (BLF) as a key operability issue for low NO_x premixed combustion of hydrogen-enriched fuels; thus design of tools to predict flashback propensity is of interest. Extensive research has already been done, and the result is three main BLF models, promise to predict the initiation of boundary layer flame flashback accurately. The first model was developed in the Paul Scherrer Institute (PSI) and was applied to an axial-dump burner operating at elevated pressure and temperature conditions with fuel mixtures of H_2-N_2 and H_2. The second model was developed at the University of California, Irvine (UCI) and was based on the flashback experimental data of 100% H_2 fuel (similar geometry with UCI) at elevated pressure and temperature conditions. Finally, the most recent BLF model was developed at TU Delft based upon the 'generalized' Stratford's turbulent boundary layer separation criterion, which is a further development of the model initially developed in TU Munich (TUM) for atmospheric confined H_2 flames in a horizontal channel burner.

In this thesis, the performance of the state-of-the-art BLF models is evaluated in a number of academic burners operating with H_2-rich and pure H_2 fuels at atmospheric and elevated operating conditions. While the TU Delft model showed good agreement with 100% H_2 flashback experiments under atmospheric conditions and simple geometries, further modifications are proposed to perform under conditions relevant for gas turbines (increased pressure and temperature). A new turbulent flame speed correlation to capture the effect of pressure on flashback propensity is applied to the model and validated in high-pressure academic burners.

Furthermore, the TU Delft model is validated for a lab-scale size of a gas turbine burner geometry, operating at atmospheric conditions and tested in the TU Delft laboratory. This validation shows that it is essential to review the outcome of the boundary layer flashback model at different locations in the boundary layer, and with minor modifications, the model can capture the test results adequately. The sensitivity of the TU Delft model on different fuel compositions is also investigated. Proper selection of the turbulent flame speed correlation is found to improve the model's performance for fuel mixtures less rich in H_2.

Acknowledgments

Foremost, I would like to express my sincere gratitude to my supervisor Sikke Klein who gave me the opportunity to do this wonderful project on the promising topic of hydrogen combustion. His patient guidance and immense knowledge helped me in all the time of research and writing this thesis. My sincere thanks also go to Luuk Altenburg for his support throughout this project and to Joris Kommen, combustion engineer in Ansaldo Thomassen, for sharing valuable data. I would like to especially thank Dirk Roekaerts and Mark Tummers for reviewing my thesis and being part of my thesis committee.

Finally, I am extremely grateful to my family for the continuous support they have given me throughout my life.

Contents

List of Abbreviations

CCT	Carbon Capture Technology
PSM	Power Systems Manufacturing
BLF	Boundary Layer Flashback
CNB	Combustion Induced Vortex Breakdown
TUM	Technical University of Munich
UCI	University of California, Irvine
PSI	Paul Scherrer Institute
ATH	Ansaldo Thomassen
CFD	Computational Fluid Dynamics
RANS	Reynolds Averaged Navier Stokes
EVM	Eddy Viscosity Model
RSM	Reynolds Stress Model
PIV	Particle Image Velocimetry
LDV	Laser Doppler Velocimetry

List of symbols

Re	Reynolds number	[-]
Re_t	Turbulent Reynolds number	[-]
Ka	Karlovitz number	[-]
Le	Lewis number	[-]
C_p	Coefficient of pressure	[-]
Pe	Peclet number	[-]
D	Mass diffusivity	[m^2/s]
S_{l0}	Unstretched laminar flame speed	[m/s]
S_t	Turbulent flame speed	[m/s]
c_p	Specific heat capacity	[kJ/(kg K)]
L	Characteristic length scale	[m]
k	Turbulent kinetic energy	[m^2/s^2]
u_t	Friction velocity	[m/s]
T_0	Inlet temperature	[K]
T_{tip}	Wall temperature	[K]
T_{ad}	Adiabatic flame temperature	[K]
P_0	Inlet pressure	[Pa]
t_{ch}	Chemical time scale	[s]
t_k	Kolmogrov time scale	[s]
g_c	Critical velocity gradient	[1/s]
g_f	Wall velocity gradient	[1/s]
l_t	Integral length scale	[m]
U_{bulk}	Bulk flow velocity	[m/s]
A_f	Flame surface area	[m^2]
$\dot{m}$	Mass flow rate	[kg/s]
d	Burner diameter	[m]

Greek Letters

ρ_u	Unburned mixture density	[kg/m^3]
ρ_b	Burned mixture density	[kg/m^3]
μ	Fluid viscosity	[Pa s]
ν	Kinematic fluid viscosity	[m^2/s]
ρ	Fluid density	[kg/m^3]
μ_t	Turbulent viscosity	[Pa s]
ε	Turbulent dissipation rate	[m^2/s^3]
ω	Specific dissipation rate	[1/s]
δ	Boundary layer thickness	[m]
τ_w	Wall shear stress	[Pa]
φ	Equivalence ratio	[-]
α	Thermal diffusivity	[m^2/s]

δ_{l0}	Unstretched laminar flame thickness	[m]
λ_u	Unburnt mixture thermal conductivity	[W/(m K)]
η_k	Kolmogrov length scale	[m]
δ_p	Penetration distance	[m]
δ_q	Quenching distance	[m]
κ	Flame stretch rate	[1/s]

1. Introduction

The increasing use of fossil fuels in the energy sector since the Industrial Revolution causes a significant increase in greenhouse gas emissions. Carbon dioxide CO_2 is one of the most prominent greenhouse gases in the atmosphere, having a significant impact on global warming. The energy sector is strongly based on the combustion of hydrocarbon fuels leading to a large amount of CO_2 emissions (almost 60%) [1]. Furthermore, the CO_2 emissions from the burning of hydrocarbon fuels are considered the most important greenhouse gas contributing to the northern hemisphere's climate change [2].

The global decarbonization of the energy sector can be accomplished by increasing the share of renewable energy sources such as solar and wind. Even though the renewable energy sources have become cost-competitive and environment-friendly over the last years [3], the fluctuating profile of those renewable sources needs to be balanced by other forms of reliable and sustainable power generation. Innovative systems are required to store the energy from these renewable sources during periods of excess supply and generate electricity during periods of excess demand.

Most renewable electricity systems use a battery as a storage system, which is highly efficient but has the disadvantage of being expensive and large per unit of stored energy [3]. Hydrogen is an attractive option to overcome the storage difficulty of renewable energy. It can be easily produced via electrolysis, a process in which the excess electricity is used to split water into hydrogen and oxygen [4]. Regarding fossil fuels, hydrogen can be produced by the process of natural gas reformation, which can also be a carbon-neutral resource if carbon capture technology (CCT) is used [5]. In the case of excess energy demand, the stored hydrogen can be burned in a gas turbine configuration with modified hydrogen combustors. The gas turbines are considered a promising option to sufficiently balance the intermittent nature of the renewable energy sources (i.e., wind, solar) due to their high turn-down ratios, short start-up times, and high efficiency [6].

The modern gas turbine combustors are primarily operated in a lean premixed mode to comply with the emission regulations of nitrous oxide NO_X [6]. The lean premixed combustion is used to reduce the flame temperature, leading to a significant reduction of the NO_x emissions. However, the premixed combustion of H_2-rich fuel in gas turbines imposes certain risks due to the differences in the physical properties of 100% H_2 and H_2-rich fueled mixtures compared to other fuels (i.e., natural gas). The high burning velocity of H_2-rich fuels intensifies the risk of upstream flame propagation into the premixing section of the combustor. This phenomenon is called flame flashback and is considered a significant challenge to achieve safe operation of combustors that use highly reactive fuels like hydrogen [6].

A promising technology for hydrogen lean premixed combustion is the FlameSheet™ combustor developed by Power Systems Manufacturing (PSM). The FlameSheet™ burner is based on a two-stage combustor design (see Figure 1.1), which allows staged operation under various load conditions [7]. This design reduces emissions and provides extended fuel flexibility with a H_2 capability of up to 80% vol. [8]. Further development of the FlameSheet™ system is in progress within the HighHydrogen project, a cooperation between academic and industrial partners aiming to achieve 100% H_2 operation at gas turbine relevant conditions [9].

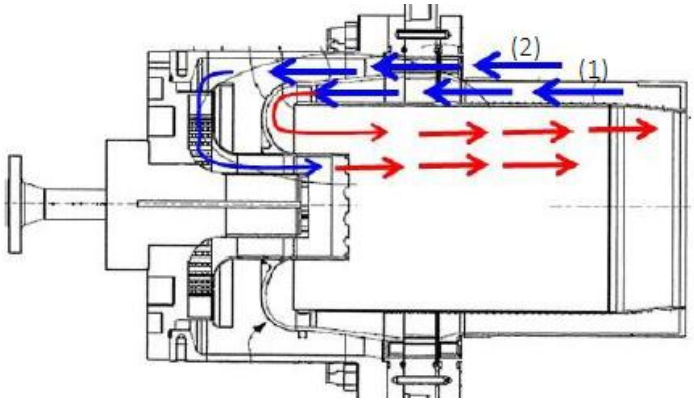

Figure 1.1: Cross-section of the FlameSheet™ combustor developed by PSM [8]. The airflow through the main (1) and the pilot (2) stage is shown with the blue arrows. The red arrows refer to the fuel-air mixture.

1.1 Main challenges in hydrogen combustion

The main technical challenge associated with converting lean, premixed combustion systems from natural gas operation to high hydrogen content fuels operation is flame flashback, as discussed in the previous section. Flame flashback is described as the process where the flame can propagate upstream into the premixer region, with the possibility of causing severe damage to the engine's critical components. Flashback can be initiated via four mechanisms [10] [11] [12]:

- Core flow flashback: This occurs when the flow velocity drops below the flame speed in the flow's core area. However, the bulk flow velocity in the premixer commonly exceeds the burning velocity during normal gas turbine operation; thus, flashback is unlikely to occur via this mechanism [11].

- Flashback due to combustion instabilities: Large amplitude fluctuations of the flow field caused by instabilities due to, i.e., unsteady heat release, pressure oscillations can trigger flame flashback.

- Combustion Induced Vortex Breakdown (CIVB): This mechanism occurs in swirl-stabilized burners. Swirling flows are used to generate a recirculation area in the combustion chamber, stabilizing the flame. Special circumstances (i.e., an increase in the fuel rate) lead to an upstream propagation of the recirculation zone into the premixing section, the vortex then breaks down, and the flame travels further upstream.

- Boundary layer flashback (BLF): The flow velocity decreases adjacent to the wall due to the no-slip boundary condition. This imposes an increased risk for the onset of flame flashback within the boundary layer of the flow. Boundary layer flashback can occur when the local flame speed is higher than the local air-fuel mixture velocity adjacent to the wall.

The present thesis focus on the boundary layer mechanism, which is the primary flashback mechanism and has been studied extensively in the literature [12]. A brief overview of the BLF research is given in the following section.

1.1.1 Research in boundary layer flashback prediction

Boundary layer flashback of laminar flames was initially investigated in 1943 by Lewis and von Elbe [13] [14], who developed a simple model that describes flashback in terms of the wall gradient of the streamwise velocity at flashback. This is the widely known critical velocity gradient concept used to predict blow off and flame flashback of laminar flames. According to the model, the velocity profile adjacent to the wall is assumed to be linear, and flashback initiation occurs when the local flow speed drops below the laminar burning velocity at a location close to the wall.

More recent studies in H_2 and H_2-rich turbulent flames showed that flashback propensity strongly depends on the fuel composition, the wall tip temperature, and the mixture's pressure and temperature [15][16]. Researchers from TU Munich also contributed to the investigation of BLF by challenging the accuracy of the well-established critical velocity gradient model. An experimental study by Eichler [11] showed that flame confinement significantly increases boundary layer flashback propensity. Contrary to the fundamental assumption used for developing the critical velocity gradient theory (i.e., the flame's effect on the flow field is negligible), they showed that the flame, with its back-pressure effect, will affect the incoming flow. Direct numerical simulations in turbulent channel flow, performed by Gruber et al. [17], validated the theory mentioned above.

Further research was conducted by Hoferichter et al. [6] [18][19], developing a semi-analytical model for both confined and unconfined flames based on Stratford's turbulent boundary layer separation criterion [20]. Hoferichter's primary assumption is that boundary layer flashback is triggered due to the flow separation upstream of the flame front [19]. Hoferichter's flashback model for confined flames was further improved at Delft University of Technology (TU Delft). Tober [21] included thermo-diffusive flame instabilities and flame stretch effects, resulting in an improved version of the Hoferichter's confined flashback model. Additional modifications were performed by Björnsson [22]. He used a generic boundary layer stability criterion from Stratford [20], and the boundary layer velocity profile was derived from steady-state cold-flow CFD simulations. Björnsson's updated flashback model showed a good comparison with Eichler's flashback experiments in channel and diffuser flows [11]. However, it was still tested at simple geometries. The need to validate the improved TU Delft flashback model to complex burner geometries and elevated operating conditions is the main research area of this thesis.

1.2 Research questions

The present thesis aims to answer the following research questions:

- What modifications are required to the TU Delft flashback model to adequately capture boundary layer flashback at gas turbine relevant conditions?

Well defined validation cases of burners at elevated operating conditions are limited in the literature. Modifications of the TU Delft flashback model based on the data from the high-pressure flashback experiments performed in the University of California Irvine (UCI) and Paul Scherrer Institute (PSI) combustors is expected to extend its applicability.

- Can the most recent flashback models developed in the PSI, UCI, and TU Delft, by coupling to CFD simulations, be extended to predict flashback limits in a lab-scale gas turbine burner geometry accurately?

Both the PSI and UCI models describe flashback in terms of similar non-dimensional parameters, including the known preheating temperature and operating pressure, as well as the Lewis number and the turbulence/flame length scale, which can be easily calculated. Furthermore, the fuel-air mixture properties and the mean velocity profile in the boundary layer required by the TU Delft model can be easily extracted from chemical kinetics software (e.g., Cantera) and steady-state CFD simulations (e.g., ANSYS Fluent), respectively. Thus, the broader applicability of the flashback models can add simple tools for boundary layer flashback prediction during the preliminary design of hydrogen combustors.

1.3 Thesis outline

This thesis is structured as follows: In chapter 2, the basic fluid flow and premixed combustion principles are introduced. Furthermore, chapter 2 includes a discussion of the first BLF model and the most recent boundary layer flashback models developed in the University of California Irvine (UCI), the Paul Scherrer Institute (PSI), and the Delft University of Technology (TU Delft). This theoretical background is essential to understand the underlying principles of the flashback models used in the following chapters.

In chapter 3, the flashback models are applied to a number of atmospheric and high-pressure academic burners and validated with H_2 flashback experimental data from literature. In the same chapter, the adaptation of the TU Delft model to perform under gas turbine relevant conditions based on experimental flashback data from high-pressure burners will be described.

In chapter 4, the flashback models are further tested for a complex combustor geometry. The validity of the models is tested to a lab-scale size burner designed at TU Delft using both H_2 and H_2-CH_4 fuel mixtures. Finally, chapter 5 ends with concluding remarks and recommendations for future research.

2. Theory

In this chapter, the basic principles of the turbulent flow and the premixed combustion are presented in section 2.1 and section 2.2. A description of the different boundary layer flashback models used in this thesis follows in section 2.3. The discussion of the boundary layer flashback models is essential to evaluate their outcome in the academic combustors discussed in chapter 3 and chapter 4.

2.1 Turbulent flow

Turbulent flow occurs at high Reynolds numbers *Re* in which the inertial forces (described by the numerator of Eq. (2.1)) dominate the viscous forces (denominator of Eq. (2.1)), and eddies, vortices and other flow instabilities occur [23].

$$Re = \frac{\rho u L}{\mu} \tag{2.1}$$

In order to describe turbulent flow, the solution variables in the exact Navier-Stokes equations are decomposed into the mean and the fluctuating components using the method known as Reynolds decomposition [24]. The decomposition of the velocity component is shown in Eq. (2.2), where $\bar{\boldsymbol{u}}_i$ and $\boldsymbol{u}_i'$ are the mean and fluctuating velocity components (i=1,2,3).

$$\boldsymbol{u}_i = \bar{\boldsymbol{u}}_i + \boldsymbol{u}_i' \tag{2.2}$$

Using Eq. (2.2) for the flow variables in the Navier-Stokes equations and taking a time average results to the Reynolds-averaged Navier-Stokes equations (RANS), as can be seen in Eq. (2.3) and (2.4).

$$\frac{\partial \rho}{\partial t} + \frac{\partial}{\partial x_i}(\rho u_i) = 0 \tag{2.3}$$

$$\frac{\partial}{\partial t}(\rho u_i) + \frac{\partial}{\partial x_j}(\rho u_i u_j) = -\frac{\partial p}{\partial x_i} + \frac{\partial}{\partial x_j}\left[\mu\left(\frac{\partial u_i}{\partial x_j} + \frac{\partial u_j}{\partial x_i} - \frac{2}{3}\delta_{ij}\frac{\partial u_i}{\partial x_i}\right)\right] + \frac{\partial}{\partial x_j}\left(-\rho\overline{u_i' u_j'}\right) \tag{2.4}$$

The equations have the same form as the Navier-Stokes equations; however additional terms, called Reynolds stresses $\rho\overline{u_i' u_j'}$ appear, and represent the effect of turbulence. These Reynolds stress terms can be modeled to close the set of equations using either the eddy viscosity models (EVM) or the Reynolds stress model (RSM).

The eddy viscosity models use the Boussinesq hypothesis [25]. According to the Boussinesq hypothesis, a relationship between the Reynolds stresses and the mean velocity gradients can be established using an effective turbulent viscosity μ_t (see Eq. (2.5)). The most widely used eddy viscosity models for computational fluid dynamics are the Spalart-Allmaras, the k-ε, and the k-ω [26].

$$-\rho\overline{u_i' u_j'} = \mu_t\left(\frac{\partial u_i}{\partial x_j} + \frac{\partial u_j}{\partial x_i}\right) - \frac{2}{3}\left(\rho k + \mu_t\frac{\partial u_k}{\partial x_k}\right)\delta_{ij} \tag{2.5}$$

For the k-ε and k-ω models, two additional transport equations (one for the turbulent kinetic energy *k*, and one for the turbulent dissipation rate *ε* or the specific dissipation rate *ω*) are solved. The turbulent viscosity μ_t is then computed as a function of *k* and *ε* or *k* and *ω*. For example, the turbulent viscosity for the widely used standard k-ε model can be modeled using Eq. (2.7), where C_μ=0.09 [26].

$$\mu_t = \rho C_\mu \frac{k^2}{\varepsilon} \tag{2.6}$$

The limitation of the Boussinesq hypothesis is that it assumes μ_t is an isotropic scalar quantity. For flows in which the Reynolds stresses are highly anisotropic, the Reynolds stress equation model (RSM) can be used. The RSM model is more complex than the eddy viscosity models since it solves additional transport equations for each Reynolds stress term. Nevertheless, the Boussinesq hypothesis performs very well in many cases, and the excess computational cost of the RSM model is not justified (except for cases where the anisotropy of turbulence is significant) [26].

2.1.1 **Boundary layer**

Ludwig Prandtl has initially introduced the turbulent boundary layer concept to describe the flow field near bodies of various shapes. He concluded that the viscous forces are negligible for low viscosity flows everywhere in the fluid domain, except for the region adjacent to the wall due to the no-slip boundary condition [24]. This no-slip boundary condition leads to the development of a thin layer along the solid surface, as shown in Figure 2.1.

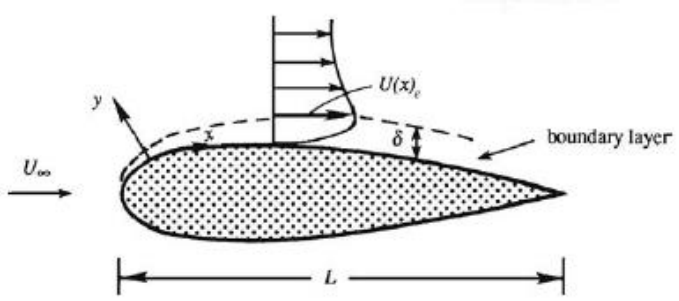

Figure 2.1: Formation of the boundary layer over a solid surface with length *L*. The thickness of the boundary layer is *δ*, the free-stream velocity is U_∞, and the velocity at the edge of the boundary layer is U_e. Source: [24].

For a thin boundary layer (δ<<L) and a constant density and viscosity fluid, the continuity and x-momentum equations for a two-dimensional flow are simplified to Eq.(2.7) and Eq.(2.8). The y-momentum equation is given by Eq. (2.9), which implies that the pressure is uniform through the thickness of the boundary layer.

$$\frac{\partial u}{\partial x} + \frac{\partial v}{\partial y} = 0 \tag{2.7}$$

$$u\frac{\partial u}{\partial x} + v\frac{\partial u}{\partial y} = -\frac{1}{\rho}\frac{\partial p}{\partial x} + \nu\left(\frac{\partial^2 u}{\partial^2 y}\right) \tag{2.8}$$

$$\frac{\partial p}{\partial y} = 0 \tag{2.9}$$

Non-dimensional parameters of the wall distance y^+, and the velocity u^+ are widely used to describe the turbulence boundary layers [6]:

$$y^+ = \frac{\rho u_\tau(x) y}{\mu} \tag{2.10}$$

$$u^+ = \frac{u(x,y)}{u_\tau(x)} \tag{2.11}$$

The shear stress velocity u_t is defined as $u_t = \sqrt{\frac{\tau_w}{\rho}}$, where τ_w is the shear stress at the wall. Based on the value of y^+, the boundary layer can be divided into the following regions [6], shown in Figure 2.2 :

- Viscous sublayer ($y^+<5$). The velocity profile is significantly affected by the viscous shear stress and have the following form:

$$u^+ = y^+ \tag{2.12}$$

- Buffer layer ($5<y^+<30$). Transition region between the viscous sublayer and the logarithmic region.

- Logarithmic region ($30\leq y^+\leq 350$). The velocity profile follows the logarithmic law of the wall, and both viscous and turbulent shear are significant. The von Kármán constant is K=0.41, and the model parameter *B=5.0*, as suggested by [27].

$$u^+ = \frac{1}{K}\ln y^+ + B \tag{2.13}$$

- Outer region ($y^+>350$). The velocity profile depends on the pressure gradient of the flow, and the turbulent shear dominates against the viscous shear.

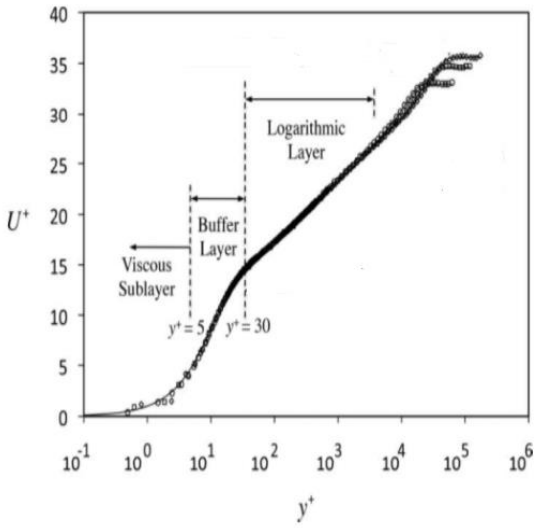

Figure 2.2: Different regions of the turbulent boundary layer profile (Source: [28]).

2.2 Premixed combustion

Premixed combustion is the process in which the mixing of the fuel and oxidizer takes place upstream of the flame front [6]. This combustion mode is used in modern gas turbines to minimize thermal NO_x formation. The equivalence ratio φ of the premixed gases can be controlled, resulting in lower flame temperature and lower NO_x emissions. It is defined as the ratio of the actual fuel/air ratio to the stoichiometric fuel/air ratio, shown in Eq. (2.14). Stoichiometric combustion occurs when $\varphi=1$, whereas $\varphi<1$ indicates lean mixture and $\varphi>1$ rich mixture.

$$\varphi = \frac{\left({}^{m_f}/_{m_a}\right)}{\left({}^{m_f}/_{m_a}\right)_{st}} \tag{2.14}$$

The laminar flame properties, such as the laminar flame speed S_l and the flame thickness δ_l, vary with the equivalence ratio. These properties are essential to describe boundary layer flame flashback and will be discussed in the next section.

2.2.1 Laminar flame properties

A premixed laminar flame can be described as a one-dimensional and unstretched flame front, shown in Figure 2.3. The premixed mixture is burned with an unstretched laminar burning velocity S_{l0}, which is equal to the reactants' velocity u_u, if the flame front is stationary [6]. The temperature of the reactants initially increases from T_u to T_{lL} within the preheat zone. It then increases further to the temperature T_b of the products (within the reaction zone) due to the heat released by the chemical reaction. Temperature T_b equals to the adiabatic flame temperature T_{ad} if the system is adiabatic. The mass fraction Y_R of the reactants rapidly decreases within the reaction zone, and this gradient leads to mass diffusion of reactants into the reaction zone. On the other hand, heat diffuses from the reaction zone into the preheat

zone. The ratio between the thermal α and the mass D diffusivity is described by the Lewis number Le:

$$Le = \frac{a}{D} \tag{2.15}$$

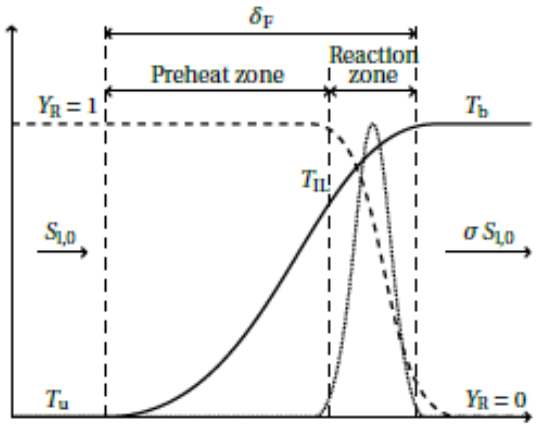

Figure 2.3: Schematic of a one-dimensional and unstretched premixed laminar flame (adapted from [29]). The solid line refers to the fuel-air mixture's temperature, the dashed line to the mass fraction Y_R of the reactants, and the dotted line to the reaction rate.

The laminar unstretched flame thickness δ_{l0} describes the preheat and the reaction zone, as shown in Figure 2.3. It can be described as the distance in which the gases are heated from T_u to the adiabatic T_b using a linear slope with the maximum gradient of the temperature with respect to x (see Figure 2.4), according to the following equation [11] :

$$\delta_{l0} = \frac{T_b - T_u}{max\left(\frac{dT}{dx}\right)} \tag{2.16}$$

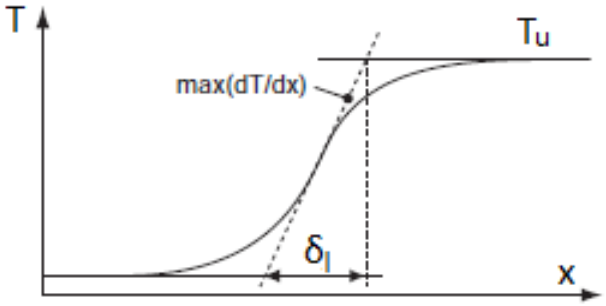

Figure 2.4: Laminar flame thickness defined by the maximum gradient of the temperature profile (adapted from [11]).

Alternative correlations for the laminar flame thickness δ_l depend on density ρ, thermal conductivity λ, specific heat capacity c_p, and laminar flame speed S_{l0}. Under the assumption of Le=1, Turns [30] proposes:

$$\delta_{l0} = \frac{2\lambda_u}{\rho_u c_{p,u} S_{l0}} \tag{2.17}$$

The laminar unstretched flame speed S_{l0} can be calculated by Cantera software [31], which performs one-dimensional steady-state flame simulations using an appropriate reaction mechanism such as the GRIMech 3.0 [32] or the Ó Conaire reaction mechanism [33].

2.2.2 Turbulent flame properties

In most industrial applications, turbulence occurs, aiding the premixed burning process by enhancing the fuel and oxidizer's mixing process. Under these conditions, the flame front of a turbulent premixed flame is wrinkled, increasing the surface area and the burning velocity. The premixed turbulent flames can be divided into different regimes in terms of length (l_t/δ_{l0}) and velocity scale ratios (u'/S_{l0}), according to Peters [34]. Figure 2.5 shows the flame regimes, in which the velocity fluctuations u' and the length scale of the large eddies l_t are divided with the laminar flame speed S_{l0} and the laminar flame thickness δ_{l0}, respectively.

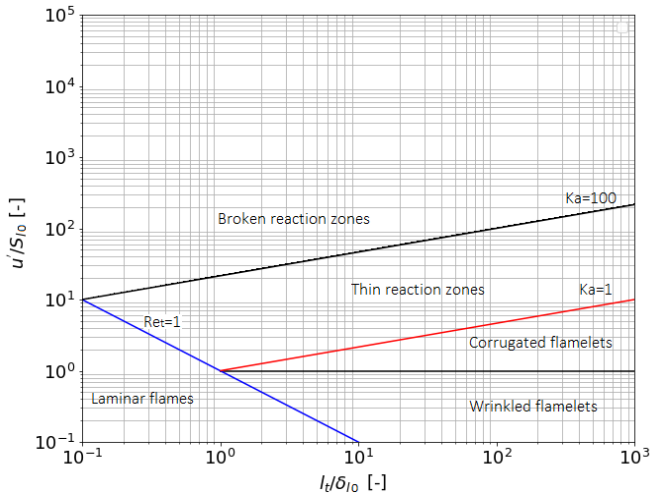

Figure 2.5: Premixed turbulent combustion regime diagram, according to Peters [34].

Peter introduces the turbulent Reynolds number Re_t in Figure 2.5. The Re_t number is used to separate the laminar ($Re_t<1$) from the turbulent ($Re_t>1$) flames.

$$Re_t = \frac{u' l_t}{v} \tag{2.18}$$

The turbulent flame regimes can be further distinguished based on the Karlovitz number Ka shown in Figure 2.5, which is defined as the ratio of the chemical time scale t_{ch} to the Kolmogorov time scale t_k of the smallest turbulent eddies, according to [34]:

$$Ka = \frac{t_{ch}}{t_k} = \frac{u'(\eta_k)\delta_{l0}}{\eta_k S_{l0}} \tag{2.19}$$

The line with *Ka=1* separates the thin reaction zones regime from the corrugated and the wrinkled flamelets. If the Karlovitz number is *Ka=1*, the laminar flame thickness δ_{l0} scales with the length scale of the small eddies n_k and the small eddies can affect the flame front, whereas if *Ka<1*, the smallest turbulent eddies do not perturb the flame structure (corrugated and wrinkled flamelets) [19]. The corrugated flamelets are strongly wrinkled flamelets with turbulent velocity fluctuations *u'* higher than the laminar burning velocity S_l [22].

In the thin reaction zone *1<Ka<100*, the Kolmogorov turbulence eddies η_k are smaller than the laminar flame thickness δ_l and can penetrate the preheat zone of the flame. The small eddies' interaction with the preheat zone enhances scalar mixing; thus, the reaction rate and the turbulent burning velocity increase. For *Ka>100* (broken reaction zones), the small eddies η_k scale with the thickness of the inner reaction zone δ_r and can penetrate the reaction zone. Due to the transport of cold reactants in the reaction zone, local quenching may occur, setting a limit to the increase of the turbulent flame speed [6].

The wrinkled-corrugated flames and flames within the thin reaction zone can be modeled based on the flamelet concept [35]. According to the flamelet concept, the turbulent flame can be viewed as an ensemble of thin, laminar, locally one-dimensional flamelet structures embedded within the turbulent flow field [10]. Damköhler was the first to develop a theoretical expression for the turbulent flame speed S_t in 1940. He proposed that the turbulent and laminar flame speed ratio can be defined by the ratio of the flame surface area and the cross-sectional flow area [34].

$$\frac{S_t}{S_{l0}} = \frac{A_F}{A} \tag{2.20}$$

A correlation based on Damköhler's idea has been widely used to estimate the turbulent burning velocity [6]:

$$\frac{S_t}{S_{l0}} = 1 + C\left(\frac{u'}{S_{l0}}\right)^{\mathrm{n}} \tag{2.21}$$

According to Damkoher, parameter *C* depends on the length scale ratio (l_t/δ_l), and the exponent *n* varies between 0.5 and 1 [36].

In more recent studies, Burke et al. investigated the accuracy of 16 turbulent flame speed S_t correlations for over 200 sets of laboratory flames at different pressures, turbulent conditions, and hydrocarbon fuel types [37]. According to their research, the correlation proposed by Muppala et al. [38] showed the best overall agreement with the experimental data (see Eq. (2.22)). Muppala's correlation showed a good agreement with the experimental data of lean methane, ethylene, and propane-air fuel mixtures for operating pressures between 0.1 and 1.0 MPa. Furthermore, Muppala's correlation accurately predicted the turbulent flame of lean hydrogen-methane fuel mixtures (ϕ=0.8) at atmospheric operating conditions [39].

$$\frac{S_t}{S_{l0}} = 1 + \frac{0.46}{Le} Re_t^{0.25} \left(\frac{u'}{S_{l0}}\right)^{0.3} \left(\frac{P_o}{0.1\ MPa}\right)^{0.2} \tag{2.22}$$

Daniele et al. performed experiments in premixed turbulent flames at gas turbine relevant conditions [40]. Based on measurements in syngas (H_2-CO), CH_4, and CH_4-H_2 fuel mixtures, they proposed the following turbulent flame speed correlation:

$$\frac{S_t}{S_{l0}} = 337.5 \left(\frac{u'}{S_{l0}}\right)^{0.63} \left(\frac{l_t}{\delta_l}\right)^{-0.37} \left(\frac{P_o}{0.1\ MPa}\right)^{0.63} \left(\frac{T_0}{298\ K}\right)^{-0.63} \tag{2.23}$$

Finally, Lin et al. published a correlation for a number of H_2-rich flames and syngas flames (H_2-CO 50-50) investigated at the high-pressure burner of Paul Scherrer Institute (PSI) [41][42]. The ratio of the turbulent flame speed S_t to the unstretched laminar burning velocity S_{l0} was represented as a function of the Lewis number Le, the mean velocity fluctuations u', the integral length scale l_t, the unstretched laminar flame thickness δ_{l0} and the operating pressure and temperature:

$$\frac{S_t}{S_{l0}} = 10.5 \times Le^{-0.82} \left(\frac{u'}{S_{l0}}\right)^{0.45} \left(\frac{l_t}{\delta_{l0}}\right)^{-0.41} \left(\frac{P_o}{0.1\ MPa}\right)^{0.75} \left(\frac{T_0}{298\ K}\right)^{-1.33} \tag{2.24}$$

The ratio of the turbulence intensity u' and the laminar flame speed S_{l0} raised to a suitable exponent is used by all turbulent flame speed correlation discussed above. Contrary to the initial Damköhler correlation shown in Eq. (2.21), the effect of the Lewis number was added to most of the recently developed turbulent flame speed correlations to take into account the increase of the flame speed due to thermodiffusive instabilities, especially for H_2-rich fuel mixtures (discussed in section 2.3.5.1). Furthermore, the most recent correlations include a pressure and a temperature term, powered to a specific constant, to consider the effect of the elevated operating pressure and temperature on the turbulent flame speed.

The turbulent flame speed correlations discussed above will be integrated into the boundary layer flashback models described in the next section. It has to be noted that the maximum streamwise turbulent fluctuations u' near the wall (y^+<40) will be applied to the turbulent flame speed correlations used in the flashback models, based on the assumption that boundary layer flashback is initiated at the wall distance of maximum turbulent burning velocity [6][22].

2.3 State-of-the-art flashback models

In this section, the first boundary layer flashback model, developed by Lewis and von Elbe [13] [14], will be initially presented. Then, the recently developed boundary layer flashback models (BLF) will be described. First, the empirical flashback models developed in the Paul Scherrer Institute (PSI) [41] and the University of California Irvine (UCI) [43] are presented. The semi-empirical flashback model based on Stratford's separation criterion and initially proposed by Hoferichter [19] is then described. Finally, the revised version of Hoferichter's flashback model (TU Delft model) [21][22] used in this thesis is presented. Understanding the PSI and the UCI models, as well as the improved TU Delft flashback model, is essential before applying the models to the academic burners in chapters 3 and 4.

2.3.1 Critical velocity gradient model

Lewis and von Elbe [13] [14] were the first to develop a boundary layer flashback model based on flashback experiments in laminar methane-air flames at atmospheric conditions. They introduced the concept of the critical velocity gradient g_c, which focuses on the velocity gradient at the wall during flashback initiation. Their concept can be described using Figure 2.6. In this figure, the velocity profile adjacent to the wall is assumed to be linear. Lewis and von Elbe proposed that the laminar flame speed equals the local flow velocity at a distance δ_p (penetration distance) when flashback occurs. Furthermore, the burning velocity is assumed to be equal to the one-dimensional laminar flame speed at the penetration distance. The critical velocity gradient g_c is then derived as $g_c = \frac{S_l}{\delta_p}$ and flashback occurs when the flow velocity gradient $\frac{\partial u}{\partial y}$ at the wall is lower than the critical velocity gradient g_c.

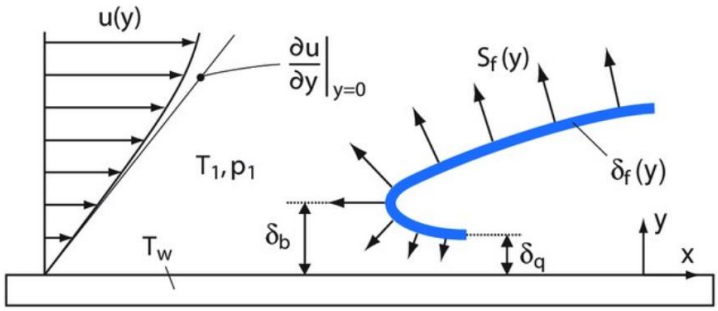

Figure 2.6: Schematic of the critical velocity gradient concept. Source: [11]

2.3.2 PSI flashback model

Lin et al. [44] proposed a flashback criterion that correlates the turbulent flame speed S_t and the flashback propensity of the H_2-rich fuel gases. They proposed a correlation for the critical velocity gradient of the flame g_c to be compared with the velocity gradient established by the flow g_f. To compose the critical velocity gradient g_c, the turbulent flame speed S_t and the laminar flame thickness δ_l are selected to be the characteristic velocity and length scale, respectively [44]. The Lewis number is also included in the definition of the critical velocity gradient (see Eq. (2.25)) to capture the influence of H_2 in the mixture, according to previous studies [45] [46].

$$g_c = \frac{S_t}{Le \times \delta_{l0}} \tag{2.25}$$

The velocity gradient of the flow g_f is calculated from Eq. (2.26), where τ_w is the shear stress at the wall and μ the fuel-air mixture's dynamic viscosity. According to the critical velocity gradient concept discussed in the previous section, boundary layer flashback occurs when the flow velocity gradient g_f drops below the critical velocity gradient g_c.

$$g_f = \frac{\tau_w}{\mu} \tag{2.26}$$

The laminar flame thickness δ_{l0} used in Eq. (2.25) is computed using Cantera software, as discussed in section 2.2.1. The Lewis number is derived from Eq. (2.15) as the ratio of the thermal diffusivity α to the mass diffusivity D of the deficient species (H_2). The latter term is calculated as the multicomponent diffusion coefficient of the H_2-N_2 pair [44]. The PSI flashback model was validated by Lin using flashback experiments for H_2-rich fuel gases at elevated operating conditions [44]. It has to be noted that the turbulent fame speed S_t is calculated according to Eq. (2.24). Substituting equation (2.24) to Eq. (2.25) gives:

$$g_c = 10.5 \times \frac{S_{l0}}{\delta_{l0}} Le^{-1.82} \left(\frac{u'}{S_{l0}}\right)^{0.45} \left(\frac{l_t}{\delta_{l0}}\right)^{-0.41} \left(\frac{P_0}{0.1\ MPa}\right)^{0.75} \left(\frac{T_0}{298\ K}\right)^{-1.33} \quad (2.27)$$

The results from this analysis are shown in Figure 2.7, in which the straight green lines represent the flow velocity gradient g_f, and the black lines are the critical velocity gradient g_c calculated from the PSI model according to Eq. (2.27). The intersection of the two lines results in the predicted equivalence ratio at flashback φ_{fb}, which is close to the experimental equivalence ratio at flashback (not shown in Figure 2.7), reported by Lin et al. [44].

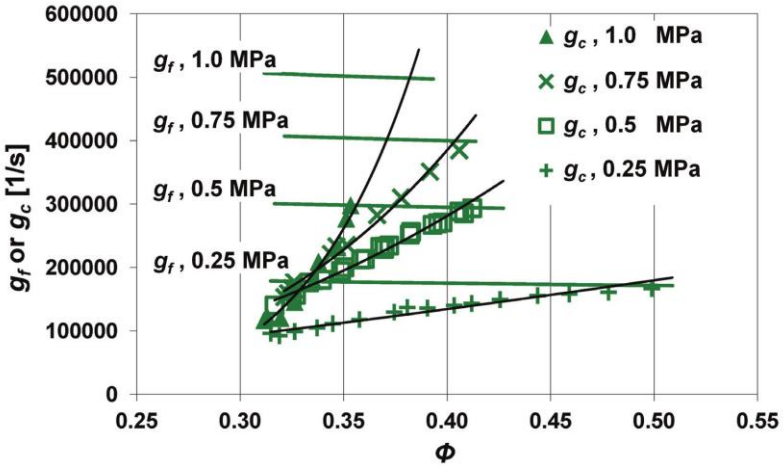

Figure 2.7: Flow g_f and critical velocity gradients g_c as a function of the equivalence ratio φ for H_2-N_2 fuel mixture (85-15 %vol) at preheated mixture temperature T=623 K (adapted from Lin's flashback experiments [41]).

2.3.3 **UCI model**

Kalantari et al. [43] developed a non-dimensional correlation, using the Buckingham Pi theorem, based upon the flashback experiments conducted at the facilities of the University of California Irvine (UCI). The correlation was optimized for pure H_2 fuel at absolute pressures between 3 and 8 atm and inlet H_2-air mixture temperature between 300 and 500 K. The inlet bulk velocity was varied between 30 and 40 m/s, resulting in highly turbulent flow (5×10^4<Re<3×10^5). The resulting non-dimensional correlation used to describe initiation of flame flashback in terms of a critical Damköhler number is given by:

$$Da_{UCI} = 5.79 \times 10^{-6} Le^{1.68} Pe_f^{1.91} \left(\frac{T_0}{300\ \mathrm{K}}\right)^{2.57} \left(\frac{T_{tip}}{300\ \mathrm{K}}\right)^{-0.49} \left(\frac{P_0}{0.1\ \mathrm{MPa}}\right)^{-2.1} \quad (2.28)$$

Eq. (2.28) shows that the Damköhler number *Da* was selected as the flashback propensity indicator. According to Kalantari, the Damköhler number is a reasonable selection because it includes flashback parameters, such as the critical velocity gradient g_c and the laminar flame speed S_l. Furthermore, Eq. (2.28) includes the effect of the Lewis number in flashback propensity, as well as the effect of the flame stretch [47] in terms of a Peclet number $\left(Pe_f = \frac{dS_{l0}}{a}\right)$, where *a* is the thermal diffusivity of the unburned fuel-air mixture and *d* the burner diameter. Finally, the preheat temperature of the fuel-air mixture T_0, the operating pressure P_0 and the burner rim temperature T_{tip} are included in Kalantari's correlation.

Figure 2.8 shows the UCI model's application to the flashback experiments conducted at the conditions discussed above [43]. The predicted Damköhler number was calculated from Eq. (2.28), whereas the actual Damköhler number was obtained from the definition of the Damköhler number (see Eq. (2.29)) evaluated at the experimentally determined flashback conditions. A good agreement is observed between the experimental data and the predicted flashback limits for 100% H_2 fuels at elevated operating conditions, as shown in Figure 2.8. Furthermore, Kalantari tested his model with the flashback data published by Daniele et al. [48] for syngas mixtures at elevated operating conditions, showing overall good agreement [43].

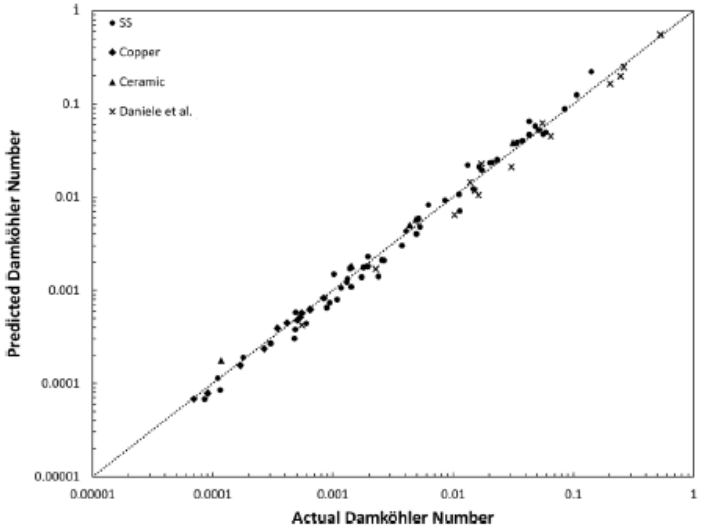

Figure 2.8: Comparison of the predicted Damköhler number (Eq. (2.28)) with the actual Damköhler number (Eq. (2.29)). Flashback experiments of H_2-air and syngas mixtures at elevated operating conditions with different burner materials were used (stainless steel, copper, and zirconia ceramic). Source: [47]

$$Da = \frac{S_{l0}^2}{a g_c} \tag{2.29}$$

The UCI flashback model can be applied in terms of a critical velocity gradient g_c instead of a predicted Damköhler number Da_{UCI} by simply substituting Eq. (2.28) into the definition of the Damköhler number given by Eq. (2.29):

$$g_c = \frac{1}{5.79} \times 10^6 Le^{-1.68} Pe_f^{-1.91} \frac{S_{l0}^2}{a} \left(\frac{T_0}{300\ \mathrm{K}}\right)^{-2.57} \left(\frac{T_{tip}}{300\ \mathrm{K}}\right)^{0.49} \left(\frac{P_0}{0.1\ \mathrm{MPa}}\right)^{2.1} \quad (2.30)$$

The critical velocity gradient g_c derived from Eq. (2.30) can then be compared with the flow velocity gradient g_f (see Eq. (2.26)) to investigate boundary layer flashback, following the same methodology described in section 2.3.2.

Comparison of Eq. (2.30) with Eq. (2.27) shows that both the PSI and UCI flashback models characterize flashback in terms of the same non-dimensional parameters, including the Lewis number and the unburned temperature and pressure ratio. The Lewis number's effect on the critical velocity gradient g_c is considered similarly, given that the (negative) exponent of the Lewis number is almost the same for both flashback models. On the contrary, the exponents of the (positive) pressure term and (negative) temperature term are higher in the UCI model's critical velocity gradient correlation, as shown in Eq. (2.30) and (2.27). Finally, two main differences between the PSI and the UCI models can be observed. The UCI model includes the effect of the wall tip temperature using the term $\left(\frac{T_{tip}}{T_0}\right)^{0.49}$ for the calculation of the critical velocity gradient, whereas a similar term is not represented in the PSI model. On the other hand, the PSI model takes into account the turbulence of the flow by introducing the term $\left(\frac{u'}{S_{l0}}\right)^{0.45}$ in Eq. (2.27), while the UCI model (see Eq.(2.30)) does not have any relevant term representing the flow field properties.

2.3.4 TU Munich model

Eichler provided a new insight into the confined wall flashback mechanism, showing that the increase of the pressure upstream of the flame tip can induce flow separation resulting in upstream flame propagation [11]. The mechanism of boundary layer flashback of confined turbulent flame, proposed by Eichler, is shown in Figure 2.9. The undisturbed velocity profile (1) is distorted at the flame tip's vicinity due to the pressure rise induced by the flame front (2). In case that the pressure rise exceeds a critical value, the boundary layer separates (3), and the flame propagates further upstream through the recirculation region formed [6].

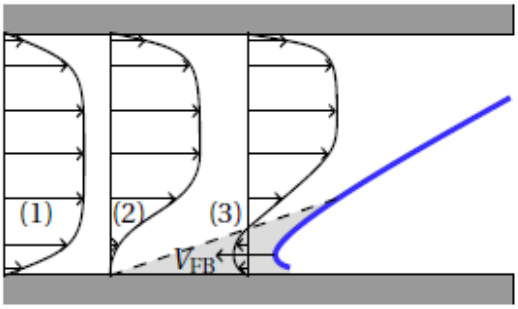

Figure 2.9: Schematic of the boundary layer flashback mechanism of confined turbulent flame (adapted from [11]). (1): Undisturbed velocity profile, (2) onset of boundary layer separation, (3) separation of boundary layer and flame flashback.

Based on Eichler's findings, Hoferichter developed a flashback model to predict the flashback limits for both unconfined and confined turbulent flames [6]. It has to be noted that a flame can be characterized as confined if the flame stabilizes inside the duct before flashback. On the contrary, flames in a free atmosphere or a combustion chamber with a considerable cross-section jump are categorized as unconfined flames [11]. Unconfined flames are beyond this thesis's scope; thus, Hoferichter's model for confined turbulent flames will be further discussed.

Hoferichter's flashback model for confined flames is based upon the turbulent boundary layer separation criterion from Stratford [20]. Stratford considered a flow over a flat plate, where a sudden increase of pressure leads eventually to separation at $x=x_s$, as shown in Figure 2.10.

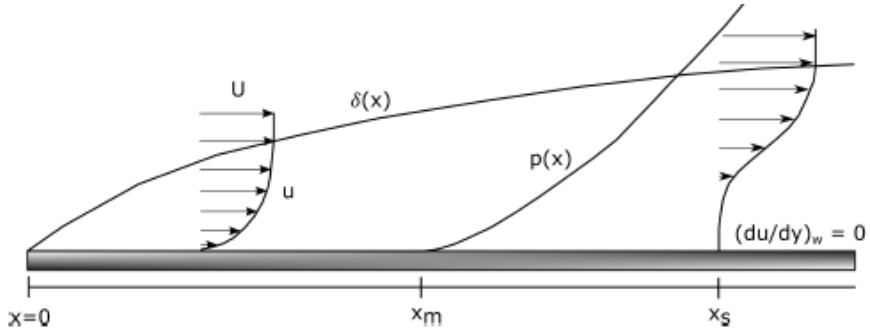

Figure 2.10: Boundary layer separation on a flat plate due to an increase in pressure at $x=x_m$ (adapted from [22]). Flow separates at $x=x_s$, where the shear stress at the wall is zero $\left(\left(\frac{\partial u}{\partial y}\right)_w = 0\right)$.

Under the effect of the adverse pressure gradient $\left(\frac{\partial P}{\partial x} > 0\right)$ Stratford divided the boundary layer into the inner and the outer region. The shape of the inner region changes with changing pressure, whereas the outer region is retarded but keeps its shape, as shown in Figure 2.11. Stratford's separation criterion for turbulent boundary layer separation is a result of the mathematical join of the inner and the outer velocity profiles at separation [20] given by:

$$\left(2C_p\right)^{\frac{1}{4}(n-2)}\left(x\frac{dC_p}{dx}\right)^{\frac{1}{2}} = 1.06\beta(10^{-6}Re_x)^{\frac{1}{10}} \tag{2.31}$$

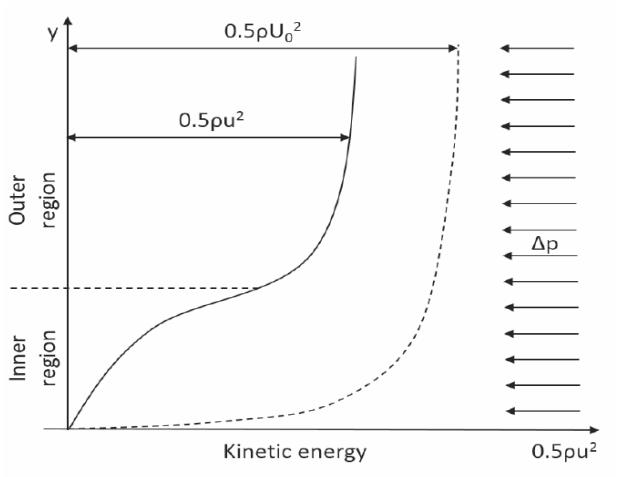

Figure 2.11: Shape of the dynamic head in the boundary layer. The dotted line refers to zero pressure gradient flow, and the solid line refers to adverse pressure gradient flow. (adapted from [10]).

Solving Eq. (2.31), the separation location *x* along a flat plate can be predicted for a given pressure distribution C_p and a local Reynolds number ($Re_x=\frac{Ux}{\nu}$). The pressure coefficient C_p is given by:

$$C_p(x) = \frac{p(x) - p_{x=0}}{\frac{1}{2}\rho_u U^2} \tag{2.32}$$

where *U* is the velocity at the edge of the boundary layer.

Hoferichter based her model on Eq. (2.31), and she further used n=6 for channel flow and β=0.73 [20] for positive curvature of the pressure distribution *p(x)* before separation resulting in [6]:

$$C_p\left(x\frac{dC_p}{dx}\right)^{\frac{1}{2}} = 0.39(10^{-6}Re_x)^{\frac{1}{10}} \tag{2.33}$$

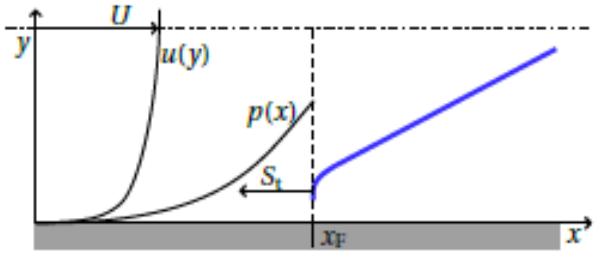

Figure 2.12: Premixed flame confined in a burner duct (adapted from [19]). Pressure increases upstream of the flame tip at x_f.

According to Eichler [11] and Baumgartner [10], a quadratic correlation is used for the pressure profile upstream the flame tip (see Figure 2.12), according to:

$$p(x) = p_{x=0} + \frac{\Delta p}{x_f^2} x^2 \tag{2.34}$$

Substituting Eq. (2.34) to Eq. (2.32) results to:

$$C_p(x) = \frac{2\Delta p x^2}{\rho_u U^2 x_f^2} \tag{2.35}$$

and then taking the derivative of Eq. (2.35) gives:

$$\frac{dC_p(x)}{dx} = \frac{4\Delta p}{\rho_u U^2} \frac{x}{x_f^2} \tag{2.36}$$

Hoferichter then inserted Eq. (2.36) to Stratford's criterion (Eq. (2.33)), resulting in Eq. (2.37). It has to be noted that Stratford's criterion is evaluated at the flame tip ($x=x_f$), and the centerline velocity of the channel U is replaced by the centerline velocity at flashback U_{fb}.

$$\sqrt{2}\left(\frac{2\Delta p}{\rho_u U_{fb}^2}\right)^{\frac{3}{2}} = 0.39\left(10^{-6}\frac{U_{fb}x_f}{\nu_u}\right)^{a} \tag{2.37}$$

Hoferichter claimed that for a fully developed flow, the U_{fb} should not depend on the position of the flame tip x_f; thus, she set the exponent α to zero. Eq. (2.37) is then further simplified to:

$$\sqrt{2}\left(\frac{2\Delta p}{\rho_u U_{fb}^2}\right)^{\frac{3}{2}} = 0.39 \tag{2.38}$$

The pressure rise Δp is derived using the standard Rankine-Huginoit conditions for mass conservation equation:

$$\rho_u u_u = \rho_b u_b \tag{2.39}$$

and momentum conservation:

$$\rho_u u_u^2 + p_u = \rho_b u_b^2 + p_b \tag{2.40}$$

Combination of Eq. (2.39) and (2.40) results to:

$$\Delta p = p_u - p_b = \rho_u u_u^2 \left(\frac{\rho_u}{\rho_b} - 1\right) \tag{2.41}$$

The flame front is assumed to be stationary, and the local velocity of the unburned mixture u_u can be replaced with the turbulent burning velocity S_t:

$$\Delta p = \rho_u S_t^2 \left(\frac{\rho_u}{\rho_b} - 1\right) \tag{2.42}$$

The turbulent flame speed is calculated from the Damköhler correlation (see Eq. (2.21)) and the air-fuel mixture properties using Cantera software. Hoferichter performed free flame simulations using Cantera at different preheating temperatures to generate third-order polynomials for the calculation of the laminar flame speed S_{l0} (see Eq. (2.43)), where the coefficients b_7-b_{10} depend on the equivalence ratio [6].

$$S_{l0}(T_u) = b_7 T_u^3 + b_8 T_u^2 + b_9 T_u + b_{10} \tag{2.43}$$

Hoferichter also included the effect of the flame stretch in her flashback model by defining a stretched laminar flame speed:

$$S_{ls} = S_{l0} - L_M \kappa \tag{2.44}$$

where L_M is the Markstein length, and κ is the flame stretch rate. It has to be noted that Eq. (2.44) is only valid in the region of the turbulent combustion diagram, where the Karlovitz number Ka is smaller than unity [49]. The Markstein length is used to describe the effect of the flame stretch on the fuel-air mixture, according to [6]. The flame stretch rate κ is defined as the normalized temporal change of the flame surface area A_F, according to the following derivative [6]:

$$\kappa = \frac{1}{A_F} \frac{dA_F}{dt} \tag{2.45}$$

For a detailed discussion of the derivation of the Markstein length L_M and the flame stretch rate κ, the reader is referred to the work of Hoferichter [6].

Hoferichter's flashback model is validated upon the experimental flashback data from Eichler [11] for channel and tube burners with premixed H_2-air mixtures. The comparison of the predicted flashback limits with the experimental data for the tube and the channel burner at atmospheric conditions and different preheating temperatures T_u is shown in Figure 2.13. Hoferichter's calculated flashback limits show good agreement with the experimental data at room temperature for both the channel and the tube burner. At preheating temperatures, however, Hoferichter's model underpredicts for equivalence ratio below 0.6. This underprediction is improved in the TU Delft model by considering the increase of the turbulent burning velocity of H_2-air mixtures at low equivalence ratios due to flame instabilities (see section 2.3.5.1).

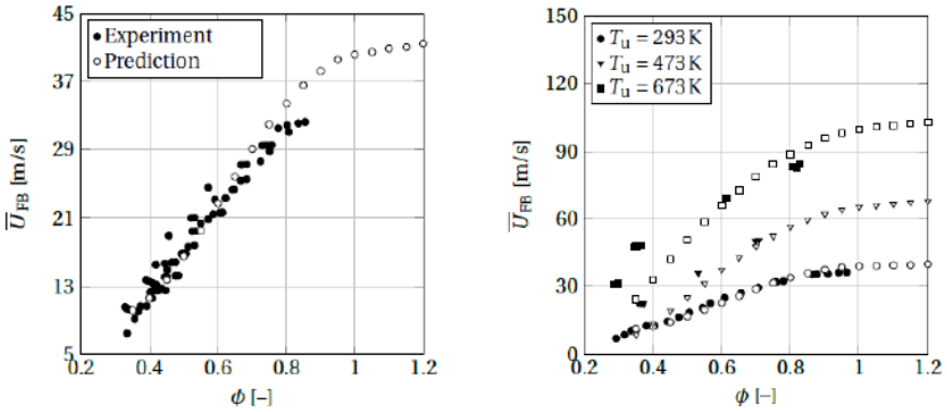

a) Tube burner d_h=40 mm. b) Channel geometry d_h=31.5 mm.

Figure 2.13: Comparison of the Hoferichter's predicted bulk velocity at flashback U_{fb} with Eichler's experimental data for tube (a) and channel (b) burners (adapted from [6]). Empty symbols refer to the predicted values and filled symbols to the experimental data [11].

2.3.5 TU Delft model

The TU Delft flashback model, developed by Björnsson et al. [50], is an improvement of the flashback model initially proposed by Hoferichter [6]. One main difference is that Björnsson took a few steps back in the derivation of Stratford's criterion [20] and proposed a generalized turbulent boundary layer separation criterion [22], whereas Hoferichter used the Stratford criterion for a developing turbulent boundary layer at a flat plate exposed to an adverse pressure gradient:

$$C_p^{\frac{1}{4}(n-2)}\left(\delta\frac{dC_p}{dx}\right)^{\frac{1}{2}} = \left(\frac{3(0.41\beta)^4}{(n+1)n^2}\right)^{\frac{1}{4}}\left(1-\frac{3}{n+1}\right)^{\frac{1}{4}(n-2)} \tag{2.46}$$

Stratford's separation criterion predicts the mean velocity profile at flow separation (zero wall shear stress) by joining the inner and the outer region of the boundary layer, as discussed in section 2.3.4. The inner region's velocity profile is derived from the mixing length theory under the assumption of zero wall stress at separation. The outer region is described by the $1/n^{th}$ power law, according to:

$$\frac{u}{U} = \left(\frac{y}{\delta}\right)^{\frac{1}{n}} \tag{2.47}$$

where the outer velocity U and boundary layer thickness δ should match, meaning that the value of U should be taken at y=δ. Since Stratford's separation criterion derives by joining the inner and the outer layer, the main idea is that Eq. (2.47) should represent the outer layer of the boundary layer velocity profile as accurately as possible close to the inner layer [22]. It is assumed that Stratford's inner region ends at y^+=30 (end of the transition region, as discussed in section 2.1.1). Thus, the value of n is determined by a least-squares method such that the calculated velocity profile from Eq. (2.47) is as close as possible to the boundary layer velocity profile at the transition region of the boundary layer ($30<y^+<50$) [50]. Finally, the mean velocity profile in the boundary layer is derived from steady-state cold-flow CFD simulations,

allowing the application of the TU Delft model to more complex geometries [50]. An example of the method discussed above is shown in Figure 2.14, where the outer layer of a strong diffusing flow (4^0 diffuser) is accurately captured from Eq. (2.47) near the transition region ($30<y^+<50$).

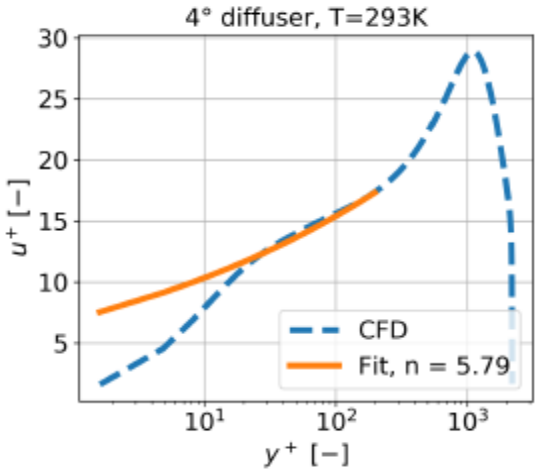

Figure 2.14: Application of the $1/n^{th}$ power law in a 4° diffuser (adapted from [50]. The fitted profile (Eq. (2.47)) shows good agreement with the velocity profile (CFD) near the transition region ($30<y^+<50$).

The empirical factor β is set equal to 0.73, according to Stratford suggestions for positive curvature of the pressure distribution at separation $\left(\frac{\partial p^2}{\partial x^2} \geq 0\right)$ [20]. Furthermore, the pressure coefficient C_p and its derivative were computed in the same way as in Hoferichter's model (see section 2.3.4).

Björnsson [22] also included the effect of flame stretch on the TU Delft model and validated it upon the Eichler's [11] flashback data for channel and tube burners. He showed that at lower equivalence ratios, the Markstein length L_M reaches unphysical values causing significant overprediction of the flashback limits. He finally concluded that removing the flame stretch effect on the TU Delft model extends the model's validity to lower equivalence ratios without affecting the model's accuracy at higher equivalence ratios. Following this observation, the Markstein length L_M will also be set to zero in this thesis, using the unstretched laminar burning velocity S_{l0} in the TU Delft flashback model.

2.3.5.1 Low Lewis number effect on flame speed

The improved TU Delft flashback model includes the effect of Lewis numbers lower than unity on the turbulent flame speed [21]. Poinson and Veynante [49] explained that flame front instabilities occur at Lewis number below unity, leading to the formation of cellular flames (flames with curved surface). This thermo-diffusive instability is caused by the faster molecular diffusion of reactants from the preheat zone into the reaction zone, compared with the heat diffusion from the reaction zone into the preheat zone. Aspden [51] investigated low Lewis number cellular flames numerically, and his results showed local maximum flame speed significantly higher than the laminar burning velocity. Kadowaki [52] also performed

numerical studies on the flame speed of cellular flames with low Lewis number. According to Kadowaki's research, the flame-velocity increment is greater than the surface-area increment at low Lewis numbers, whereas the flame speed is proportional to the surface area for unity Lewis numbers. Kadowaki's results were implicitly applied to the improved TU Delft flashback model to take into account the increase of the turbulent flame speed at lower Lewis number, using the following polynomial fit [50]:

$$\frac{S_{t,cf}}{S_t} = 0.6052\left(\frac{1}{Le}\right)^2 - 1.1314\left(\frac{1}{Le}\right) + 1.5224 \tag{2.48}$$

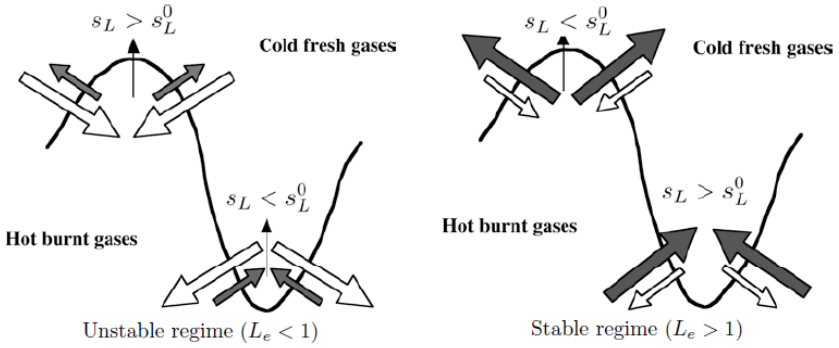

Figure 2.15: Schematic of the thermos-diffusive instabilities. White arrows represent the mass diffusion, whereas the grey arrows depict the heat diffusion. Source: [49]

Eq. (2.48) applies for H_2-air mixtures with Lewis number 0.5≤Le≤1. Mixtures with Lewis numbers above unity do not show a cellular flame structure. On the contrary, for flames with Lewis number below 0.5, the multiplication factor at Le=0.5 is used, based on the assumption that the trend described by Eq. (2.48) levels off for Le<0.5 [50].

2.3.5.2 **Effect of mean flow pressure gradient**

The last modification applied to the TU Delft model is to include the underlying flow pressure gradient effect. The adverse pressure gradient ($\frac{\partial p}{\partial x} > 0$) will contribute to the separation of the boundary layer in the same way the flame backpressure Δp does, whereas the favorable pressure gradient ($\frac{\partial p}{\partial x} < 0$) should mitigate the possibility of flow separation. Thus, the flow pressure gradient is included in Eq. (2.34), resulting in a combined pressure profile [50]:

$$p(x) = p_m + \frac{\Delta p}{x_f^2}x^2 + \frac{\partial p_{flow}}{\partial x}x \tag{2.49}$$

2.3.5.3 **Validation upon experimental data**

Björnsson et al. [50] compared the calculated flashback limits from the updated TU Delft model with Eichler's flashback data in channel confined flames [11]. Figure 2.16 shows that the TU Delft model extends the original model's applicability to very low equivalence ratios

for the preheated mixture (see Figure 2.16b), given that the low Lewis number effect on the flame speed discussed in section 2.3.5.1 is taken into account.

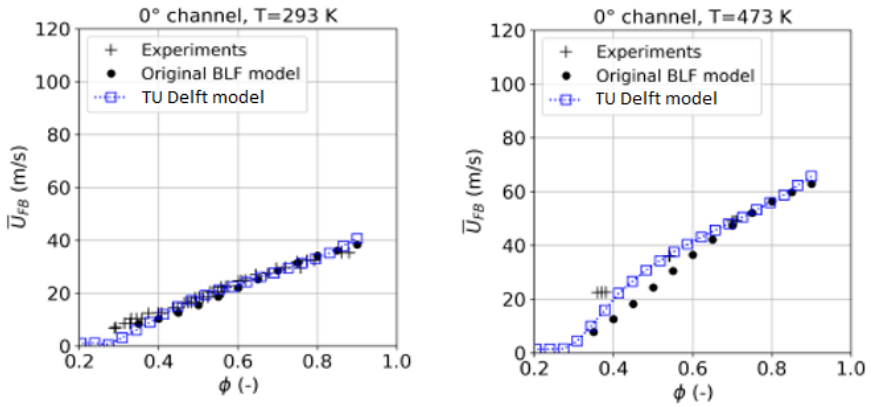

a) Channel geometry, room temperature.

b) Channel geometry, preheated mixture temperature (200°C).

Figure 2.16: Comparison of the TU Delft model's predicted flashback limits to Hoferichter's [6] original flashback model (adapted from [22]). Experimental flashback data from Eichler [11] are used at room and preheated mixture temperatures.

Björnsson et al. [50] also evaluated the updated TU Delft model upon the flashback experimental data of Eichler in adverse pressure gradient flows (2°-4° diffusers) [11]. Figure 2.17 shows that, with a number of modifications, the TU Delft model captures the flashback limits for the 2° diffuser adequately. However, the flashback limits are underpredicted for higher adverse pressure gradients flows (4°). According to Björnsson, this was probably attributed to the low-velocity streaks in the diffusing flow [11], which may not be included well in the updated TU Delft flashback model [50].

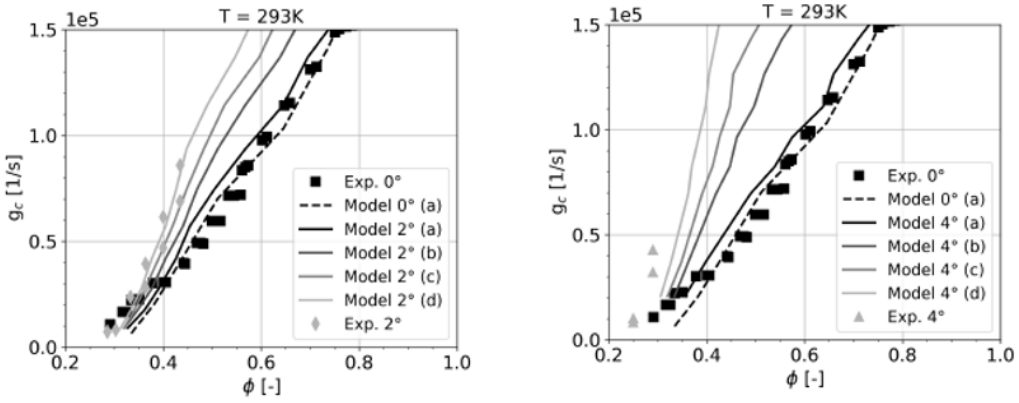

a) Calculated flashback limits in the 2° diffuser.

b) Calculated flashback limits in the 4° diffuser.

Figure 2.17: TU Delft model's flashback limits in the 2° and 4° diffusers (adapted from [50]). (a) Coupling of the flashback model with CFD simulations. (b-c) Including mean flow adverse pressure gradient and correcting the u' to experimental values. (d) Adjusting of the tuning constant C used in the Damköhler turbulent flame speed correlation.

3. Application of BLF models to academic burners

In this section, the three flashback models (PSI, UCI, and TU Delft discussed in section 2.3) are benchmarked against the flashback experiments on a number of academic burners (atmospheric set-up TU Munich (TUM), pressurized set-up for the Paul Scherrer Institute (PSI) and the University of California Irvine (UCI)). First, cold flow CFD simulations using ANSYS Fluent are performed on the three burners, and the turbulence properties within the boundary layer (i.e., u') are coupled with the three flashback models to predict flashback initiation. The empirical models of PSI and UCI are applied in their original form [15] [47], whereas the TU Delft model [50] is adapted to perform at gas turbine relevant conditions (i.e., increased pressure and temperature), based upon the flashback data of the UCI high-pressure burner [47]. Finally, the modified TU Delft model is further validated against both the high-pressure PSI combustor and the TUM atmospheric burner.

3.1 Evaluation of BLF models at atmospheric operating conditions

According to Eichler [11], the pressure rise upstream of the turbulent flame (flame backpressure) interacts with the incoming flow and can cause flame flashback. This finding challenges the validity of the fundamental concept of the 'critical velocity gradient' to predict boundary layer flashback [14], in which the existing empirical models from PSI [15] and UCI [53] are based in. In this section, both empirical models will be compared with the improved (semi-empirical) TU Delft model. Thus, all three flashback models will be investigated for confined flames in the 0° channel and 2°–4° diffuser experiments (all atmospheric operating conditions) performed by Eichler [11].

3.1.1 Channel and 2°-4° diffuser cold flow CFD simulations

As discussed in section 2.3.4, Eichler performed flashback experiments in a burner with a modular structure such that zero pressure gradients and adverse pressure gradient flows can be established. A cross-section of the combustion chamber and the TUM burner's measurement section is shown in Figure 3.1. The channel and the 2°-4° diffuser geometries can be generated by inserting stainless steel plates in the measurement section with inclination angles of ϕ=0°, 2°, and 4°, respectively [11]. The premixed H_2-air mixture enters the combustor through an inlet with height h=17.5 mm (right-hand side of Figure 3.1) and width w=157 mm. This high aspect ratio allows the assumption of a quasi-two-dimensional flow; thus, the flow section in the ramp's center region can be used for the cold flow CFD simulations [11].

Björnsson [22] already performed cold flow CFD simulations in the channel, 2°, and 4° diffuser, showing good agreement with the Particle Image Velocimetry (PIV) experiments carried out by Eichler [11]. The schematic of the two-dimensional fluid domain, used by Björnsson to simulate the flow in the different configurations, can be seen in Figure 3.2. Due to the good agreement with the experiments, the same set-up was adopted in the thesis to solve the governing equations of the fluid flow in ANSYS Fluent. The Fluent mesh and solver settings for both the channel and the diffusers are discussed in detail in Appendix A.1.

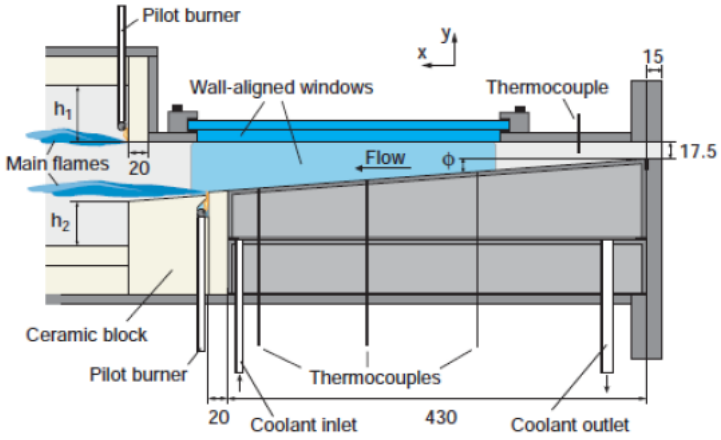

Figure 3.1: Geometry of the burner used for Eichler's flashback experiments (Source: [11]). The measurement section was used for flashback detection, and the combustion chamber was used for the safe burnout of the premixed gases, according to Eichler [11].

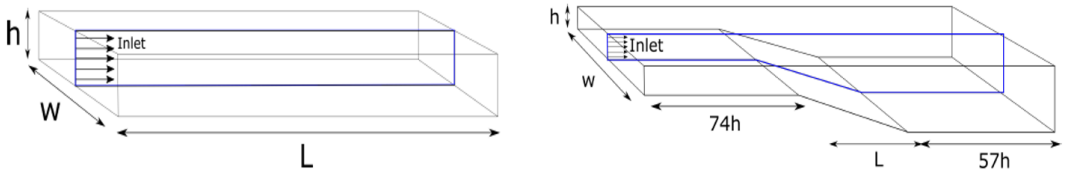

a) Channel fluid domain.

b) Diffusers fluid domain.

Figure 3.2: Schematic of the channel's (a) and diffuser's (b) fluid domain (blue) used for the cold flow CFD simulations, according to Björnsson [22].

Figure 3.3 and Figure 3.4 show the dimensionless axial velocity u and fluctuating velocities u', v' of the channel geometry, respectively. The velocities are dimensionless, using the friction velocity u_τ, and plotted with respect to the non-dimension wall distance y^+. Figure 3.3 shows that the mean velocity CFD results show good agreement with both the Spalding profile and the experiments in the logarithmic region of the boundary layer (up to y^+=300). The velocity fluctuations in the axial direction u' are slightly underpredicted in the viscous sublayer and the buffer layer (y^+<20), whereas they are overpredicted inside the logarithmic region (see Figure 3.4). The radial velocity fluctuations v' are well predicted.

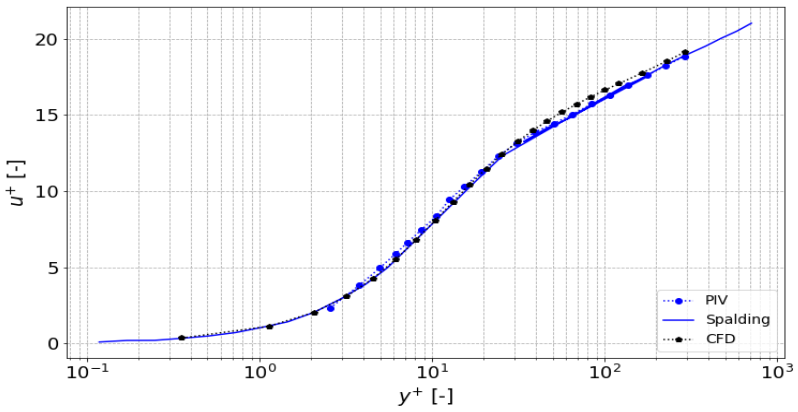

Figure 3.3: PIV values of dimensionless velocity and wall distance [11] compared with CFD and empirical Spalding function [54] in channel geometry. Ambient air mass flow inlet 60 g/s.

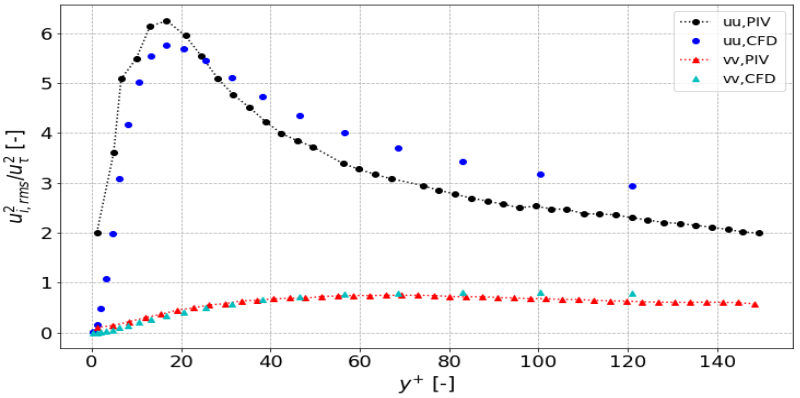

Figure 3.4: Dimensionless turbulent fluctuations in the channel geometry derived by PIV [11] and CFD simulations. Ambient air mass flow inlet 60 g/s.

For the diffusers, the velocity magnitude, velocity fluctuations, and the wall shear stress are extracted from ANSYS Fluent at sections E1, E2, E3 (see Figure 3.5) and used to calculate the friction velocity u_τ and the non-dimensional quantities u^+ and y^+. In Figure 3.6, Eichler's PIV experiments are compared with the CFD results in the 2° diffuser. It can be seen that the mean velocities are captured well in the CFD simulations, especially adjacent to the wall. The non-dimensional velocity fluctuations profiles of the CFD results have a similar shape along the different sections. The peak velocity fluctuations are underpredicted in the CFD results further downstream (sections E2, E3), while the peak values are similar near the wall in section E1.

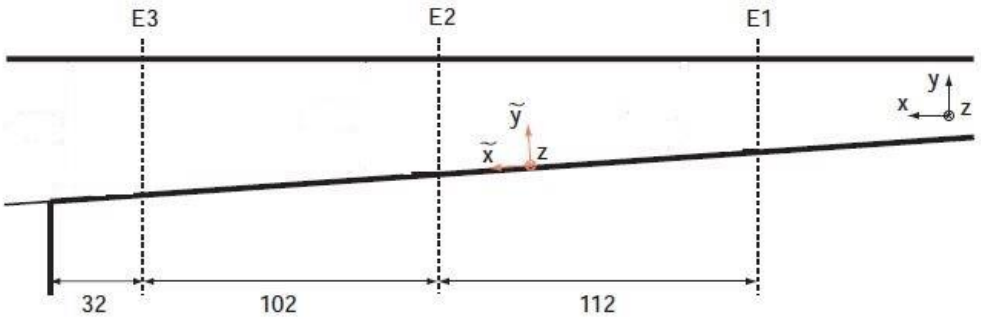

Figure 3.5: PIV measurement sections along the 2° and 4° diffuser [11].

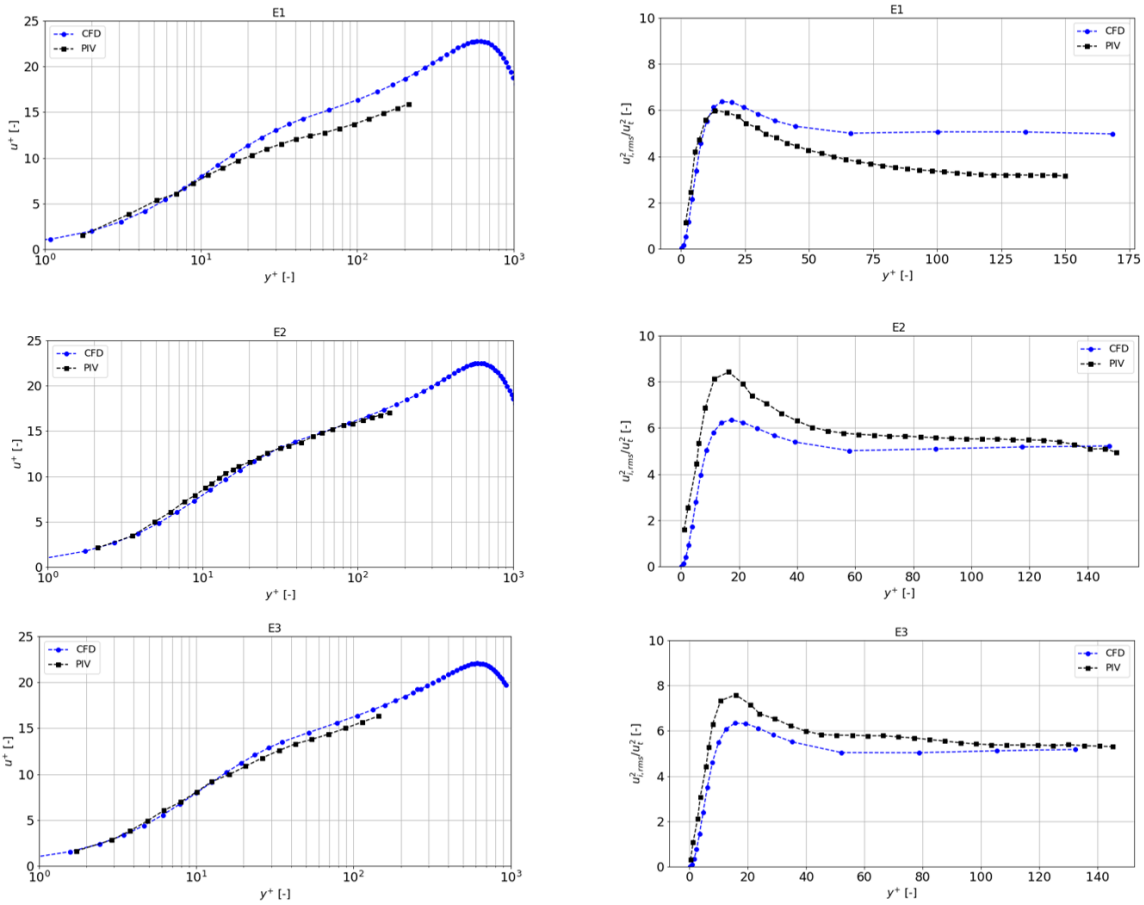

Figure 3.6: CFD and PIV [11] results of the mean velocity and turbulent velocity fluctuations across the different sections (E1-E3) of the 2° diffuser. Ambient air mass flow 60 g/s.

The comparison of the CFD results with the experimental data for the 4° diffuser is shown in Figure 3.7. In addition to the PIV experiments, LDA measurements were performed on the 4° degree diffuser due to the less uniform flow field than the 0° and 2° diffuser cases [11]. The non-dimensional mean velocity is almost the same as the experimental data within the boundary layer (y^+<200), while it is underpredicted further away from the wall. A similar trend with the 2° diffuser is observed for the non-dimensional velocity fluctuations, which are underpredicted by the CFD results throughout the measurement section.

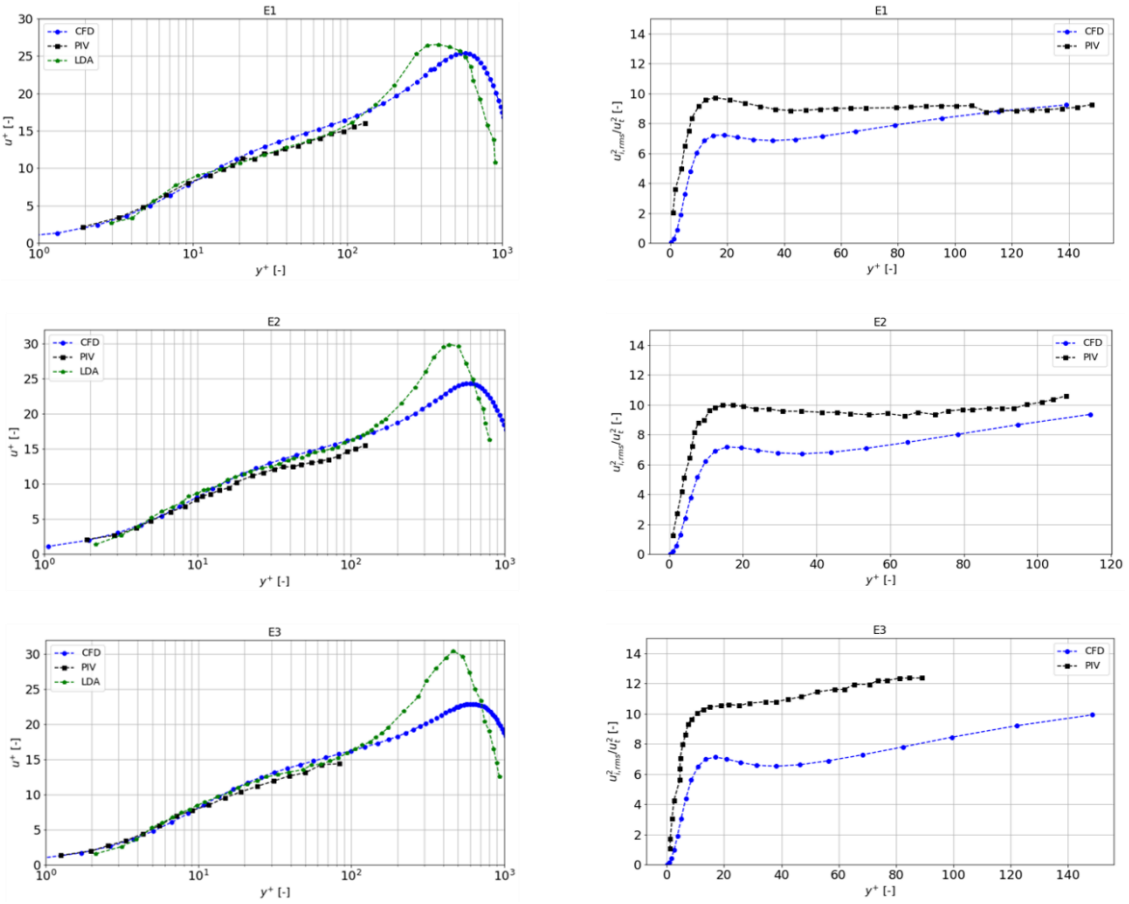

Figure 3.7: CFD and PIV [11] results of the mean velocity and turbulent velocity fluctuations across the different sections of the 4° diffuser. Air mass flow 60 g/s.

The above analysis showed that the outer mean velocity profile and the maxima of the velocity fluctuations are captured correctly for both the channel and the diffusers, following the results from Björnsson's CFD cold flow simulations [22]. The importance of the mean velocity profile and the maximum velocity fluctuations in the flashback models (PSI, UCI, TU Delft) has been already addressed in section 2.3.

In the next section, a map of flashback limits will be obtained for the channel and 2°-4° diffusers for different combinations of inlet bulk velocity and equivalence ratio. Thus, separate cold flow CFD simulations are required for each inlet velocity. However, the density and the viscosity of the H_2-air mixture need to be defined prior to the CFD simulations. According to Björnsson [22], a reasonable simplification is to use the density and viscosity of the H_2-air mixture based on an average equivalence ratio of ϕ=0.6. With this simplification, the flow information from the CFD results does not depend on the equivalence ratio, and the system of equations that make up the flashback models (UCI, PSI, and TU Delft) is linear and can be easily solved. Björnsson showed that the percentage variation in density and viscosity is ±10% and almost 0%, respectively. The effect of density variation, due to variation in the equivalence ratio, on the CFD results is further investigated in this section. Separate cold flow CFD simulation runs are performed at a constant inlet velocity and varying H_2-air mixture equivalence ratio in the channel. Thus, the density and viscosity of the H_2-air mixture varies in the CFD simulations due to variations of the equivalence ratio. Then the flow velocity gradient at the wall g_f, and the maximum turbulent fluctuations u' are extracted from the CFD results

at position E3 of the channel's measurement section. Figure 3.8 shows that the turbulent velocity fluctuations vary less than 2%, while the wall velocity gradient varies by up to 8% between 0.3≤ϕ≤0.9. The negligible deviation of the velocity fluctuations is not expected to influence the turbulence flame speed correlations used in the PSI and TU Delft model significantly. However, the UCI and PSI models may slightly overpredict the maximum equivalence ratio for flashback φ_{fb} at the very lean region (0.3<ϕ<0.4) due to the lower g_f value in this region compared to the wall velocity gradient of the average H_2-air mixture (ϕ=0.6). The validity of the last statement will be examined in the next section.

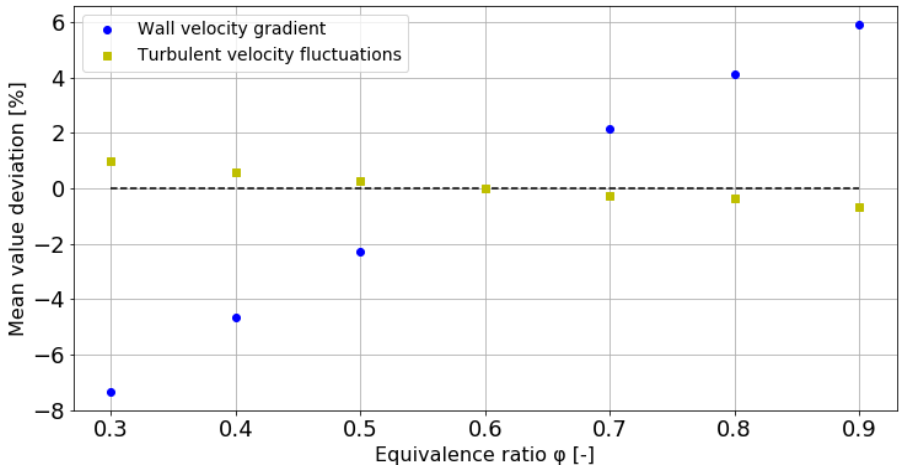

Figure 3.8: Wall velocity gradient and turbulent velocity fluctuations for unburned H_2-air mixtures at atmospheric conditions (channel geometry).

3.1.2 **Flashback limits calculation**

In this section, the flashback models (UCI, PSI, and TU Delft) will be applied to the turbulent flashback experiments carried out by Eichler [11] in the channel and the 2°-4° diffusers. This analysis aims to obtain a map with the predicted flashback limits for both the channel and the 2°-4° diffusers and compare it with Eichler's experimental data. Thus, separate cold flow CFD simulations are carried out at different inlet velocities, and then the flow properties (i.e., u, u') and the flow velocity gradient at the wall g_f are extracted at the different positions of the measurement section (see Figure 3.5). As discussed in section 2.3, the mean velocity profile affects the separation criterion used in the TU Delft model, the velocity fluctuations u' are essential for the turbulent flame speed correlations used in the PSI and TU Delft models, and the wall velocity gradient g_f is used in the UCI and PSI models.

3.1.2.1 **Channel geometry**

Björnsson has calibrated the TU Delft model to predict flashback initiation accurately in the channel configuration [22]; thus, the same configuration will be used in this analysis. More specifically, the tuning constant C for the Damköhler turbulent flame speed correlation is selected C=1.1, and the laminar unstretched burning velocity S_{l0} is calculated using the third-order polynomials proposed by Hoferichter [6]. Additionally, the Lewis number's effect on the turbulent flame speed is captured by implementing the Lewis number correction proposed by

Tober [21] (see section 2.3.5.1). A detailed discussion of the TU Delft model can be found in section 2.3.5.

Regarding the PSI and UCI flashback models, the critical velocity gradient g_c is calculated using Eq. (2.27) and (2.30), respectively. It is then compared with the wall velocity gradient of the flow g_f derived from the CFD simulations. According to Eichler's experiments, the flame stabilizes at the upstream end of the ceramic tile (section E3 of the measurement section) seconds before flashback. Thus, the CFD results for each inlet bulk velocity are extracted in section E3 (see Figure 3.5). Boundary layer flashback occurs when the critical velocity gradient g_c exceeds the wall velocity gradient of the flow g_f, as discussed in section 2.3.1.

The results from the analysis described above are shown in Figure 3.9. The critical velocity gradient g_c derived by the UCI model is overall lower than the flow velocity gradient g_f (see Figure 3.9b,c); thus, the UCI model cannot capture the TUM burner's flashback limits at all. This can be attributed to the fact that the UCI model was developed based on flashback experiments in unconfined flames and the flashback limits for these flames are lower than the confined configurations [10]. On the other hand, the PSI model's predicted equivalence ratio at flashback φ_{fb} (intersection of the g_c with the g_f line) shift to higher values with increasing bulk velocities. The predicted flashback limits derived by the PSI model are plotted in the same diagram with the TU Delft model's results and the experimental data for better comparison, as will be discussed below.

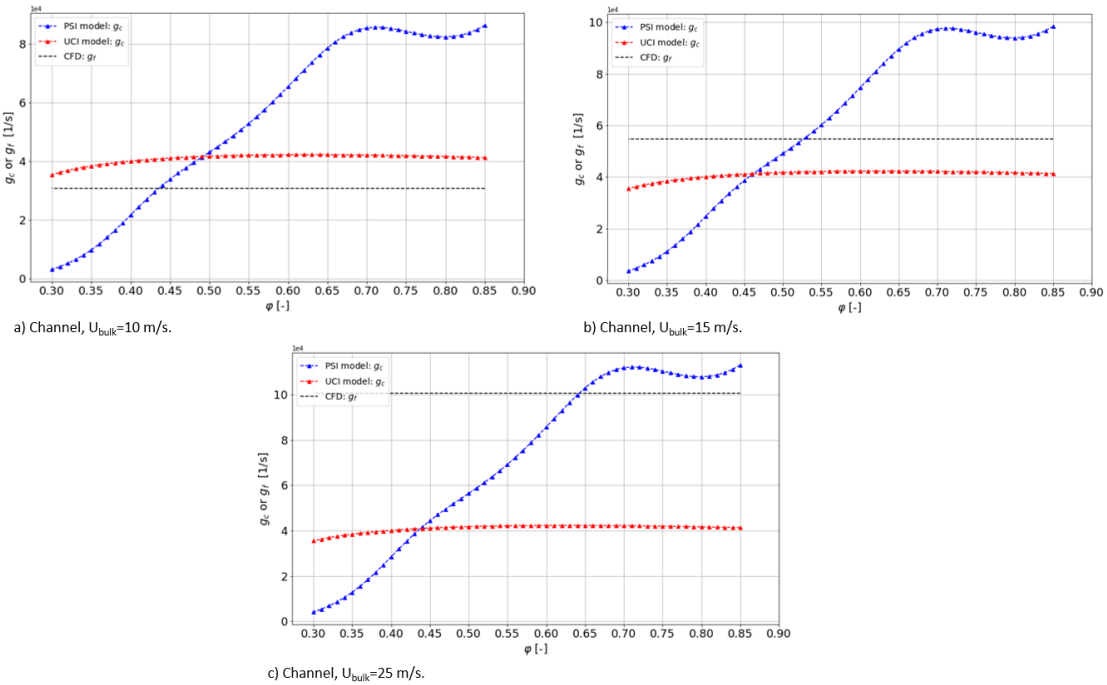

Figure 3.9: Critical velocity gradient g_c (PSI, UCI flashback models) compared with the flow velocity gradient at the wall g_f (CFD simulations). The inlet bulk velocity of the channel U_{bulk} is varied between 10 and 25 m/s.

The predicted flashback limits from the PSI and TU Delft models are shown in Figure 3.10. The TU Delft model shows a strong correlation with the experimental data at higher equivalence ratios. At lower values of equivalence ratio (ϕ<0.45), the TU Delft model overpredicts the

maximum equivalent ratio for flashback φ_{fb} following Björnsson's observations [22]. On the other hand, the TU Delft model slightly underpredicts φ_{fb} values at higher equivalence ratios, but it is very close to the experimental trend line. The PSI model also shows overall a good agreement with the experimental data. While the PSI model predicts flashback initiation at a higher equivalence ratio than the experiments in the very lean region (0.3<ϕ<0.45), the model shows better agreement with the experimental data at higher equivalence ratios.

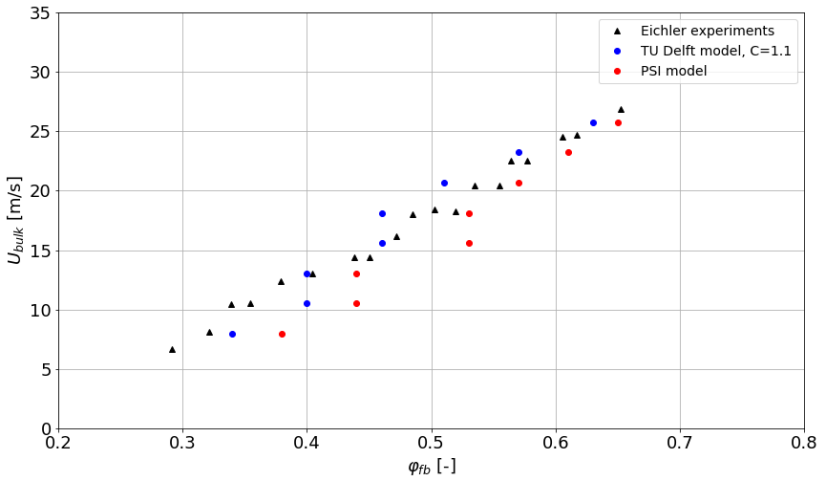

Figure 3.10: Predicted flashback limits from TU Delft and PSI model in the Eichler's channel. The experimental flashback data are also presented [11].

The overprediction of the PSI model's predicted φ_{fb} at the very lean region (see Figure 3.10) is further investigated based on the analysis in section 3.1.1, in which the wall velocity gradient calculated at real lean conditions is a little lower than the calculated velocity gradient based on an average equivalence ratio of ϕ=0.6. In this context, the flow velocity gradient g_f (CFD) of the H_2-air mixture with not only ϕ=0.6 but also ϕ=0.3 is compared with the predicted critical velocity gradient g_c in Figure 3.11. It can be seen that the minor decrease of the flow velocity gradient g_f has a negligible effect on the predicted maximum equivalence ratio φ_{fb}, given that both g_f lines intersect the PSI model's g_c line at almost the same equivalence ratio φ.

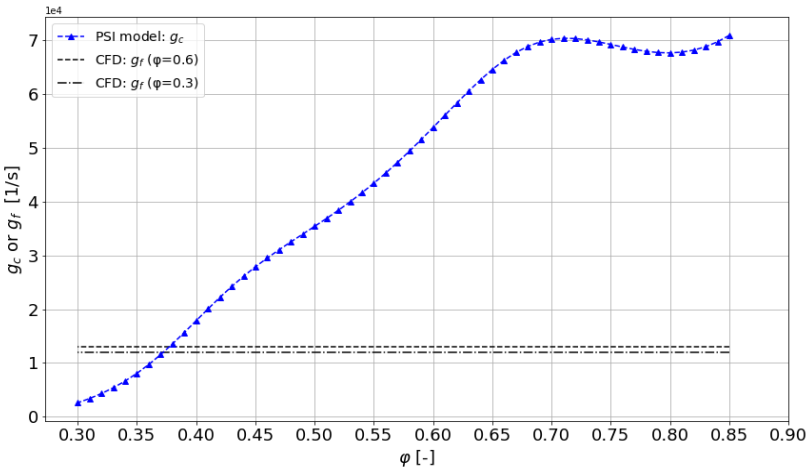

Figure 3.11: Predicted critical velocity gradient g_c (PSI model) and calculated flow gradient g_f (extracted from CFD in section E3) of the channel geometry. The inlet bulk velocity is U_{bulk}=8 m/s.

3.1.2.2 **2°-4° diffuser geometry**

The adverse pressure gradient flows of the 2° and 4° diffusers were realized by inserting ramps with different angles in the measurement section, as was discussed in section 3.1.1. Similar to the channel case discussed in the previous section, Björnsson [50] tuned the TU Delft model to accurately predict the flashback limits in the 2° and 4° diffusers. According to his suggestions, the tuning constant *C* (used in the turbulent flame speed correlation) is increased to 1.1 and 1.3 for the 2° and 4° diffuser, respectively, and the velocity fluctuations are corrected to the experimental values, as they were underpredicted by the CFD simulations (see Figure 3.6 and Figure 3.7) [50]. Moreover, the streamwise adverse pressure gradient $\left(\frac{\partial P}{\partial x} > 0\right)$ induced by the flow, due to the deceleration of the flow inside the diffuser, is also added to the Stratford's turbulent boundary layer separation criterion (see section 2.3.5.2).

Both the TU Delft and the PSI model are evaluated at the three positions of the Eichler's burner [11] measurement section (E1, E2, and E3 in Figure 3.5), and the results are plotted in Figure 3.12. For a given inlet bulk velocity, the TU Delft model's flashback limits in the 2° and 4° diffuser shift to lower critical velocity gradient g_c values further downstream (from section E1 to E3), which can be attributed to the deceleration of the flow due to the increase of the flow area. Nevertheless, the TU Delft model predicts overall flashback accurately in the diffusers, following Björnsson's research [50].

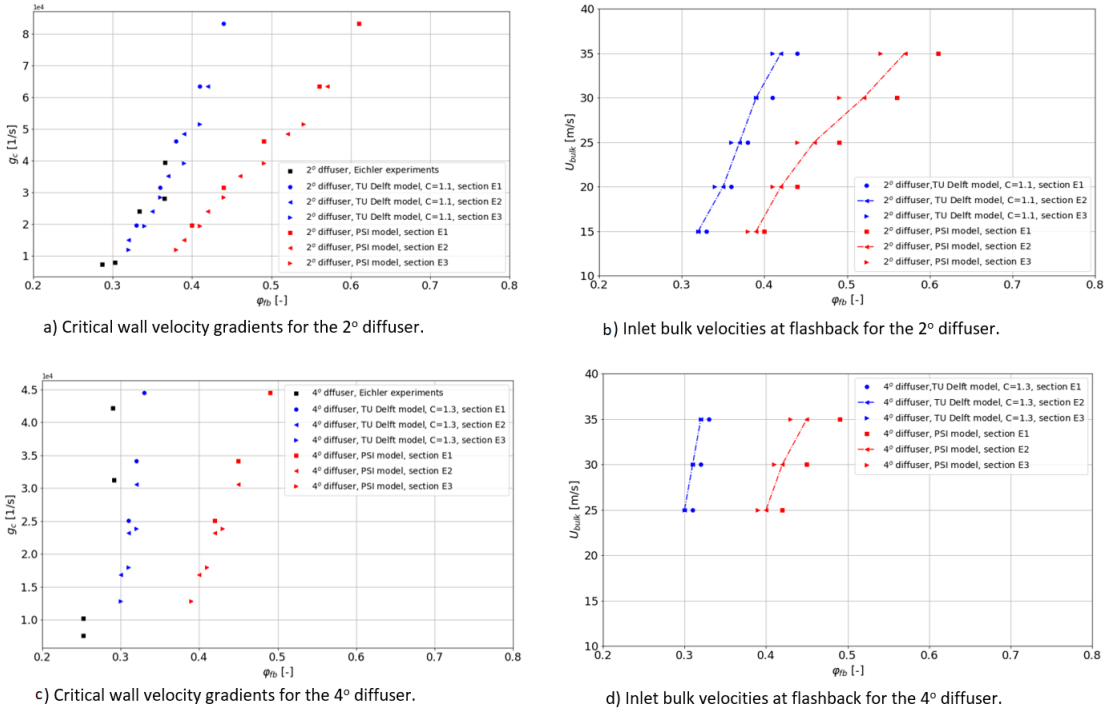

a) Critical wall velocity gradients for the 2° diffuser.

b) Inlet bulk velocities at flashback for the 2° diffuser.

c) Critical wall velocity gradients for the 4° diffuser.

d) Inlet bulk velocities at flashback for the 4° diffuser.

Figure 3.12: Comparison of the TU Delft predicted flashback limits with the PSI model results. Both models are applied to the Eichler's [11] 2° and 4° diffuser. The U_{bulk} refers to the bulk velocity at the inlet of the diffusers.

On the other hand, the PSI model predicts flashback at a higher equivalence ratio than Eichler's experimental data in the 2°-4° diffusers (see Figure 3.12). This can be attributed to the fact that the PSI model may not adequately consider the effect of the diffuser's underlying adverse pressure gradient on flashback initiation, which is shown to have a non-negligible effect on the flashback limits [22]. Moreover, the PSI model's variation of the predicted equivalence ratio φ_{fb} in the E1, E2, and E3 positions of the measurement section (see Figure 3.5) is significantly higher than the TU Delft model's. Figure 3.12b and Figure 3.12d show a noticeable split between the PSI results at the diffusers' different sections due to the difference in the wall velocity gradient along positions E1, E2, and E3 of the measurement section.

3.2 Elevated pressure and temperature operating conditions

The capability of the TU Delft model to predict flashback at the pressurized burners of the University of California Irvine (UCI) [43] and the Paul Scheerer Institute (PSI) [15] will be investigated in this section. The TU Delft model has been calibrated for atmospheric flames (see section 2.3.4); thus, modifications will be made to capture the increased flashback propensity at higher pressure and temperature. First, the flashback model will be tuned based on the UCI burner's flashback experiments and validated on the high-pressure PSI combustor. The main modification to the TU Delft model is the application of a customized turbulent flame speed correlation based on the Damköhler correlation used in the original TU Delft model. The mean velocity profile and the maximum turbulence fluctuations u' required to the TU Delft model (see section 2.3.4) have been calculated using cold flow CFD simulations in both

the UCI and the PSI burners. The updated version of the TU Delft model is finally tested on the atmospheric TUM burner discussed in section 3.1.

3.2.1 **UCI burner cold flow simulation**

Kalantari et al. conducted flashback experiments at elevated pressure and temperature conditions at the University of California Irvine (UCI), using the combustor shown in Figure 3.13. More details about the experimental set-up and the flashback experiments can be found in Kalantari's dissertation [47].

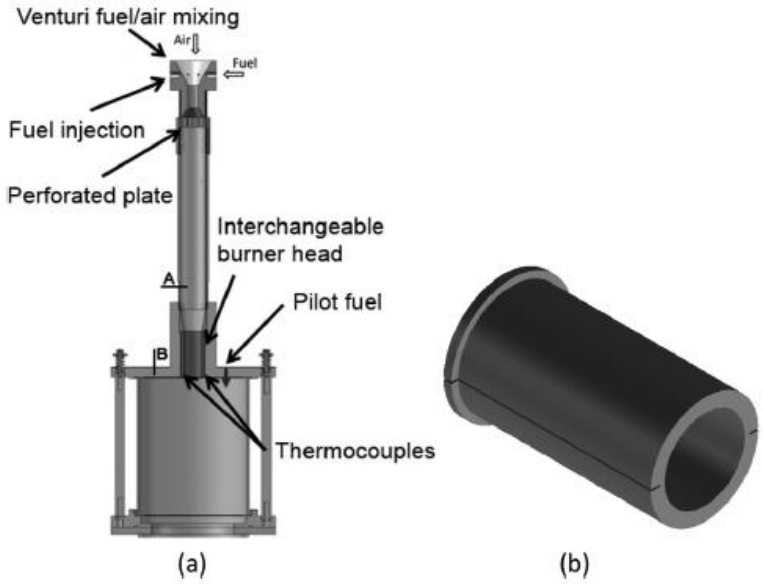

Figure 3.13: Cross-section of the mixing and combustor test sections (a) and the burner head (b) (Source: [43]). This set-up was used for the flashback experiment performed by Kalantari et al. [43]

The UCI burner's flow domain is modeled as 2-D axisymmetric using 141835 quadrilateral elements (see Figure 3.14), and the Reynolds-Averaged Navier-Stokes equations are solved using the hybrid SST k-ω turbulence model due to its superior performance for wall-bounded boundary layer [55]. The RSM turbulence model is not used in this analysis due to poor convergence of the residuals. The conservation equations are solved using a second-order scheme, and the pressure-velocity coupling is performed using the Fluent solver's SIMPLE algorithm. The boundary conditions are set as velocity-inlet and pressure-outlet, and the convergence of the residuals is up to 1e-06.

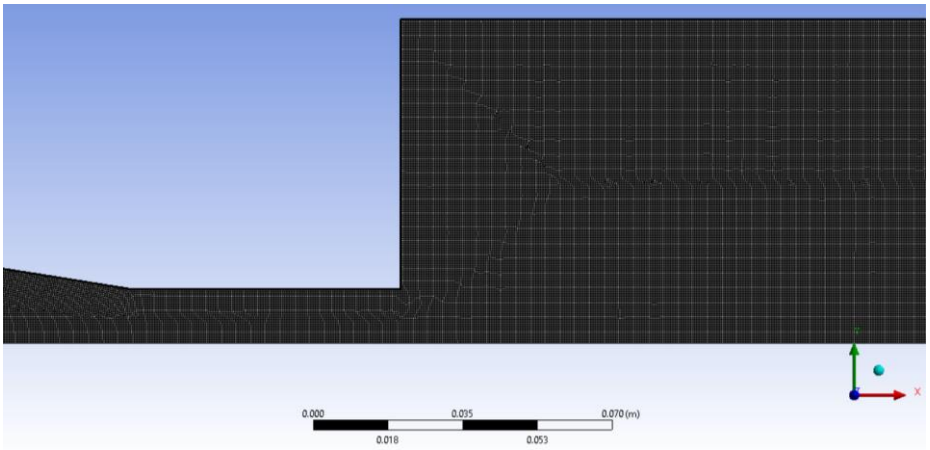

Figure 3.14: UCI burner geometry with the unstructured mesh.

Kalantari [47] performed Laser Doppler Velocimetry (LDV) experiments on the non-reacting flow (P=1 atm, T=300 K) to ensure a fully developed flow was established at the UCI burner's exit. The flow bulk velocity at the exit was varied between 37 and 55 m/s, and the measurements were performed at a plane 7 mm above the burner. The resulting velocity profile at the exit of the burner can be seen in Figure 3.15.

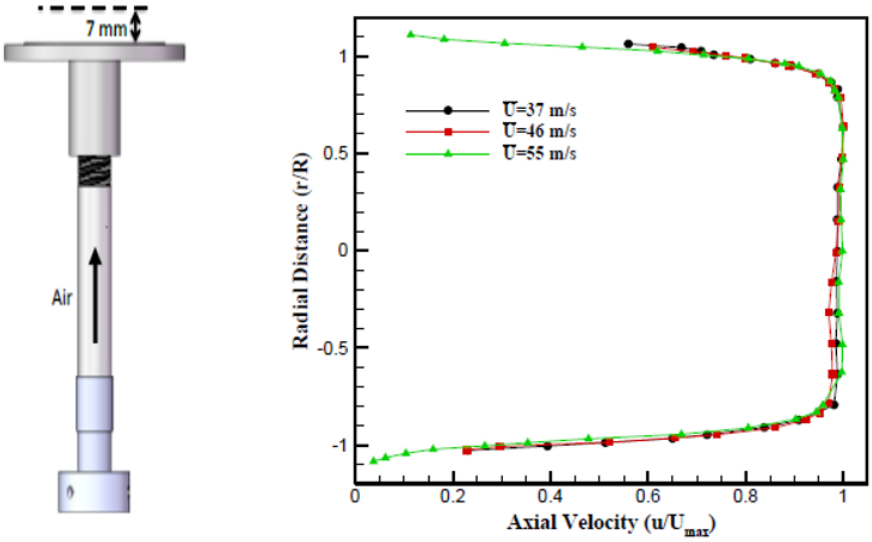

Figure 3.15: Velocity profile for different bulk velocities at the exit plane (7mm above the burner exit) derived by LDV experiments (Source: [47]).

The cold flow CFD simulations are validated by comparing with the results from Kalantari's LDV experiments shown in Figure 3.15. Thus, a CFD simulation run is performed at a bulk velocity of 37 m/s, and the resulting velocity profile at the exit plane (7 mm above the burner exit) is extracted from the CFD results. Figure 3.16 shows the velocity profile obtained by the CFD simulations and the LDV experiments. The velocity profile is fully developed, and the CFD results lay close to the experiments at the wall and the center of the burner. The experimental velocities are slightly lower than the CFD results at the burner's center and closer to one side.

This disturbance of the velocity profile can be attributed to the water injection during the LDV experiments, according to Kalantari [47].

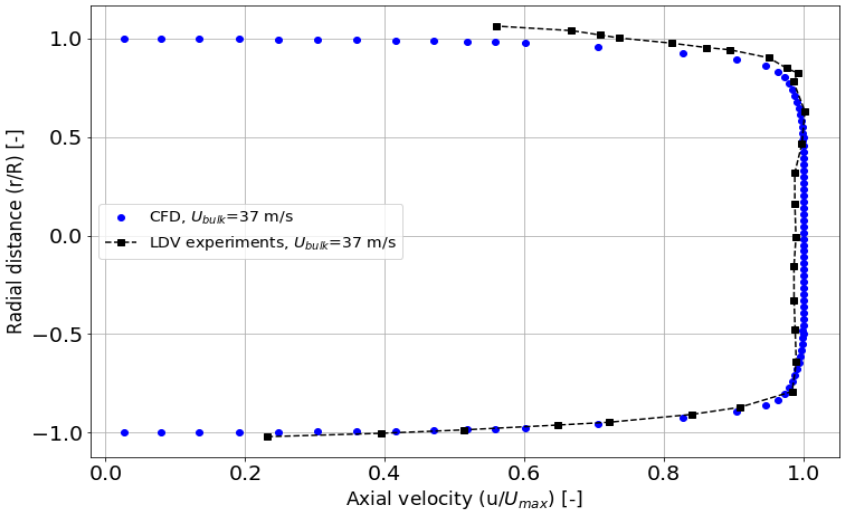

Figure 3.16: CFD velocity profile at the burner's exit compared with the LDV experiments performed by Kalantari.

Separate cold flow CFD simulations are performed using ANSYS Fluent to calculate the UCI burner's turbulent flow properties at every flashback data set of Figure 3.17. The burner head bulk velocity varied between 30 and 40 m/s, according to the UCI flashback experiments [43], and these values are used as boundary conditions during the CFD simulations set-up. It should be noted that the density and the viscosity of the H_2-air mixture had to be explicitly specified before the cold flow simulations. Similar to the TUM burner (see section 4.1), an average equivalence ratio of ϕ=0.6 is assumed for the H_2-air mixture. Its density and viscosity varies according to each flashback case's pressure and temperature from Figure 3.17.

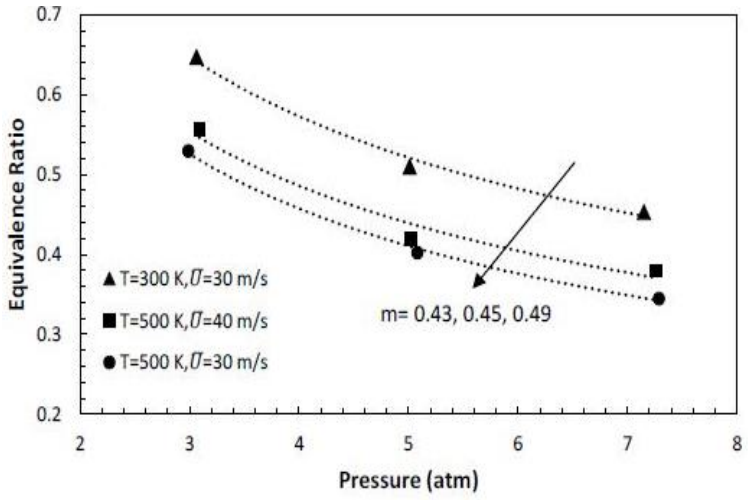

Figure 3.17: Flashback equivalence ratio as a function of pressure and temperature for the UCI burner. Trend lines represent $\varphi_{fb} = P^{-m}$ and exponent m increases according to the direction of the arrow. Experimental data provided by Kalantari et al. [47].

According to Kalantari's flashback experiments [47], the flame starts to propagate upstream from the left side at point (b) (exit of the burner) before partially enters the burner head at point (c) (see Figure 3.18). Finally, a full flame flashback occurs at point (d), in which the flame propagates further upstream inside the burner head. This observation indicates that a suitable region to apply the (confined) TU Delft flashback model is inside the premixing tube and adjacent to the burner's exit. Thus, the TU Delft model is coupled to the CFD results in this region of the burner and then validated with the flashback experiments of Figure 3.17.

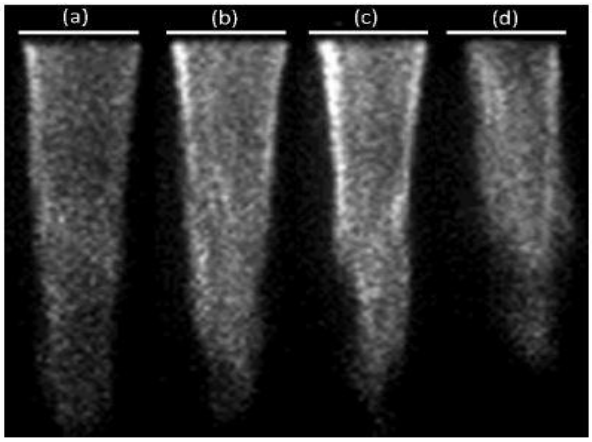

Figure 3.18: Flashback detection of H_2 jet flame at elevated operating conditions (P=5 atm and T=400K) in the UCI burner (Source: [47]).

Finally, Kalantari [47] monitored the UCI burner's tip temperature (use of thermocouples along the burner head shown in Figure 3.13) at different operating temperatures and pressures during flashback initiation (see Figure 3.19). The increased wall tip temperature at higher operating pressures and temperatures was showed to be an essential factor in determining the flashback propensity, according to [47]. Thus, the effect of the wall temperature on the TU Delft flashback model's accuracy will be further investigated in section 3.2.3 using the data of Figure 3.19.

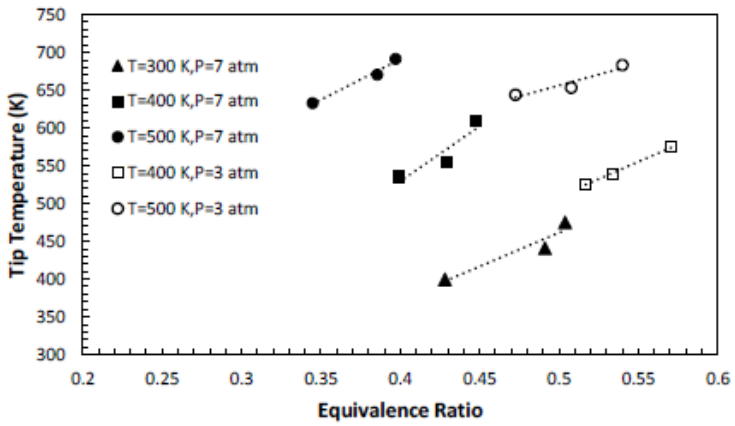

Figure 3.19: Variation of UCI burner's tip temperature at different operating temperatures and pressures. Measurements performed by Kalantari [47].

3.2.2 **PSI burner cold flow simulation**

A schematic of the high-pressure PSI combustor is shown in Figure 3.20. Both the UCI and PSI combustors have almost the same design (axial-dump burners); thus, the numerical modeling approach is similar to the details mentioned in section 3.2.1. and will not be repeated in this section.

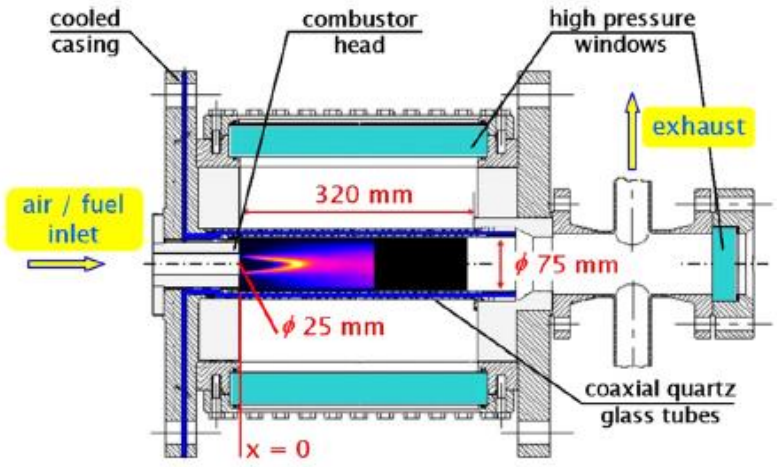

Figure 3.20: Schematic of the PSI high-pressure combustor [41]

The validity of the CFD results is compared to the results from Siewert's Particle Image Velocimetry (PIV) experiments [56]. Siewert performed cold flow experiments in the PSI combustor setup using air at atmospheric and room temperature conditions. Moreover, the turbulence intensity at the burner's inlet was varied using different turbulence grids, as shown in Figure 3.21.

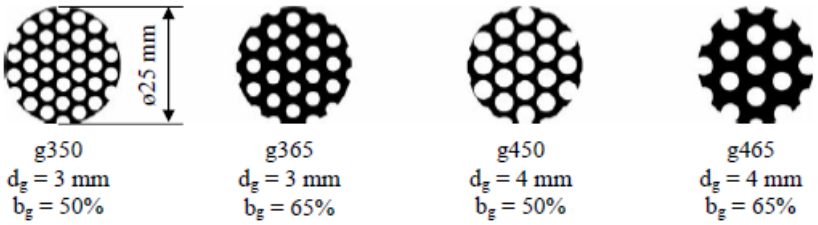

Figure 3.21: Turbulence grids used by Siewert [56] to vary the turbulence intensity at the burner's inlet. The d_g refers to the hole diameter and the b_g to the blockage ratio.

According to Siewert, the PIV experiments were performed using the g350 turbulence grid, which results in a turbulence intensity of around 8% at the burner's inlet. However, a value of 9% is defined at the inlet during the CFD simulations to account for dissipation, according to Menon's suggestions [57]. Menon also conducted numerical simulations in the PSI burner, and he concluded that with this setup, the experiment's turbulence was captured to maximum accuracy in the CFD simulations. Based on these suggestions, the velocity field is well predicted, as shown in Figure 3.22.

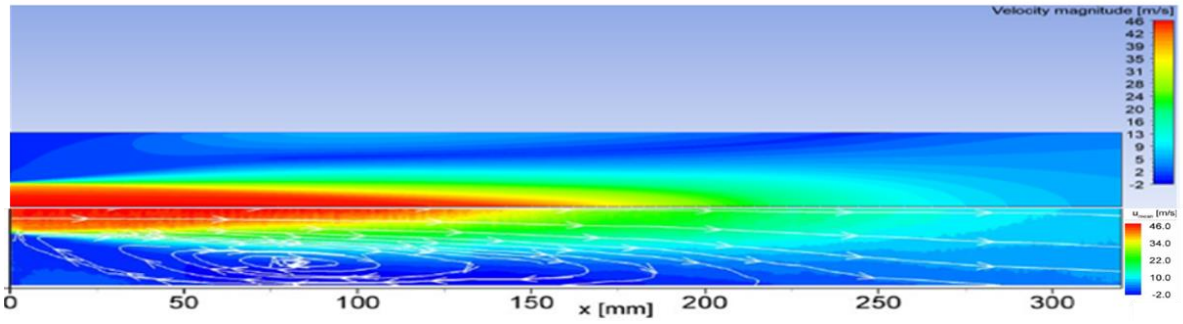

Figure 3.22: Comparison of the numerical velocity magnitude with Siewert's cold flow experiments [56]. The figure's upper half is the CFD results, while the bottom half refers to the experimental flow field. Inlet bulk velocity is set to 40 m/s.

Similar to the UCI burner (see section 3.2.1), separate cold flow CFD simulations are performed using ANSYS Fluent to calculate the PSI burner's turbulent flow properties at every flashback data set of Figure 3.23. The inlet bulk velocity was kept constant at 40 m/s throughout the flashback experiments [15]. Figure 3.23 shows the H_2-rich fuel flashback experiments conducted by Lin et al. [58]. It can be seen that flashback is observed for the cases at 7 and 10 bar with equivalence ratio at 0.41 and 0.35, respectively (data lay close to the flashback region). According to Lin, burning these H_2-rich mixtures at an equivalence ratio of ϕ=0.5 was the richest boundary that was manageable at 2.5 bar; thus, this operating data set can also be used as a flashback case. Consequently, three flashback points can be utilized from Figure 3.23, namely the cases at 2.5, 7, and 10 bar with flashback equivalence ratios φ_{exp} at 0.5, 0.41, and 0.35, respectively.

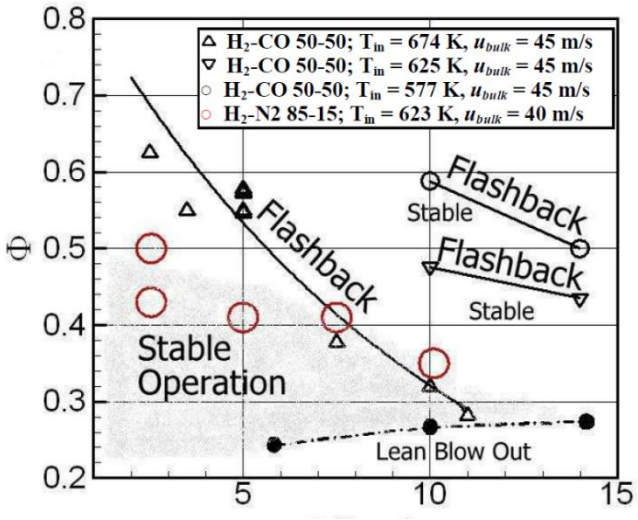

Figure 3.23: Flashback limits of a syngas mixture (H_2-CO 50-50) and the representative limits of H_2-rich mixture (H_2-N_2 85-15) in the PSI burner. Results derived by the flashback experiments of Lin et al. [58]

3.2.3 TU Delft model application at the UCI and PSI combustors

The next step is to investigate the TU Delft flashback model's performance on the high-pressure UCI and PSI burners. In this section, the effect of the elevated operating pressure and temperature on the model's parameters will be examined. As it has been discussed in section 2.3.5, the Stratford criterion for the generic boundary layer is given by Eq. (2.46):

$$C_p^{\frac{1}{4}(n-2)}\left(\delta\frac{dC_p}{dx}\right)^{\frac{1}{2}} = \left(\frac{3(0.41\beta)^4}{(n+1)n^2}\right)^{\frac{1}{4}}\left(1-\frac{3}{n+1}\right)^{\frac{1}{4}(n-2)}$$

The right-hand side (RHS) of Eq. (2.46) solely depends on the cold flow field, and the left-hand side (LHS) depends mainly on the properties of the flame front at flow separation. Thus, the elevated operating conditions' effect can be examined separately on the flow field and the flame front properties. For this study, the experimental flashback data provided by Kalantari will be used (see Figure 3.17), and the performance of the current version of the TU Delft model will be investigated.

3.2.3.1 Cold flow field variation

The cold flow in the UCI burner is simulated using CFD software (see section 3.2.1) at the different operating pressures and temperatures. It should be noted that the density and the viscosity of the H_2-air mixture are varied according to the operating conditions. The variation of the non-dimensional mean velocity for the different operating pressures is shown in Figure 3.24. It is noticeable that the velocity profiles are almost the same within the flashback sensitive region (y^+<40), while they differ farther away from the wall (y^+>100). Moreover, the effect of the temperature on the velocity profile at constant pressure conditions is negligible, as shown in Figure 3.25.

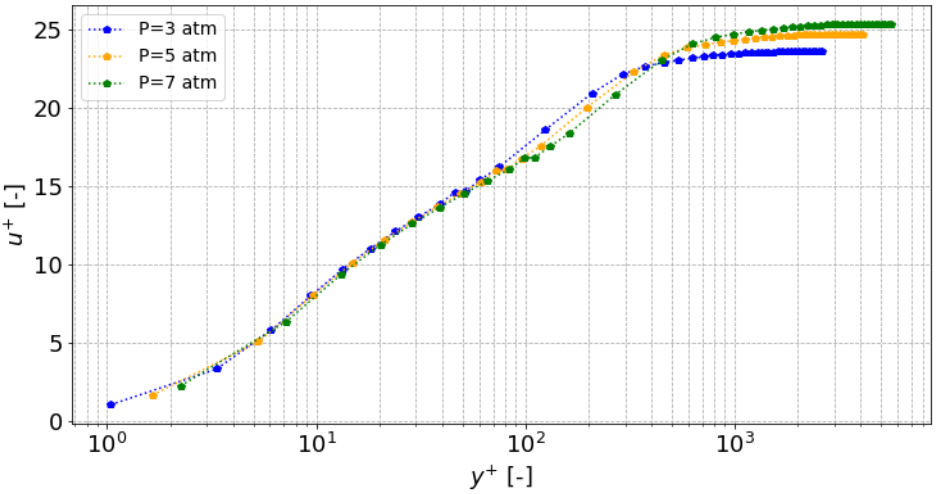

Figure 3.24: Variation of the velocity profile adjacent to the UCI burner head for different pressures. The inlet bulk velocity and operating temperature are 30 m/s and 300 K, respectively.

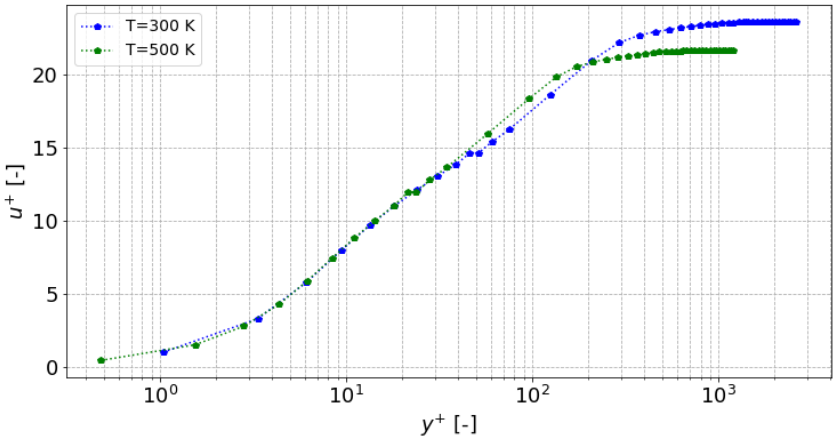

Figure 3.25: Variation of the velocity profile adjacent to the UCI burner head for different temperatures. The inlet bulk velocity and operating pressure are 30 m/s and 3 atm, respectively.

The right-hand side of Eq. (2.46) is expected to be almost the same due to the same near-wall velocity profile at the different operating conditions. According to Björnsson's recommendations, the pipe radius and the centerline velocity are used to the 1/n-th law [22]. The value of n derived by the 1/n-th law: $\frac{u}{U} = \left(\frac{y}{\delta}\right)^{1/n}$ to describe the outer layer (see section 2.3.5) varies slightly with respect to the inlet pressure and temperature, as shown in Figure 3.26. Thus, the increased flashback propensity at elevated operating conditions cannot be attributed to changes in the cold flow field.

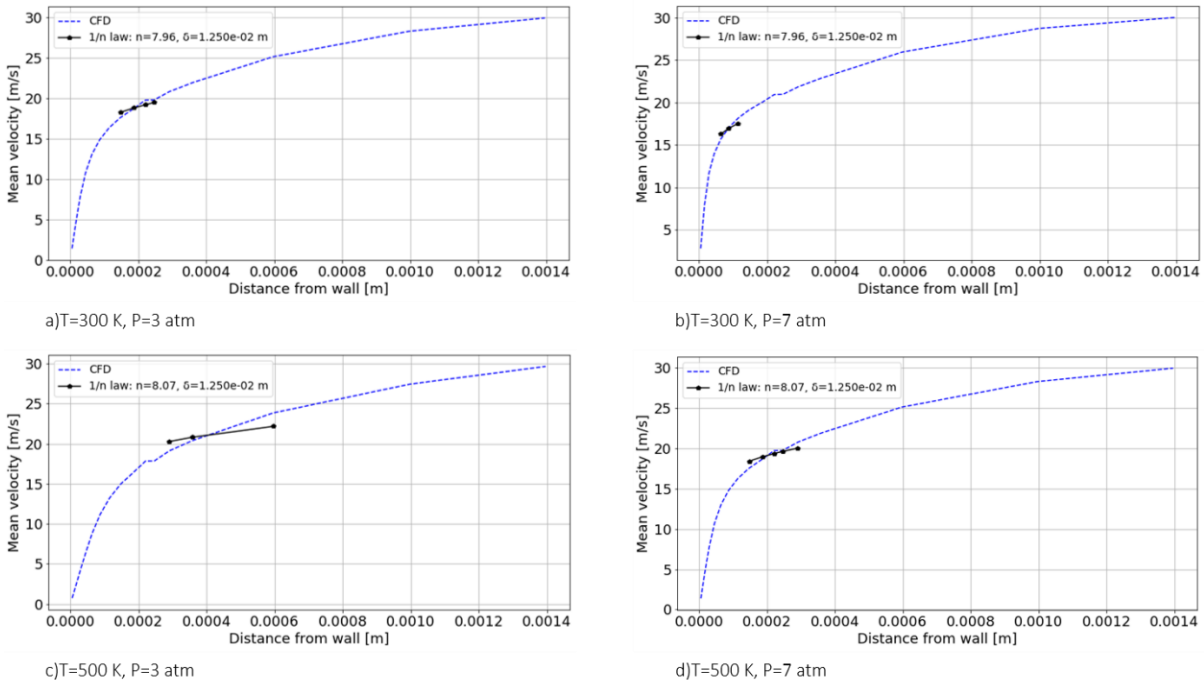

Figure 3.26: Results from applying the 1/n-th law to the mean velocity profile derived from the CFD simulation. The velocity profile is extracted from the CFD results adjacent to the UCI burner head's exit, and the inlet bulk velocity is 30 m/s.

3.2.3.2 **Flame front properties variation**

The left-hand side of Eq. (2.46) is rewritten in terms of the turbulent flame speed S_t, the expansion ratio σ, and the pressure gradient of the cold flow $\frac{\partial P}{\partial x}$ (x is the direction of the flow) by using the definition of the coefficient of pressure C_p (see section 2.3.4). The effect of each parameter on flashback prediction will be investigated in this section. As has already been discussed in section 2.3.4, the main proportion of pressure rise is assumed to take place at x_f=1 cm upstream of the flame tip, according to Baumgartner [10], and the model is applied at x=x_f.

$$LHS = \left(\frac{2\left(S_t^2(\sigma-1) + \frac{\partial P}{\partial x}\frac{x_f}{\rho_u}\right)}{U^2} \right)^{\frac{1}{4}(n-2)} \left(\delta \frac{\left(4S_t^2(\sigma-1) + 2\frac{\partial P}{\partial x}\frac{x_f}{\rho_u}\right)}{U^2 x_f} \right)^{\frac{1}{2}} \tag{3.1}$$

The variation of the expansion ratio σ of the Kalantari's flashback data (see Figure 3.17) is shown in Figure 3.27. It can be seen that the expansion ratio slightly decreases with increasing pressure for both operating temperatures; thus, the value of the LHS in Eq. (3.1) will also decrease at elevated operating conditions. In general, the decrease of the LHS value in the TU Delft model due to a change in the expansion ratio means that the predicted maximum equivalence ratio at flashback φ_{fb} shifts to higher values. However, this trend is opposite to Kalantari's experiments [59], in which flashback propensity significantly increases at higher pressure conditions.

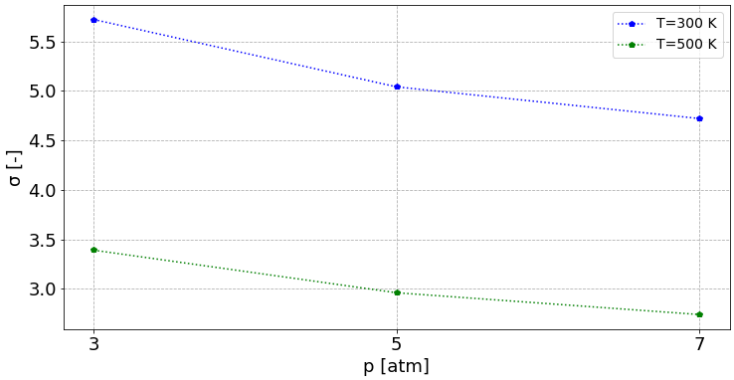

Figure 3.27: Variation of the expansion ratio with pressure and temperature. The equivalence ratios from Figure 3.17 are used.

The turbulent flame speed S_t in Eq. (3.1) is related to the unstretched laminar flame speed S_{l0}, according to the Damköhler flame speed correlation: $\frac{S_t}{S_{l0}} = 1 + C \cdot \left(\frac{u'}{S_{l0}}\right)^{0.5}$, thus the effect of the increased pressure and temperature on the laminar flame speed should also be examined. For that reason, 1-D flame simulations of H_2-air mixture at elevated operating conditions are performed in Cantera software (see Appendix A.2.1). At lean conditions (ϕ<1), the laminar flame speed of the H_2-air mixture decreases with increasing pressure, except of the very lean region (ϕ 0.3-0.35), in which the variation of the S_{l0} with the pressure is negligible (see Figure

3.28). Consequently, the value of the left-hand- side of Eq. (2.46) decreases with increasing pressure, and the predicted flashback limits will shift to higher equivalence ratios. As mentioned before, Kalantari's flashback experiments (see Figure 3.17) show a decreasing trend of the flashback limits at higher pressure, which indicates that the Damköhler flame speed correlation should be updated to include the effect of pressure on the flashback propensity. Indeed, the lack of the current version of the TU Delft model [22] to predict flashback initiation at higher operating pressures is shown in Figure 3.29. More specifically, the TU Delft model shows an increasing trend of the flashback limits at increasing pressures, whereas the opposite trend is observed in Kalantari's flashback experiments [43].

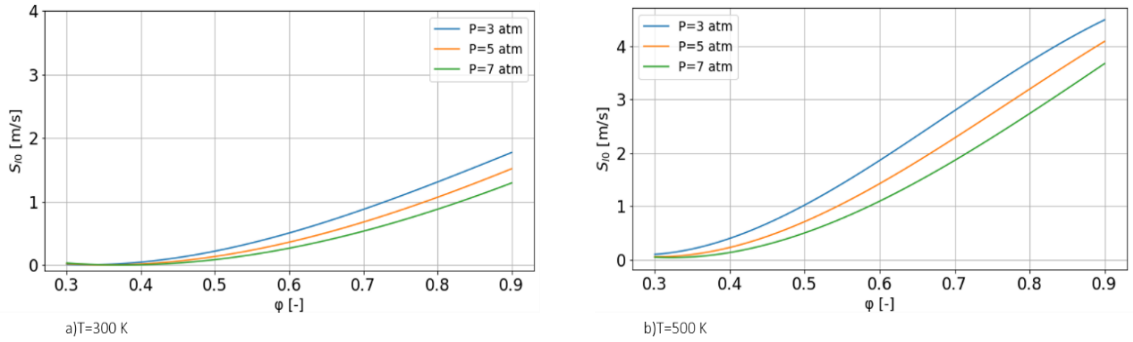

Figure 3.28: Unstretched laminar flame speed of H_2-air mixture at different operating pressure and temperature conditions. 1-D steady-state free flame simulation is performed using Cantera software.

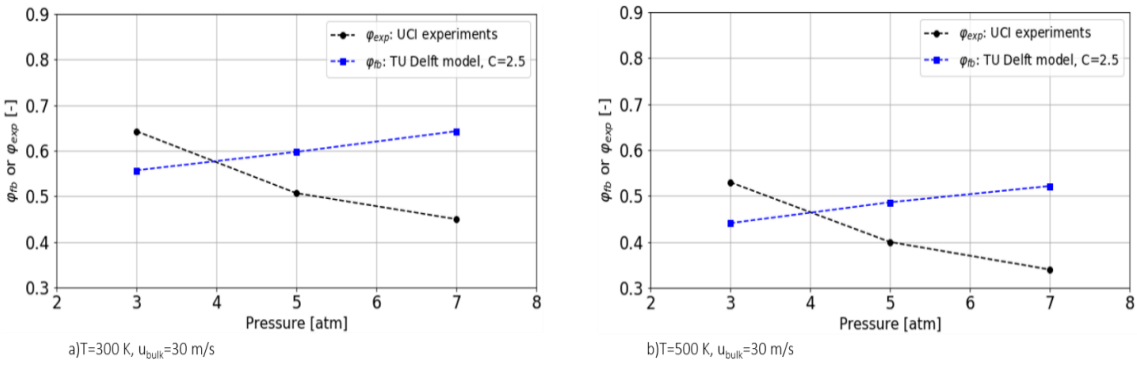

Figure 3.29: Predicted flashback limits of the UCI burner using the current version of TU Delft (C=2.5).

The effect of the pressure on flashback propensity will be included in the TU Delft model by proposing a new correlation for the turbulent flame speed closure. The new formula is an improved version of the well-established Damköhler correlation, based on the studies of Muppala and Dinkelacker [38]. According to their research, the turbulent flame speed can be described by Eq. (3.2), in which the turbulent Reynolds number is $Re_t=u' l_t/v$ (with integral length scale l_t and kinematic viscosity v). The integral length scale is calculated as $l_t=0.07L$, where L is the burner's diameter. This is a suitable approximation for fully-developed turbulent flows, proposed by [60]. Additionally, an explicit pressure term (p/p_0) is introduced to Eq. (3.2), in which $p_0=0.1$ MPa.

$$\frac{S_t}{S_{l0}} = 1 + a \cdot Re_t^{0.25} \left(\frac{u'}{S_{l0}}\right)^b \left(\frac{p}{p_0}\right)^c \tag{3.2}$$

The three fitting parameters, *a*, *b*, and *c,* are varied, and the resulting turbulent flame speed S_t is applied to the TU Delft model to predict the initiation of flashback at the UCI burner. The objective is to find the optimum set of fitting parameters at which the least-square deviation between the predicted and the experimental flashback equivalence ratio from Figure 3.17 is minimized. Eq. (3.3) is found as the best fit for the accurate prediction of flashback at the UCI combustor:

$$\frac{S_t}{S_{l0}} = 1 + 0.2 \cdot Re_t^{0.25} \left(\frac{u'}{S_{l0}}\right)^{0.6} \left(\frac{p}{p_0}\right)^{0.7} \tag{3.3}$$

The constant *α* is close to Muppala's correlation (α: 0.28-0.46), whereas the exponent *b* of the $\frac{u'}{S_{l0}}$ term and exponent *c* of the pressure term are increased to 0.6 and 0.7, respectively (Muppala reported b=0.3 and c=0.2). This was expected because Muppala's correlation is based on premixed methane, ethylene, and propane-air flames, which generally exhibit lower turbulent flame speeds than the H_2-air flames. Nevertheless, Eq. (3.3) shows a similar dependence of $\frac{S_t}{S_{l0}}$ on $\frac{p}{p_0}$ and $\frac{u'}{S_{l0}}$ with the turbulent flame speed correlation proposed by Lin [41]. Lin concluded that $\frac{S_t}{S_{l0}} \sim \left(\frac{p}{p_0}\right)^{0.75}$ and $\frac{S_t}{S_{l0}} \sim \left(\frac{u'}{S_{l0}}\right)^{0.45}$ for all the H_2-rich flames at pressures up to 2.0 MPa investigated in his work. It should be noted that the Lewis number correction proposed by Tober [21] is also included in the new turbulent flame speed correlation described by Eq. (3.3), to take into account the flame instability due to Lewis numbers below unity (see section 2.3.4).

Table 3.1: Comparison of the parameters used in the Muppala's [38] and Lin's [41] turbulent flame speed correlations with the proposed correlation described by Eq. (3.3).

Turbulent flame speed	*a*	b	c
Muppala	0.28-0.46	0.3	0.2
Lin	-	0.45	0.75
New correlation	0.2	0.6	0.7

The calculated flashback limits from the updated version of the TU Delft model are shown in Figure 3.30. A similar trend between the experimental and the predicted values is observed at the lower temperature (300 K) and for pressures up to 5 atm (see Figure 3.30a). However, a substantial deviation from the experimental trend is observed at higher pressures and higher inlet temperature, as can be seen in Figure 3.30b. It seems that the effect of the increasing pressure on the flashback limits is not captured adequately, especially for the case with the high inlet temperature (see Figure 3.30b). The exact same trend is observed for the case with u_{bulk}=40 m/s and T=500 K.

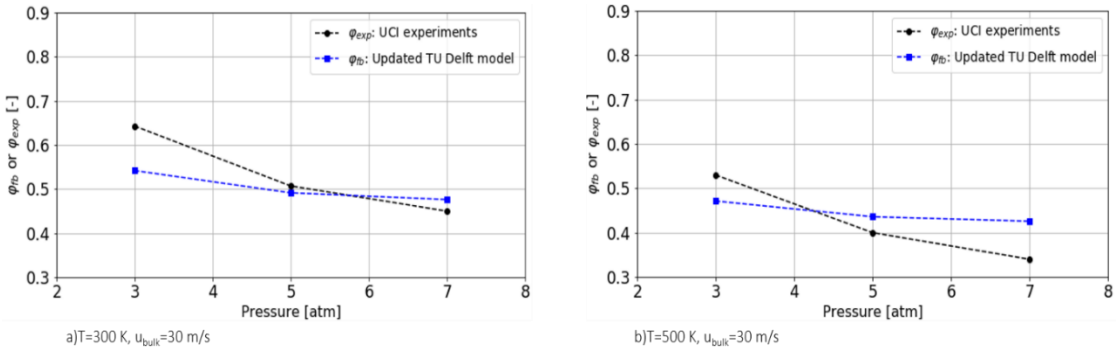

Figure 3.30: Comparison of the updated TU Delft model with the UCI burner's flashback experiments [43]. The inlet temperature and pressure were varied between 300-500 K and 3-7 atm, respectively.

Kalantari measured the variation of the burner's tip temperature at different pressures (see Figure 3.19) and concluded that the pressure increase leads to higher tip temperature and higher flashback propensity [47]. In this context, the increase of the wall temperature is expected to affect the H_2-air mixture's temperature, especially at the higher pressures. This effect can be taken into account in the TU Delft model using the tip temperature, instead of the inlet temperature, for the higher pressure cases of Figure 3.19 (p=7 atm). From this analysis, the calculated maximum equivalent ratio at flashback ϕ_{fb} decreases significantly at the higher pressure cases, and the updated TU Delft model's results have a similar trend with the experimental data (see Figure 3.31).

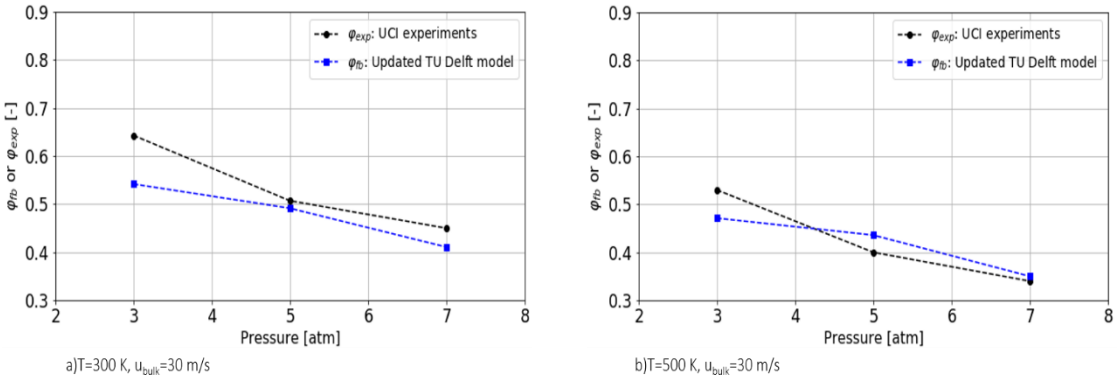

Figure 3.31: Comparison of the updated TU Delft model with the UCI burner's flashback experiments [43]. The effect of the higher tip temperature on the H_2-air mixture's temperature is included in the model. The wall tip temperature is used for the H_2-air mixture's temperature for the flashback case at p=7 atm.

The updated version of the TU Delft model is also benchmarked against the PSI combustor's flashback experiments (see Figure 3.23). Due to the cooling of the PSI burner, the effect of the decreasing stand-off distance of the flame on the H_2-air mixture's temperature is expected to be less significant than in the UCI burner. Thus, the inlet temperature of the H_2-rich mixture (T=623 K) will be used in the model to calculate the flashback limits in the PSI combustor. Figure 3.32 shows that the TU Delft model predicts flashback very well for all cases. Only a slightly higher equivalence ratio is observed for the p=10 atm case.

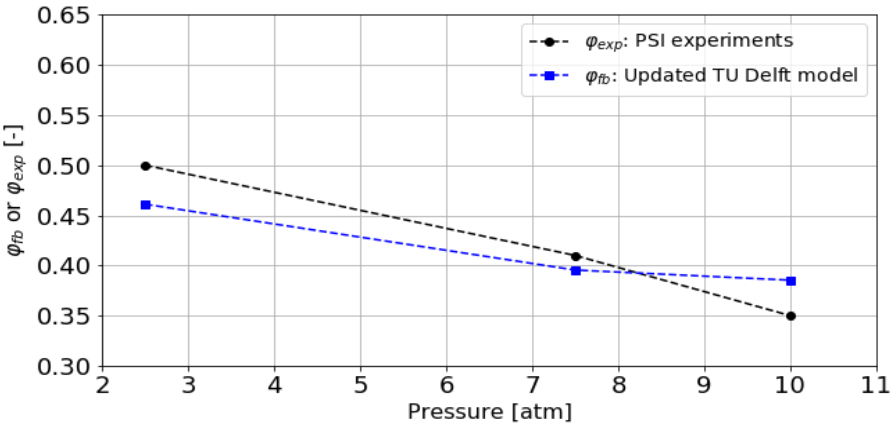

Figure 3.32: Benchmarking of the updated TU Delft model against the PSI burner's flashback experiments [58]. The inlet temperature and bulk velocity are 623 K and 40 m/s, respectively.

The final step of this analysis is to check the modified TU Delft model's applicability to the TUM burner's atmospheric cases discussed in section 3.1. The correction of the *u'* based on the experimental data in the 2° and 4° diffusers is also included in the TU Delft model (see section 3.1.2.2), and the turbulent Reynolds number Re_t is calculated according to Eq. (2.18). Figure 3.33 shows that the updated version of the model captures flashback initiation adequately for both the channel and the diffuser configurations. These findings demonstrate that the updated version of the TU Delft model for elevated operating conditions performs well also for standard flows at atmospheric conditions.

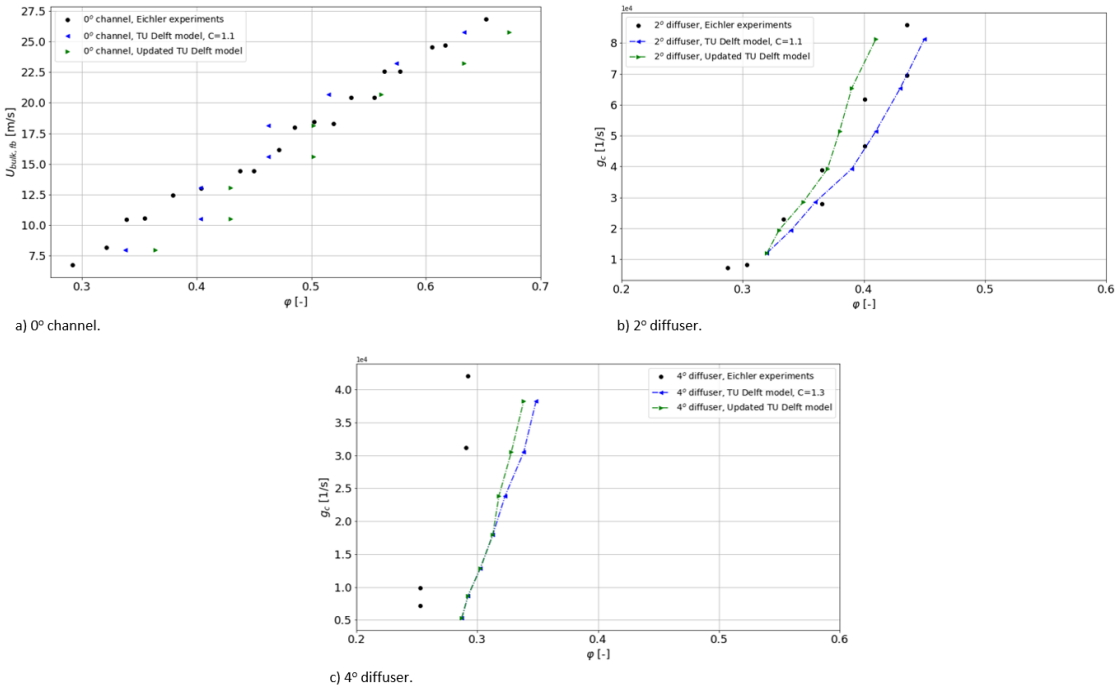

Figure 3.33: Flashback limits from the modified TU Delft model for the atmospheric TUM burner. Eichler's flashback experiments for the 0° channel and the 2°-4° diffuser [11] are used. The updated TU Delft model is applied at position E3 of the measurement section (see Figure 3.5).

3.2.4 **Summary**

The UCI and PSI model's performance was initially investigated on Eichler's flashback experiments [11]. The TU Delft model has already been evaluated and calibrated at the TUM burner [22]; thus, it is used in this thesis as a reference flashback model. On the one hand, the PSI model captured the channel's flashback trends and 2°-4° diffuser adequately. It showed a good agreement with the experiments at the higher equivalence ratios. However, the calculated equivalence ratio at flashback φ_{fb} was higher than the experimental value at the very lean region. Similarly, the predicted equivalence ratio was higher than the experimental value for the adverse pressure gradient flows (2°-4° diffuser) for all investigated cases. On the other hand, the UCI model did not capture the TUM burner's flashback limits at all.

The applicability of the TU Delft model on high-pressure burners was further investigated. The H_2 flashback experiments at elevated pressures and temperatures, provided by Kalantari et al. [43] and Lin et al. [58], were used for this analysis. It was shown that the current version of the TU Delft model could not capture the experimental flashback trend at elevated operating conditions. A sensitivity analysis was performed to identify the dominant influencing parameters. The turbulent flame speed correlation was identified as the main parameter influencing flashback at elevated operating conditions. A new approach with three empirical parameters for estimating the turbulent flame speed was proposed (see Eq. (3.2)), which includes an explicit term for the pressure. The fitting constants were adjusted till the least-square deviation between the predicted and the experimental flashback equivalence ratio was minimized for the UCI flashback experiments [47] (larger available set of data). The updated version of the TU Delft model shows overall a good agreement with the experimental data at both high pressures and temperatures, however it does not follow adequately the flashback trend at the higher examined pressures. This was attributed to the fact that the increase of the wall tip temperature at higher pressures (due to the decreasing stand off distance of the flame) influences the temperature of the H_2-air mixture adjacent to the wall and should be taken into account. It was shown that the modified TU Delft model follows significantly better the flashback trend at higher pressures, if the wall tip temperature is used to describe the temperature of the H_2-air mixture.

The updated version of the TU Delft model also captures the limited PSI flashback experimental data of 100% H_2 fuel [15] well. Moreover, the model showed a better correlation with the PSI experiments if the burner's tip temperature is not included, which is might due to the effective cooling of the PSI burner compared with the uncooled UCI burner. Thus, the improved model can be used for flashback predictions at elevated operating conditions; however, the effect of the high wall temperature on the H_2-air mixture's temperature should be taken into account, especially for uncooled burners at high operating pressures.

Lastly, the new version of the TU Delft model was benchmarked against the atmospheric TUM burner. The modified model shows a good agreement with the flashback experiments for both the favorable pressure gradient (0° channel) and the adverse pressure gradient flows (2°-4° diffusers).

4. Application of BLF models to complex burner geometry

In this chapter, the PSI and TU Delft flashback models will be validated at a gas turbine burner geometry based on flashback experimental data. The flashback models will be applied to a lab-scale burner tested in the TU Delft laboratory. Similar to the academic burners discussed in chapter 3, CFD simulations using ANSYS Fluent will be performed on this burner, and the turbulence properties within the boundary layer will be coupled with the flashback models (PSI and TU Delft) to predict flashback initiation. Minor modifications of the TU Delft model [50] will be discussed to capture flashback adequately at different locations of the combustor.

In section 4.1, the flashback models will be applied to a lab-scale burner tested in the TU Delft laboratory, which operates with a fully premixed H_2-air mixture at atmospheric operating conditions. The design of this TU Delft laboratory burner is based on the HighHydrogen Flamesheet^{TM} design from Ansaldo Thomassen/PSM [7][8]. Furthermore, both flashback models will be used to evaluate flashback propensity for different H_2-CH_4 fuel mixtures, based on TU Delft's burner flashback experiments.

4.1 TU Delft FlameSheet^{TM} burner

In this section, the flashback models (PSI and TU Delft) will be benchmarked against the flashback experiments of the TU Delft's lab-scale burner, which operates with a fully premixed fuel-air mixture at atmospheric operating conditions. Both cold and reactive flow CFD simulations will be performed to investigate the flame's effect on the flow properties (i.e., mean velocity profile, *u'*) that were coupled to the flashback models. Finally, the performance of both models will be further investigated on less H_2-rich fuel gases. The flashback models will be used to calculate the flashback propensity for H_2-CH_4 fuel mixtures, based on the TU Delft's burner flashback experiments with different fuel compositions.

4.1.1 TU Delft burner configuration

The lab-scaled TU Delft combustor's design is based on the HighHydrogen FlameSheet^{TM} burner, which was initially developed by PSM [61] [7]. The original combustor's operation is based on the injection of fuel-air mixture as an uninterrupted sheet into the reaction zone, immediately after which an aerodynamically trapped vortex is generated and used to anchor and stabilize the flame [8].

The HighHydrogen FlameSheet^{TM} combustor system consists of the pilot and the main stage, in which high-pressure air enters from the compressor outlet (blue arrows in Figure 4.1a). In the pilot stage, air passes through the radially outermost circuit, is turned 90^o, and after passing a radial inflow swirler with another 90^o turn, it is mixed with fuel that is injected from the swirler vanes and enters into the reaction zone (red arrows in Figure 4.1a). However, the design of the TU Delft FlameSheet^{TM} burner for the pilot circuit is less complicated: The pilot stage is only fed by axially flowing air (without swirl) and without fuel injection. In the HighHydrogen FlameSheet^{TM} burner's main stage, the air flows along the combustor liner's backside, mixed with the fuel, and then turns 180^o and flows into the combustor through the dome (see Figure 4.1a). The rapid change of the fuel-air mixture's direction separates the flow and results in a strong recirculation zone, stabilizing the flame at the edge of the liner (see recirculation regions in Figure 4.1). The same configuration is utilized in the TU Delft

FlameSheet™ burner's main stage to establish the recirculation zone before entering into the combustor's reaction zone. The main difference with the HighHydrogen FlameSheet™ combustor is that the air is perfectly mixed with the fuel before entering the main stage. The two aerodynamic stages (pilot and main) and the corresponding recirculation zones are shown in Figure 4.1.

Only the main stage of the TU Delft FlameSheet™ burner will be investigated, as previous tests of the HighHydrogen FlameSheet™ burner showed that the main stage is most prone to flashback.

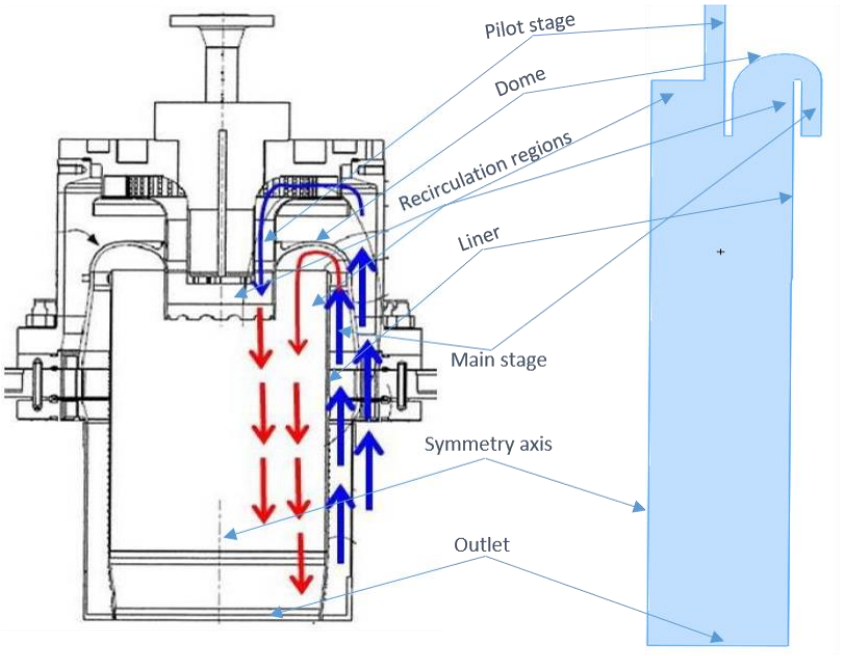

a) HighHydrogen FlameSheet™ combustor. b) TU Delft FlameSheet™ combustor.

Figure 4.1: Schematic view of the HighHydrogen FlameSheet™ combustor (Source: [8]) and the TU Delft FlameSheet™ burner cross-sections. The pilot-main stage of both burners and the recirculation zones stabilizing the flame are presented.

4.1.2 **Flashback experiments**

The experiments have been conducted using different H_2-CH_4 mixtures at atmospheric pressures, and temperatures at 293 K. Figure 4.2 shows the results from these flashback experiments. The bulk velocity at flashback (y-axis in Figure 4.2) refers to the bulk velocity at the inlet of the main stage when flashback is initiated. In the experiments, the bulk velocity was gradually decreased at constant fuel-air mixture composition and equivalence ratio until flashback occurs. The equivalence ratio at the x-axis of Figure 4.2 refers to the fuel-air mixture that flows through the main stage. The air mass flow rate through the pilot stage's annulus consisted of only air at atmospheric operating conditions and was the same as the mass flow through the main stage. Eq. (4.1) is used to derive the mass flow rate through the main stage (U_{bulk} is known) using the surface area of the main stage's annulus A_{an} (see Eq. (4.2)). Since the

mass flow rate through the main and the pilot stages are the same, the inlet bulk velocity at the pilot stage is calculated by Eq. (4.1) using the area of the pilot stage's annulus.

$$\dot{m} = \rho \cdot U_{bulk} \cdot A_{an} \tag{4.1}$$

$$A_{an} = \pi \cdot \frac{\left(D_{out}^2 - D_{in}^2\right)}{4} \tag{4.2}$$

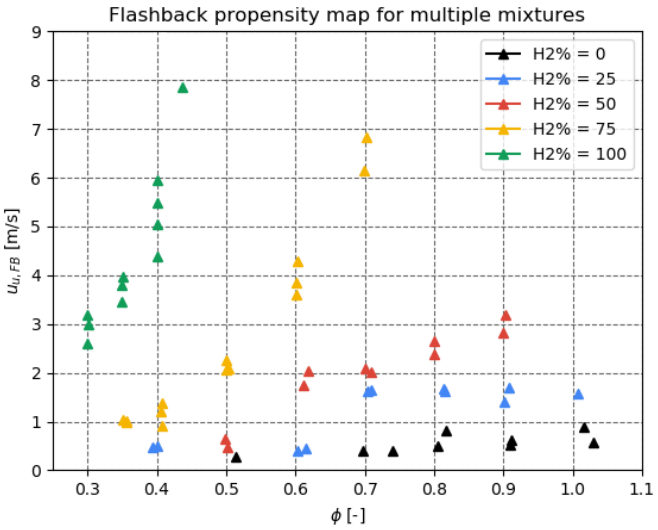

Figure 4.2: Inlet bulk velocity (main stage) at flashback with respect to the equivalence ratio. H_2-CH_4 mixtures vary from 0% H_2 up to 100% H_2. Flashback experiments were performed in the TU Delft FlameSheet™ burner.

4.1.3 Cold flow CFD simulation

Based on the flashback points of Figure 4.2 (100% H_2), the cold flow inside the TU Delft FlameSheet™ burner is simulated using the ANSYS Fluent software. A cross-section of the combustor is selected (see Figure 4.3), and the flow is solved as a two-dimensional axisymmetric problem reducing the computational cost.

The two-dimensional steady Reynolds-averaged Navier-Stokes (RANS) equations are solved using the realizable k-epsilon turbulence model due to its better performance than the RNG and the standard k-epsilon model in boundary layers and separated flows [62]. Moreover, the enhanced wall treatment option is selected for the modeling of the near-wall flow. The conservation equations are solved using a second-order scheme, and the pressure-velocity coupling is performed using the SIMPLE algorithm of the Fluent solver.

The right grid size selection for the cold flow CFD simulation is performed according to the following procedure. Three unstructured meshes with triangular and quadrilateral elements are generated using the ANSYS meshing application. The velocity magnitude variation is then monitored at two axial lines at two radial positions (see Figure 4.3) inside the combustor and adjacent to the recirculation region.

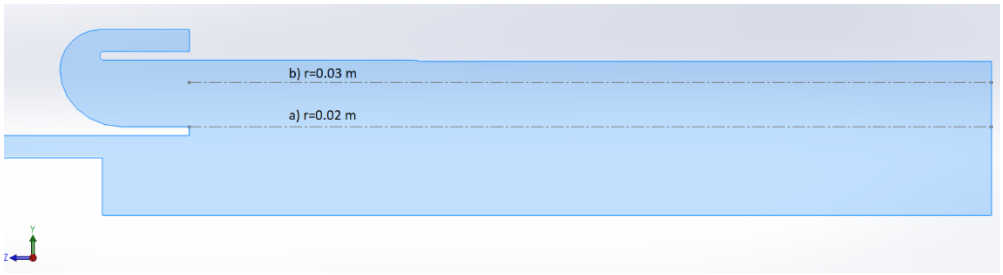

Figure 4.3: Geometry of the TU Delft's FlameSheet™ burner fluid domain used for the CFD simulation. Axial lines at r=0.02 m and r=0.03 m are used for the mesh independence analysis.

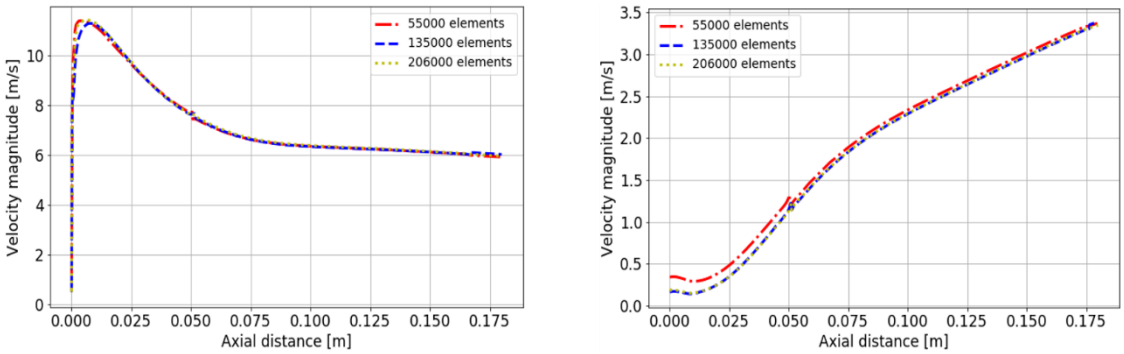

a) r=0.02 m b) r=0.03 m

Figure 4.4: Axial variation of the velocity magnitude at a) r=0.02 m and b) r= 0.03 m for different grid sizes. The inlet bulk velocity of the main stage is U_{bulk}= 7.9 m/s (flashback case selected from Figure 4.2).

The results from this analysis are presented in Figure 4.4. It can be seen that a mesh independent solution is achieved for a mesh size with over 135000 elements. Subsequently, this mesh is selected for the CFD simulations and can be seen in Figure 4.5. The significant near-wall flow is solved using ten inflation layers, and the value of the wall mesh size y^+ is kept between 0.4 – 0.8 for the different cases. It has to be noted that the y^+ value should be $y^+<5$ when the enhanced wall treatment option is selected, and the viscous sublayer is resolved [63] [55].

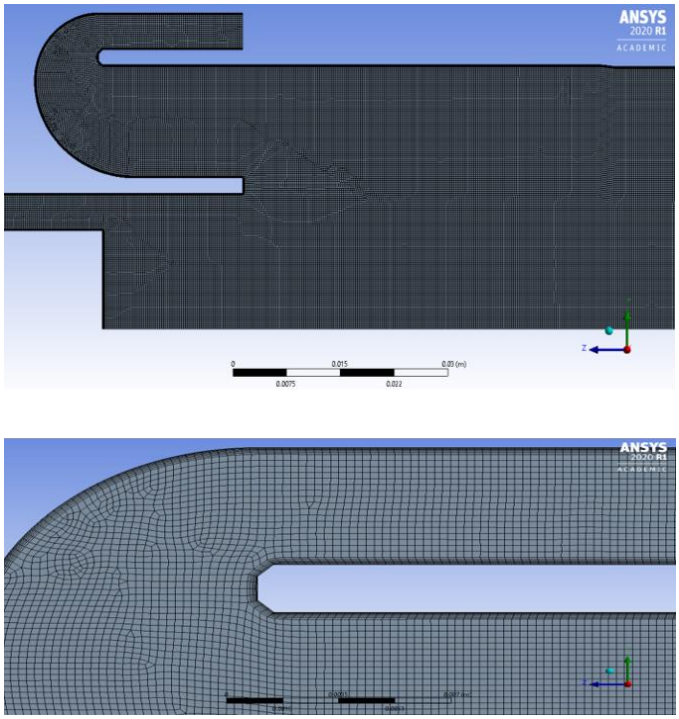

Figure 4.5: TU Delft FlameSheet™ burner mesh and wall inflation layers.

4.1.3.1 **CFD results post-processing**

Different operating scenarios of the TU Delft burner are simulated using ANSYS Fluent. The inlet bulk velocity at the main and pilot stage is varied to simulate the burner's cold flow during the flame flashback initiation, according to Figure 4.2. In this section, the results from one operating set is selected (ϕ_{fb}=0.45 at U_{bulk}=7.9 m/s) to discuss the flow field inside the combustor. It has to be noted that the variation of the most relevant quantities for the application of the PSI and TU Delft model is examined (i.e., flow velocity, velocity fluctuations, and wall velocity gradient).

The velocity contour in a cross-section of the burner is depicted in Figure 4.6. The flow enters through the outermost annulus (main stage) at an inlet bulk velocity of U_{bulk}= 7.9 m/s. A short separation region (zone 1) is formed once the H_2-air mixture enters the dome wall. The flow then quickly reattaches and accelerates once it exits the 180° turn of the dome wall. The acceleration of the flow is due to the long recirculation zone 3. This zone is formed because of the flow separation at the corner of the liner wall (zone 2). Due to this recirculation region, a narrow flow passage is formed, and the flow velocity increases according to mass conservation. The high-velocity field formed in that region (zone 4) increases the resistance of the flow to flame flashback due to the higher wall velocity gradient and favorable pressure gradient $\left(\frac{\partial P}{\partial x} < 0\right)$ that counteracts the pressure rise because of the flame presence, as discussed in section 2.3.5.2.

The bulk velocity at the inlet of the pilot stage is 16.4 m/s, and a recirculation region (zone 5) is formed at the combustor axis due to the sudden flow expansion. In the TU Delft version of the FlameSheet™ burner, no combustion will take place at this location as the pilot stage is only fed with air.

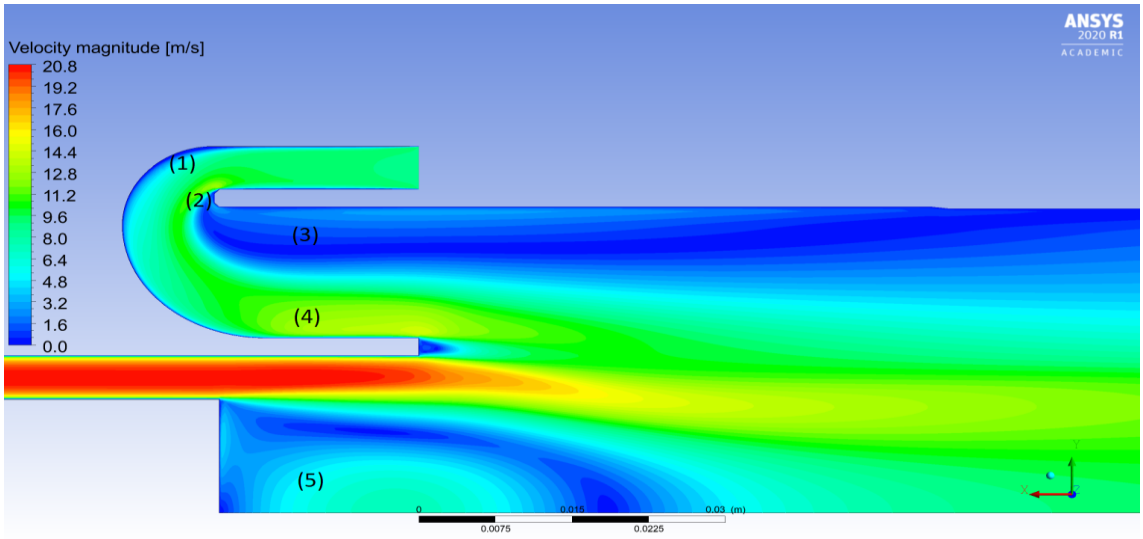

Figure 4.6: Velocity contour of TU Delft FlameSheet™ burner. The main and pilot stage inlet bulk velocities are 7.9 and 16.4 m/s, respectively.

The turbulent velocity fluctuation contour is shown in Figure 4.7. A shear layer is formed downstream the corner of the liner wall (zone 1), where the flow separates, and turbulence is generated. Another high turbulence zone 2 is generated in the long recirculation zone at the exit of the main stage. Then further downstream, the turbulence intensity decreases due to the dissipation of the turbulent kinetic energy. In zone 3, the turbulence intensity is the highest due to the significant velocity gradient between the flow exiting from the pilot and the burner's main stage. Similarly, a high turbulence region (zone 4) is formed in the recirculation region at the pilot stage exit due to the high shear stress.

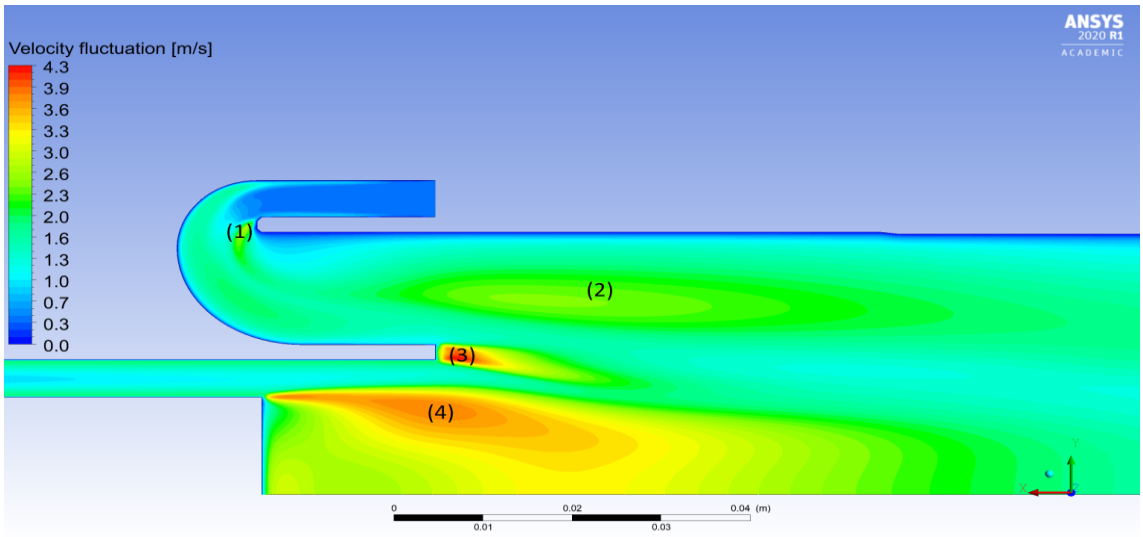

Figure 4.7: Turbulent velocity fluctuation contour in TU Delft FlameSheet™ burner. The inlet bulk velocities at the main and the pilot stage are 7.9 and 16.4 m/s, respectively.

The results of the boundary layer flashback models (PSI and TU Delft) will be evaluated at different locations of the main stage in section 4.1.4. For that reason, the flashback models' essential quantities (i.e., *u'*, wall velocity gradient) are extracted from the CFD simulations at different regions along the dome and the cold side of the liner wall (see Figure 4.8).

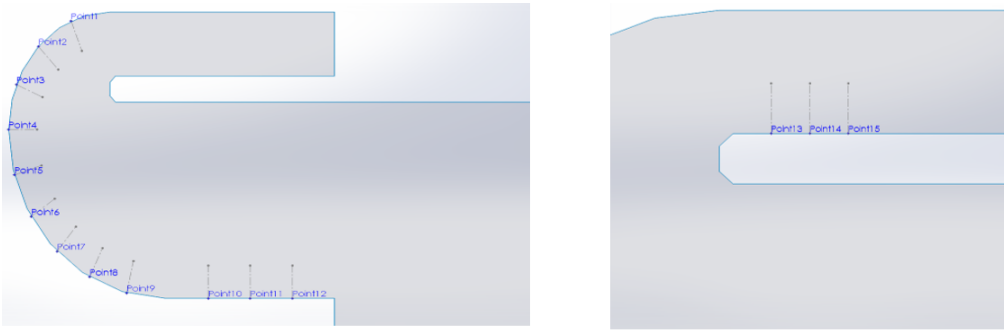

a) Dome wall. b) Liner wall.

Figure 4.8: Sections across the dome and the TU Delft FlameSheet^{TM} burner's liner wall to extract the relevant flow properties used in the flashback models.

The maximum turbulence intensity *u'* increases along the dome wall (from section 4 to section 12), as shown in Figure 4.9, where for different locations, the relative mean axial velocity u/U_{bulk} (red line) and the relative turbulence intensity u'/U_{bulk} (blue line) are plotted against the wall-normal distance. In the dome region, the velocity fluctuation reaches a peak at a distance below 2 mm from the wall for the more upstream location (see Figure 4.9a), and as the flow moves further downstream, the wall distance in which the velocity fluctuation has its maximum value increases up to 5 mm (see Figure 4.9c). On the other hand, the turbulence intensity (blue line) is lower along the liner wall, as shown in Figure 4.9d.

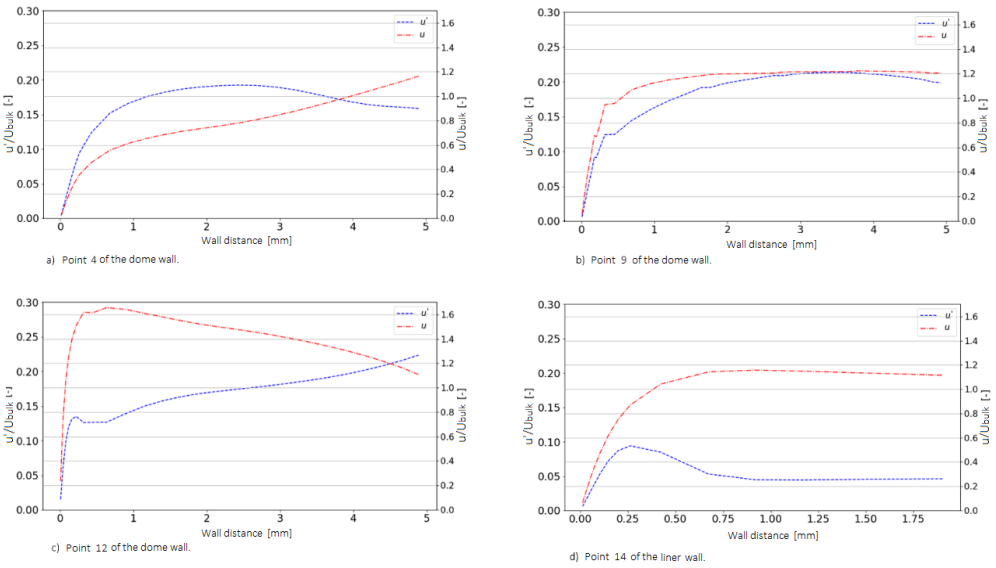

Figure 4.9: Relative mean axial velocity profile *u* and velocity fluctuations *u'* at different points in the dome (a),(b),(c), and the liner wall (d). Both *u* and *u'* are non-dimensionalized with the inlet bulk velocity at the main stage (U_{bulk}=7.9 m/s).

The velocity gradient at the wall g_f is calculated using Eq. (2.26), in which the shear stress at the wall τ_w is calculated from the ANYS Fluent solver using the properties of the flow adjacent to the wall-fluid boundary. Between sections 3 and 9, the wall velocity gradient remains at low values. In addition to the low values of g_f, the low flow velocity in this region (see Figure 4.6) further increases the risk of boundary layer flashback across the dome wall. Further downstream (sections 10 to 12), the wall velocity gradient is higher (see Figure 4.10a). These higher velocity gradients can prevent the flame from traveling upstream and closer to the dome wall. Similarly, the high-velocity gradient close to the edge of the liner wall (point 13 in Figure 4.10b) is expected to enhance the flame resistance against boundary layer flashback in this region.

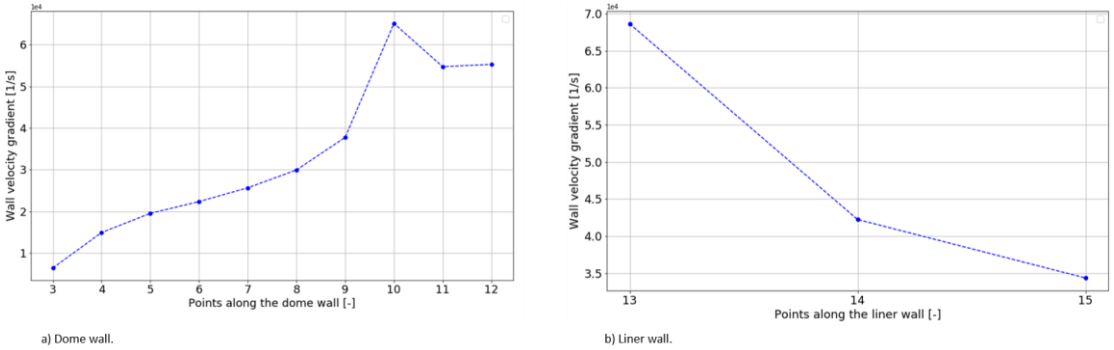

Figure 4.10: Wall velocity gradient g_f along different sections of the dome and the liner wall. Cold-flow CFD results for the H_2-air mixture at U_{bulk}=7.9 m/s and ϕ=0.45, according to Figure 4.2.

4.1.3.2 **Variation of the inlet bulk velocity**

The inlet bulk velocity of the main and pilot stage is varied to simulate the flow field of the different H_2 flashback experiments from Figure 4.2. In this section, the effect of the inlet bulk velocity on the flow properties (i.e., velocity fluctuation, wall velocity gradient) is investigated prior to applying the boundary layer flashback models.

Figure 4.11 shows that the turbulent velocity fluctuations *u'* increase with increasing inlet bulk velocities in both the liner and the dome wall. The higher inlet bulk velocity leads to higher velocity gradients in the shear layer of the flow, and these gradients are responsible for the turbulence production [57].

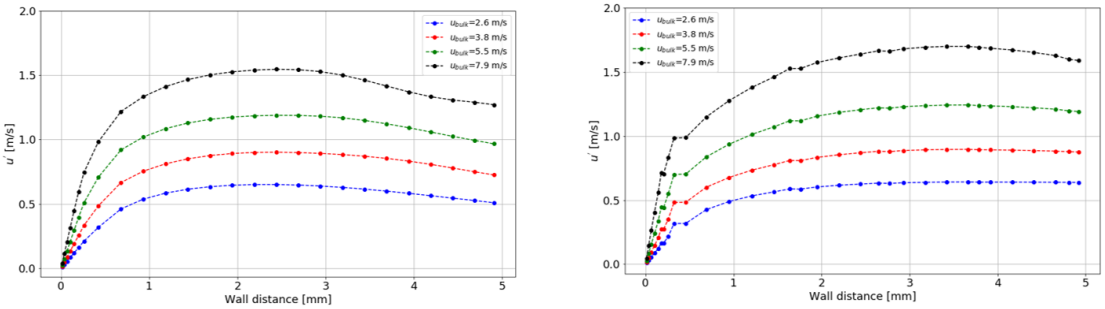

a) Velocity fluctuations profile in point 4 (dome wall).

b) Velocity fluctuations profile in point 9 (dome wall).

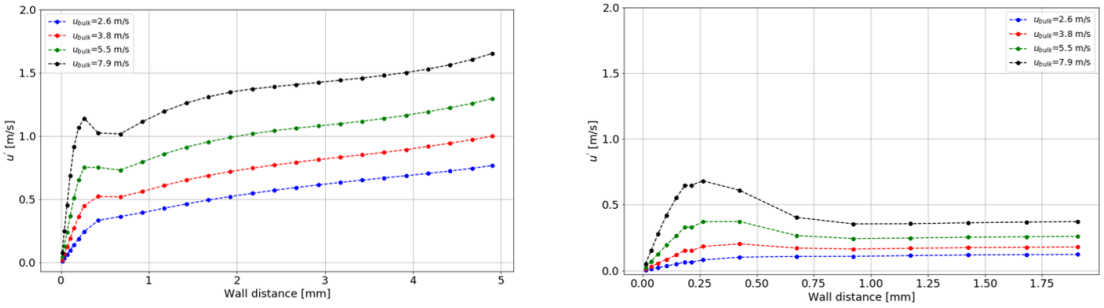

c) Velocity fluctuations profile in point 12 (dome wall).

d) Velocity fluctuations profile in point 13 (liner wall).

Figure 4.11: Velocity fluctuations for different inlet bulk velocities along the TU Delft FlameSheetTM burner's liner-dome wall. The U_{bulk} refers to the inlet bulk velocity of the main stage.

Figure 4.12 shows the effect of the inlet bulk velocity U_{bulk} on the wall velocity gradient along the dome and the liner. The wall velocity gradient only slightly increases with increasing U_{bulk} along the points 3 to 9 of the dome (see Figure 4.12a). However, once the flow exits the 180° turn of the dome wall and enters points 10 to 12, the wall velocity gradient seems to be more sensitive to changes in the inlet bulk velocity. Similarly, close to the edge of the liner wall (point 13), the increase of the U_{bulk} has a significant effect on the wall velocity gradient (see Figure 4.12b).

The ability to control the wall velocity gradient along the dome and the liner wall is essential to prevent flashback initiation, based on the critical velocity gradient concept discussed in section 2.3.1. From the above analysis, it can be concluded that an increase in the inlet velocity will affect the flashback limits more along the straight part of the dome wall (points 10-12) and the edge of the liner (point 13).

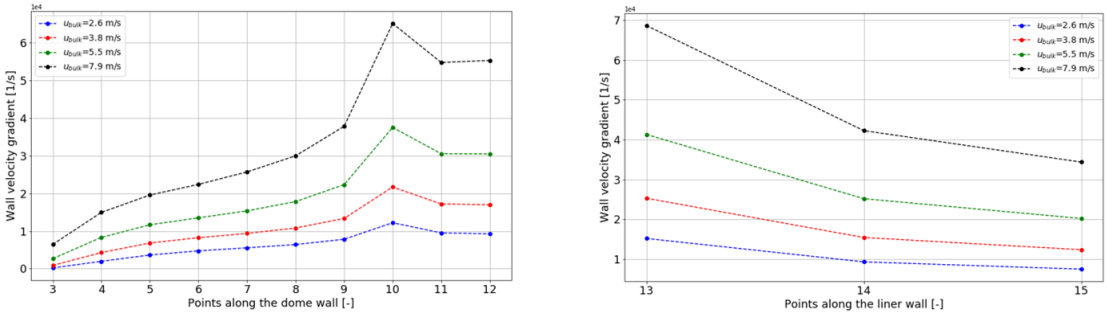

a) Dome wall.

b) Liner wall.

Figure 4.12: Wall velocity gradient for different inlet bulk velocities along the dome and the liner wall.

4.1.4 **Prediction of boundary layer flashback limits**

In this section, the flashback limits of the TU Delft FlameSheet™ burner (100% H_2) will be determined based on the flashback experiments of Figure 4.2. The PSI [15] and the TU Delft [22] models will be coupled with the CFD simulations and applied at the different positions along the dome wall and liner wall discussed in the previous section. Before applying the models, the experimental flashback data are allocated on the regime diagram for turbulent premixed combustion [46] to ensure that the Damköhler turbulent flame speed correlation used in the TU Delft model is valid, according to section 2.2.2.

4.1.4.1 **Combustion regimes**

The flame's position in the premixed turbulent combustion regimes (see Peters' diagram in section 2.2.2) is investigated for the minimum and the maximum inlet bulk velocity from the experimental cases of Figure 4.2 (i.e., U_{bulk}: 2.6, 7.9 with ϕ_{fb}: 0.3, 0.45, respectively). Two separate figures are used for the dome and the liner wall due to the different turbulence intensities in these regions.

In Figure 4.13, the flow properties(i.e., u', l_t) are calculated in the near-wall flow along the dome and the liner and at the position of maximum velocity fluctuations. The turbulence fluctuations u' are extracted from the CFD simulations, and the integral length scale l_t is computed from the following expression [22]:

$$l_t = 0.09^{3/4} \frac{k^{3/2}}{\varepsilon} \tag{4.3}$$

where the turbulence kinetic energy k and the turbulence dissipation rate ε are extracted at the wall distance of maximum turbulent intensity (y^+<40) [22]. The laminar flame thickness δ_{l0} is computed according to Eq. (2.17), and the laminar flame speed S_{l0} is calculated according to Hoferichter's [6] third-order polynomials (see Eq. (2.43)). Figure 4.13 shows that the premixed flames in both the dome and the liner are located within the thin reaction zones of the turbulent combustion regimes for both experimental cases. This is an essential condition for the validity of Damköhler's turbulent flame speed correlation [34] applied to the TU Delft model, as discussed in section 2.2.2.

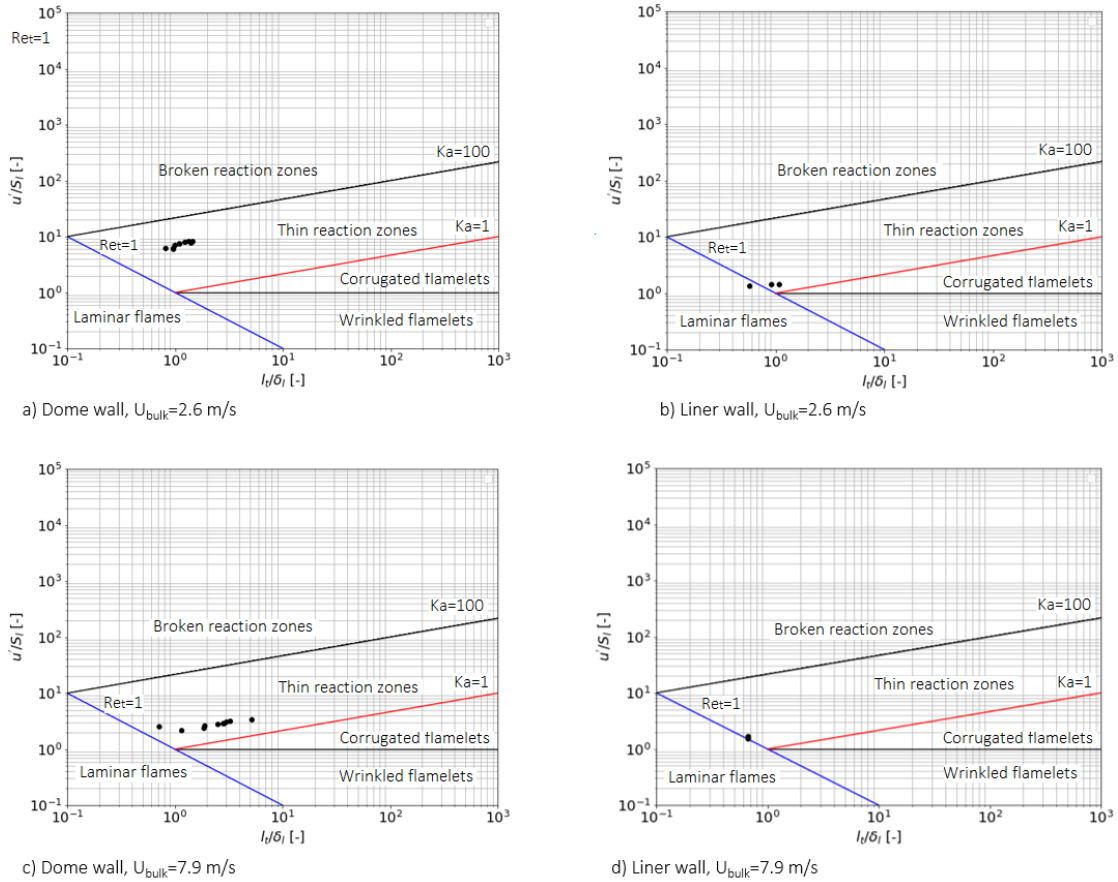

Figure 4.13: Turbulent combustion regimes at different inlet bulk velocities. The flow (u', l_t) and flame (S_l, δ_f) properties are calculated at points 3-12 along the dome wall and 13-15 along the liner (see Figure 4.8).

4.1.4.2 **Application of the BLF models**

In this section, the PSI and the TU Delft boundary layer flashback models will be evaluated to the flashback experiments of Figure 4.2. Four sets of experimental flashback data (100% H_2) will be utilized, in which the equivalence ratio varies between 0.3 and 0.45, and the corresponding inlet bulk velocity (main stage) between 2.6 and 7.9 m/s.

The equivalence ratio of the H_2-air mixture is constant along the dome, and the liner wall as the fuel and air are fully premixed upstream of the burner. With a given equivalence ratio, the flame properties (i.e., laminar burning velocity S_{l0}, laminar flame thickness δ_{l0}) can be calculated at every point along the liner and the dome (see Figure 4.8). The flashback models are applied separately to the dome and the liner wall due to the different turbulence intensity levels in these regions (see section 4.1.3.1). For these experimental cases, the equivalence ratio at which flashback occurs φ_{fb} is calculated at each location along the dome and liner wall and compared with the experimental value φ_{exp}.

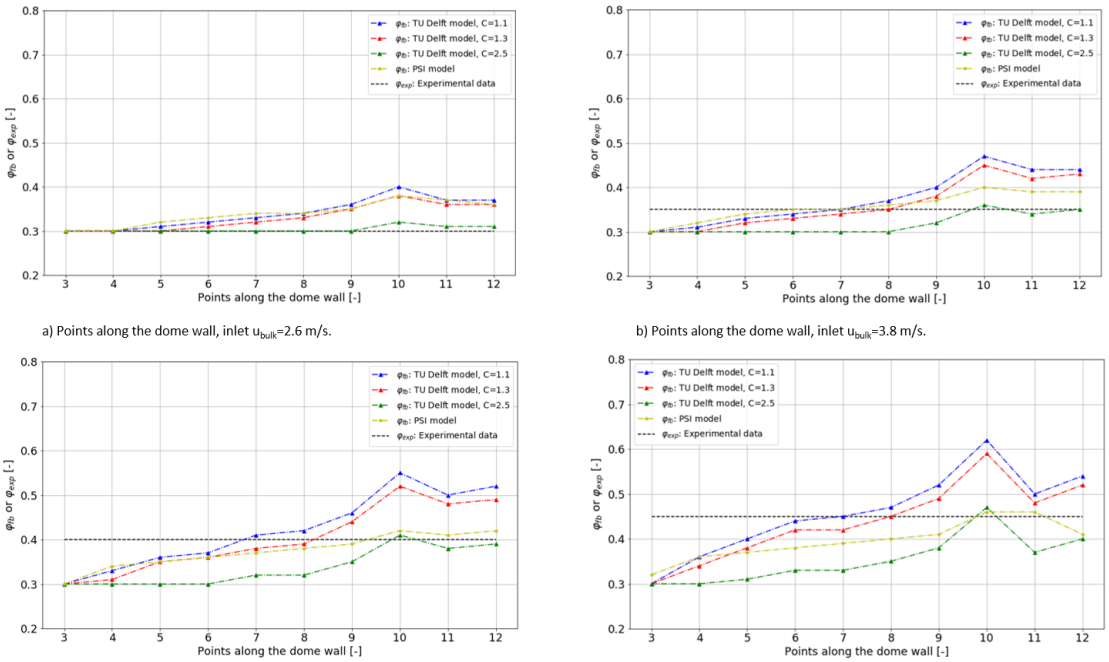

a) Points along the dome wall, inlet u_{bulk}=2.6 m/s.

b) Points along the dome wall, inlet u_{bulk}=3.8 m/s.

c) Points along the dome wall, inlet u_{bulk}=5.5 m/s.

d) Points along the dome wall, inlet u_{bulk}=7.9 m/s.

Figure 4.14: Predicted flashback limits for different inlet bulk velocities along the dome wall. Different versions of the TU Delft (variable tuning constant C) model are applied and compared with the PSI model.

Figure 4.14 shows the predicted flashback limits from the PSI and the TU Delft models at different locations of the TU Delft burner. The inlet bulk velocity is varied according to Figure 4.2 (each figure in Figure 4.14 refers to another bulk velocity), and the equivalence ratio at flashback φ_{fb} is calculated along the dome wall for both models, according to the methodology presented in sections 2.3.2 and 2.3.5. The black dotted line refers to the experimental value of the equivalent ratio at flashback φ_{exp} measured at the inlet of the burner's main stage (see Figure 4.1). It should be noted that the different versions of the TU Delft flashback model are initially applied by varying the constant *C* of the Damköhler turbulent flame speed correlation from 1.1 to 2.5 (see section 2.3.5), according to Björnsson's research [22]. The tuning constant *C* will be further optimized to capture better the TU Delft's burner experiments in the next section.

The results presented in Figure 4.14 can be used for the estimation of the position of flashback initiation, according to the following methodology:

- If the calculated value of the maximum flashback equivalence ratio φ_{fb} is greater than the experimental flashback equivalence ratio φ_{exp}, then boundary layer flashback is not expected at this position. In the opposite case ($\phi_{fb} \leq \phi_{exp}$), flashback initiation is at a critical stage ($\phi_{fb}=\phi_{exp}$) or has been already initiated.
- For example, from Figure 4.14c and at location 12, the following derives: The PSI model and the TU Delft model (C=2.5) predict that flashback would occur at this location as soon as the equivalence ratio is above 0.4. The TU Delft model (C=1.1-1.3) predicts that flashback at this location only occurs for equivalence ratios above 0.5.

According to both the PSI model and the TU Delft flashback model, the highest equivalence ratio required to initiate flashback is at the burner's exit (locations 10-12). This can be

interpreted that as soon as the flashback has been initiated at the burner exit at a certain equivalence ratio and bulk velocity, it will propagate upstream as the requirements to prevent flashback are stricter at the upstream locations (lower equivalence ratio required).

Therefore, the comparison between the models and experiments will be focused on the locations 10-12 along the dome. The maximum allowed equivalence ratio to prevent flashback from the models is compared with the experimentally observed value. Figure 4.14 shows that the high *C* constant version of the TU Delft model (C=2.5) is closer to the PSI predicted flashback limits φ_{fb} adjacent to the burner's exit (point 10-12 of Figure 4.8).

Figure 4.15 shows the results of the PSI and TU Delft models along the liner wall. It can be seen that the PSI model does not predict flashback initiation along points 13 to 15 of the liner (the equivalence ratio from the model is above the experimental one), except for the case with U_{bulk}=5.5 m/s. For these high inlet velocity cases, the plotted PSI model line is close to the constant line of equivalence ratio at flashback φ_{exp} (see Figure 4.15c), which indicates that upstream flame propagation may occur in this region. A similar trend is observed for the high *C* constant version of the TU Delft model (C=2.5), in which the predicted flashback limits φ_{fb} lay closer to the PSI model's trend line. On the other hand, the lower *C* constant version of the TU Delft model results in significantly higher φ_{fb} values than the experiments for all the examined cases.

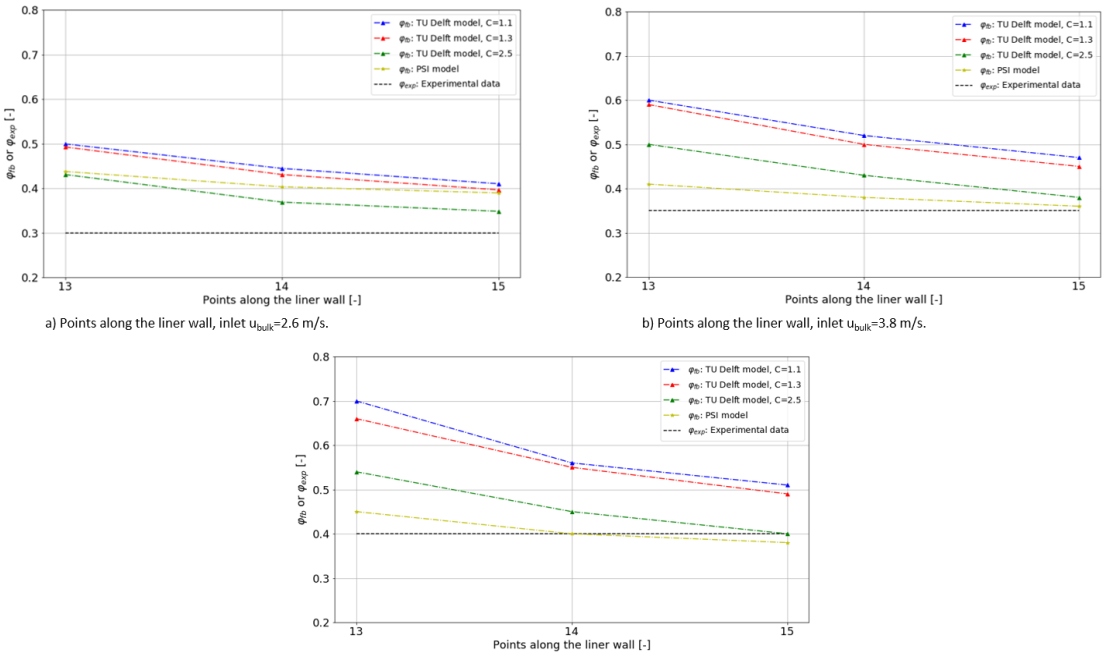

a) Points along the liner wall, inlet u_{bulk}=2.6 m/s.

b) Points along the liner wall, inlet u_{bulk}=3.8 m/s.

c) Points along the liner wall, inlet u_{bulk}=5.5 m/s.

Figure 4.15: Predicted flashback limits for different inlet bulk velocities along the liner wall.

It has to be noted that the predicted flashback limits presented in Figure 4.15 do not include the liner wall temperature effect. During the burner's normal operation, the flame anchors at the exit of the main stage (after point 12, see Figure 4.8), and the liner's (inner) wall temperature is expected to be significantly higher due to the high adiabatic flame temperature of the H_2-air mixture. The heat is transferred from the wall to the near-wall flow

and elevates the H_2-air mixture's temperature. As a result, the mixture's laminar flame speed rises, and the flashback limits presented in Figure 4.15 are expected to shift to lower equivalence ratios, closer to the experimental value of equivalence ratio at flashback φ_{exp}.

4.1.5 **Optimization of the TU Delft model**

In this section, the TU Delft model is calibrated to match the experimental flashback data (see Figure 4.2) by varying the tuning constant *C* of the Damköhler turbulent flame speed closure. The TU Delft model is adjusted to predict φ_{fb} closer to the φ_{exp} adjacent to the burner's exit (points 10-12, see Figure 4.8). A numerical optimization study is performed for the 13 H_2 flashback cases of Figure 4.2. For every case, the tuning constant C is varied between 1 and 2.5 till the least-square deviation between the calculated flashback equivalence ratio φ_{fb} and the experimentally observed φ_{exp} is minimized. The optimum value of the Damköhler turbulent flame speed correlation is derived C_{opt}=2.0, and the calculated flashback limits for the experimental cases tested in section 4.1.4 are shown in Figure 4.16. It can be seen that the flashback limits predicted by the revised version of the TU Delft model (C=2.0) show good agreement with both the PSI model and the experimental data.

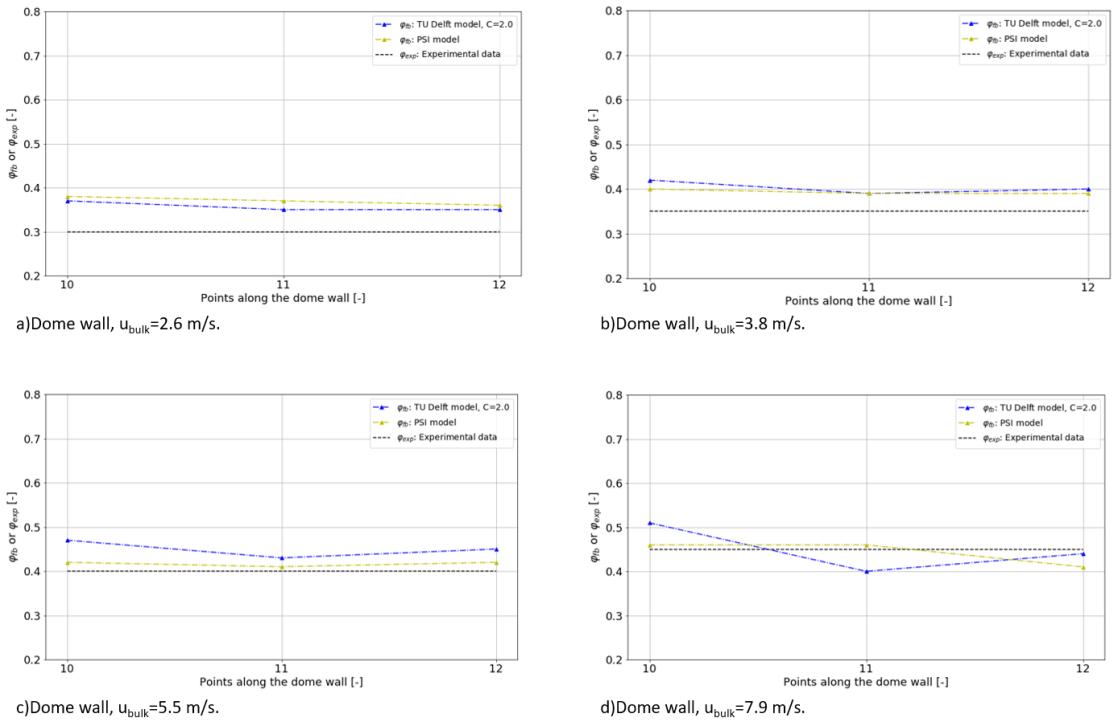

a)Dome wall, u_{bulk}=2.6 m/s.

b)Dome wall, u_{bulk}=3.8 m/s.

c)Dome wall, u_{bulk}=5.5 m/s.

d)Dome wall, u_{bulk}=7.9 m/s.

Figure 4.16: Predicted flashback limits for different inlet bulk velocities along the TU Delft's burner dome wall. Optimization of the TU Delft model based on the experimental data of Figure 4.2.

According to the TU Delft's burner flashback experiments (see Figure 4.2), flashback was observed within a range of inlet bulk velocities for a given equivalence ratio. Thus, the sensitivity of the optimized TU Delft and PSI models on changes of the inlet bulk velocity should be investigated. For that reason, the flashback limits for all the experimental cases (u_{bulk} between 2.6 and 7.9 m/s) are calculated using both flashback models. The variation of

the φ_{fb} value for different inlet bulk velocities (main stage) is shown in Figure 4.17. Overall, both models show better agreement with the experimental values adjacent to the burner's exit (see Figure 4.17a,b), whereas the predicted flashback limits are significantly higher than the experimental values near the edge of the liner (see Figure 4.17c). For this analysis, it is assumed that if boundary layer flashback is initiated adjacent to the burner exit or at the liner's edge, then the flame will propagate further upstream following the discussion in section 4.1.4. Thus, both flashback models are evaluated only to the points 11-12 along the dome wall and point 13 at the edge of the liner.

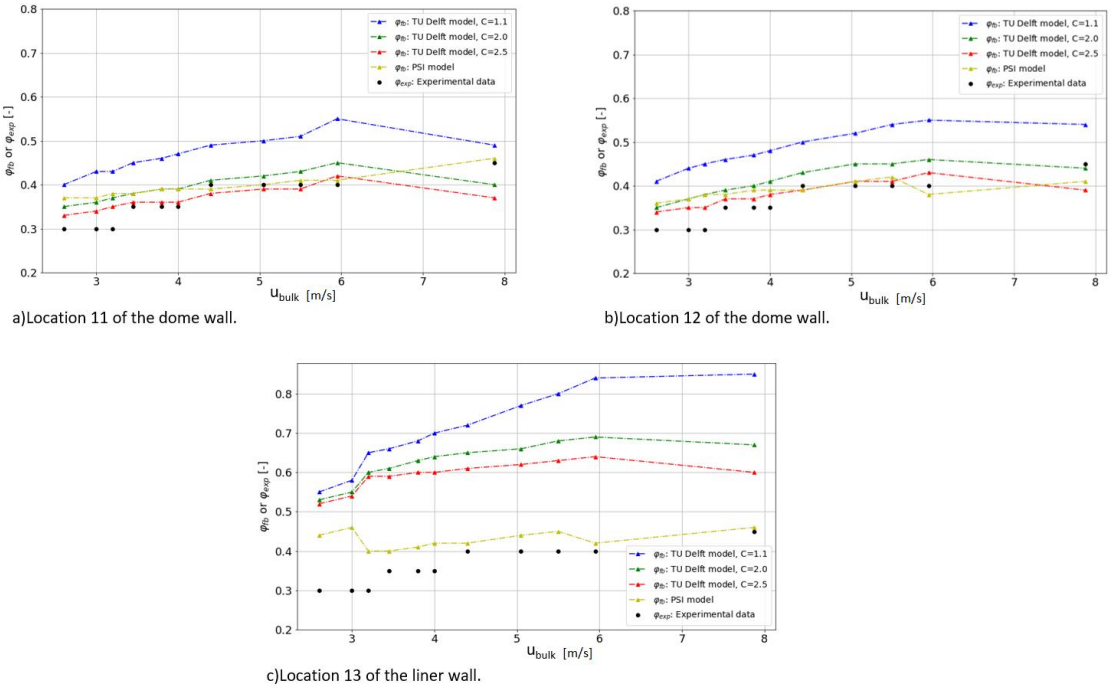

a)Location 11 of the dome wall.

b)Location 12 of the dome wall.

c)Location 13 of the liner wall.

Figure 4.17: Flashback limits derived from the optimized TU Delft and PSI model at different inlet bulk velocities. Both models are evaluated adjacent to the TU Delft's burner exit (a), (b), and close to the edge of the liner (c).

4.1.6 Evaluation of flashback models at different H_2-CH_4 fuel gases.

Flashback experiments are performed not only for H_2-air mixtures but also for H_2-CH_4 mixtures in the TU Delft FlameSheet^{TM} combustor, as has been already shown in Figure 4.2. In this section, the sensitivity of the flashback models on variations of the fuel composition will be investigated.

According to the flashback map of Figure 4.2, there are cases that, for almost the same inlet bulk velocity, flashback limits shifted to higher equivalence ratios at less H_2-rich fuel gases. This observation allows us to apply both flashback models to these H_2-rich fuel cases using the CFD results from the cold-flow simulations discussed in section 4.1.3. The thermophysical properties of the fuel-air mixture (i.e., density, laminar flame speed) had to be calculated again based on the fuel composition using the Cantera software. Table 4.1. presents the two cases with H_2-rich fuel gases (H_2-CH_4 75-25, H_2-CH_4 50-50; numbers are in vol. %) that will be investigated in this section.

Table 4.1: Flashback experiments at the same U_{bulk} and different fuel composition. Experimental data based on Figure 4.2.

U_{bulk} [m/s]	*Fuel composition in H_2 [%]*	*φ_{fb} [-]*
2.6	100	0.3
	50	0.9
3	100	0.3
	50	0.9
3.45	100	0.35
	75	0.6
3.8	100	0.35
	75	0.6
4	100	0.35
	75	0.6

Both the TU Delft and PSI models are applied adjacent to the exit of the burner (point 12 in Figure 4.8), following the assumption made in section 4.1.4, and benchmarked against the experimental values in Figure 4.18. Overall, the φ_{fb} values of the optimized TU Delft model (C=2.0) lay slightly closer to the different fuel compositions' experimental data. Both models deviate significantly from the experimental data when fuel's H_2 composition decreases significantly. This is evident for the 50% H_2 case, in which both models predict flashback initiation at a significantly lower equivalence ratio (ϕ: 0.6-0.7) than the experimental value of 0.9.

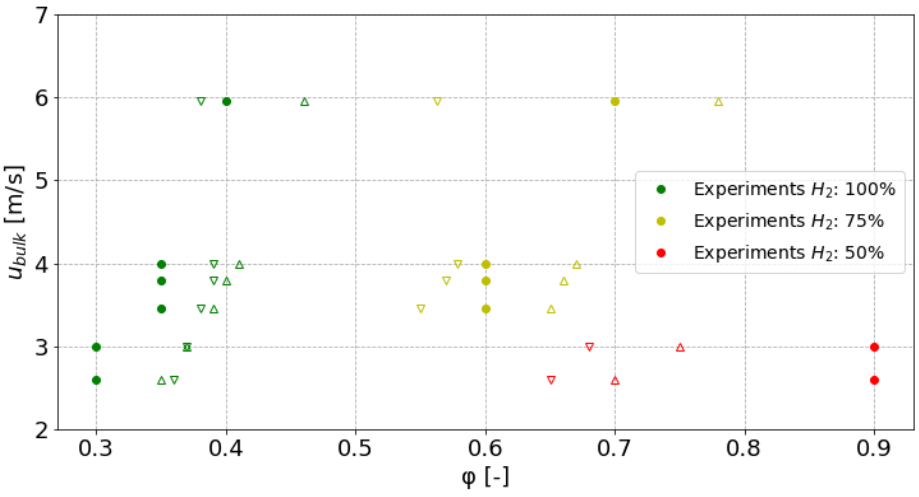

Figure 4.18: Variation of flashback limits with decreasing fuel's H_2 composition. The non-filled up-pointing triangle (△) and down-pointing triangle (▽) refer to the TU Delft and PSI model's flashback limits, respectively.

4.1.6.1 **Turbulent flame speed correlation for H_2-CH_4 fuel gas.**

The deviation between the predicted φ_{fb} and the experimental data for the 50% H_2 case, discussed in the previous section, can be attributed to the turbulent flame speed correlation used in the TU Delft model. The updated Damköhler turbulent flame speed correlation with

C=2.0 (see section 4.1.5) is benchmarked against Kido's experimental turbulent flame data [64]. Kido performed experiments to evaluate the turbulent flame speed at a near spherical chamber using a mixture of H_2-CH_4 (50-50 %vol) with an equivalence ratio ϕ=0.8. The experimental turbulent burning velocity S_t and the measured integral length scale l_t at different turbulence intensity conditions u' are shown in Table 4.2.

Table 4.2: Kido's experimental turbulent flame data in H_2-CH_4 fuel mixture (50-50 % vol) [64]. Equivalence ratio is 0.8 and operating pressure and temperature 1 atm, 298 K, respectively.

u' (m/s)	S_t (m/s)	l_t (mm)
0.00	0.25	0
0.49	0.84	2.98
0.98	1.34	3.37

Figure 4.19 shows that the turbulent flame speeds S_t predicted from the Damköhler correlation (C=2.0) are higher than Kido's experiments, which explains the lower predicted flashback limits in Figure 4.18. A promising alternative is the use of Muppala's turbulent flame speed correlation [39]. As discussed in section 2.2.2, Muppala's correlation showed the closest overall agreement to experimental data for hydrocarbon fuels at various operating conditions [37]. Furthermore, Muppala's turbulent flame speed correlation showed a good agreement with Kido's experimental data with H_2-rich fuel gases [39]. Indeed, Figure 4.19 shows that the Muppala's turbulent flame speed correlation (see Eq. (2.22)) has overall a better agreement with the experiments than the Damköhler correlation (C=2.0).

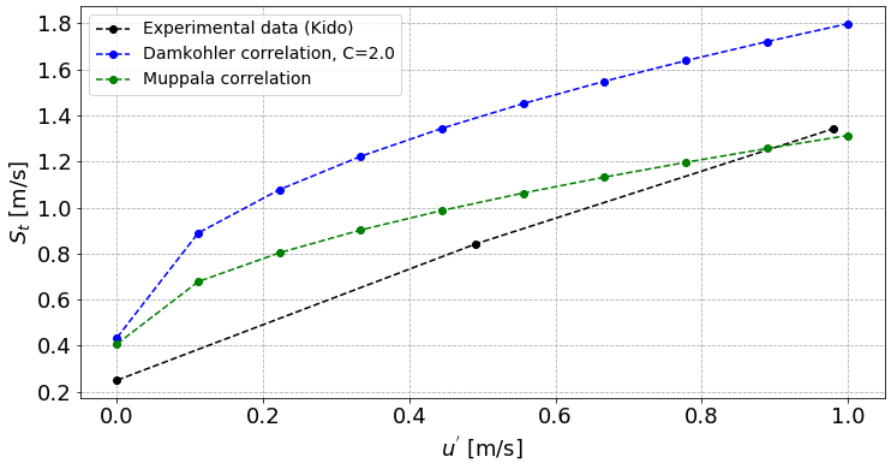

Figure 4.19: Turbulent flame speed S_t as function of the turbulence intensity u' for H_2-CH_4 (50-50) fuel mixture. The operating pressure and temperature are 1 atm and 298 K, respectively, and the equivalence ratio is 0.8. The experimental data are from Kido [64].

Following the discussion above, the TU Delft model's accuracy is expected to be enhanced for the 50% H_2 fuel case if the Damköhler turbulent flame speed correlation (C=2.0) is replaced by the Muppala correlation. This can be seen in Figure 4.20, in which the coupling of the Muppala correlation with the TU Delft flashback model shifts the flashback limits to higher values and closer to the experiments for the 50% H_2 fuel case. From this analysis, it can be

concluded that the TU Delft model can still adequately capture the flashback limits for fuel gases less rich in H_2, provided that a proper correlation for the turbulent flame speed (e.g., Muppala correlation) is selected.

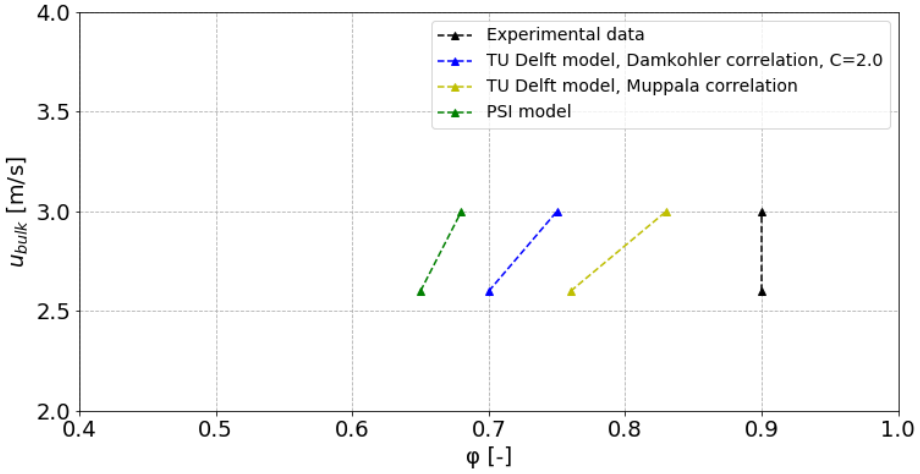

Figure 4.20: Predicted flashback limits (PSI, TU Delft models) for the 50% H_2 flashback cases. Different flame speed correlations are applied to the TU Delft flashback model.

4.1.7 Effect of reactive flow on the flashback models

In this section, reactive flow simulations are performed in the flashback experiments of Figure 4.2. The objective of this analysis is to determine whether the presence of a flame has a significant effect on the flow field close to the wall and thereby on the (calculated) flashback propensity. The same set-up is used for the turbulence modeling as in section 4.1.2, and the premixed turbulent combustion model of ANSYS Fluent is used for the flame modeling [65]. The turbulent flame speed is modeled using the Zimont turbulent flame closure, and the Non-Adiabatic feature is selected to determine the temperature of the H_2-air mixture. Moreover, the unburnt mixture's physical properties (i.e., α, C_p, k, μ, ρ_u, S_{l0}) are calculated using Cantera software and then used as input to the premixed combustion model of ANSYS. Finally, the heat of combustion is selected 120 MJ/kg (value for H_2 fuel), and the unburnt fuel mass fraction is calculated from the equivalence ratio φ and the single-step reaction of H_2 with air (21% O_2 – 79% N_2) shown in Eq. (4.4).

$$\varphi H_2 + \frac{1}{2}(O_2 + 3.76N_2) \rightarrow (\varphi H_2O + 1.88N_2) + \frac{1}{2}(1-\varphi)O_2 \tag{4.4}$$

The contour of the progress variable for the ϕ=0.4 and U_{bulk}=5.5 m/s case is shown in Figure 4.21. The progress variable varies between 0 (unburnt mixture) and 1 (burnt mixture). It can be seen that the flame is anchored on the edge of the liner, and its thickness increases, moving further downstream. Nevertheless, the reactive flow effect on the velocity field is negligible at the examined flashback regions adjacent to the exit of the burner (point 12) and close to the edge of the liner wall (point 13). This can be seen from the velocity profiles of the cold and reactive flow at points 12 and 13 of Figure 4.8, for the ϕ=0.4 and U_{bulk}=5.5 m/s flashback case. The mean velocity profile is almost the same within the boundary layer for both cold and

reactive flow, whereas the mean velocity increases for the reactive flow further away from the dome wall (see Figure 4.22a). Similarly, the velocity profile in the liner region is not influenced by the flame's presence, as can be seen in Figure 4.22b. The velocity fluctuations *u'* are also the same for both cold and reactive flow, according to Figure 4.22c-d.

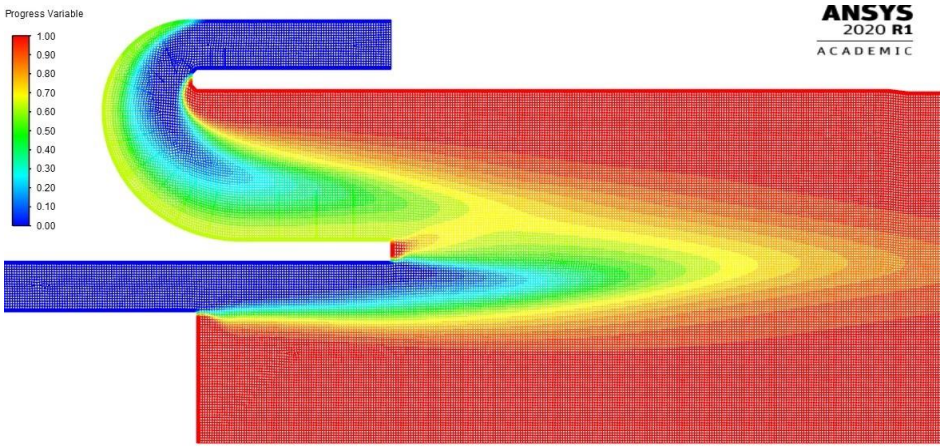

Figure 4.21: Contour of the progress variable *c* in the TU Delft burner (c=0: unburnt, c=1: burnt mixture). The inlet bulk velocity (main stage) is 5.5 m/s, and the equivalence ratio of the H_2-air mixture is ϕ=0.4.

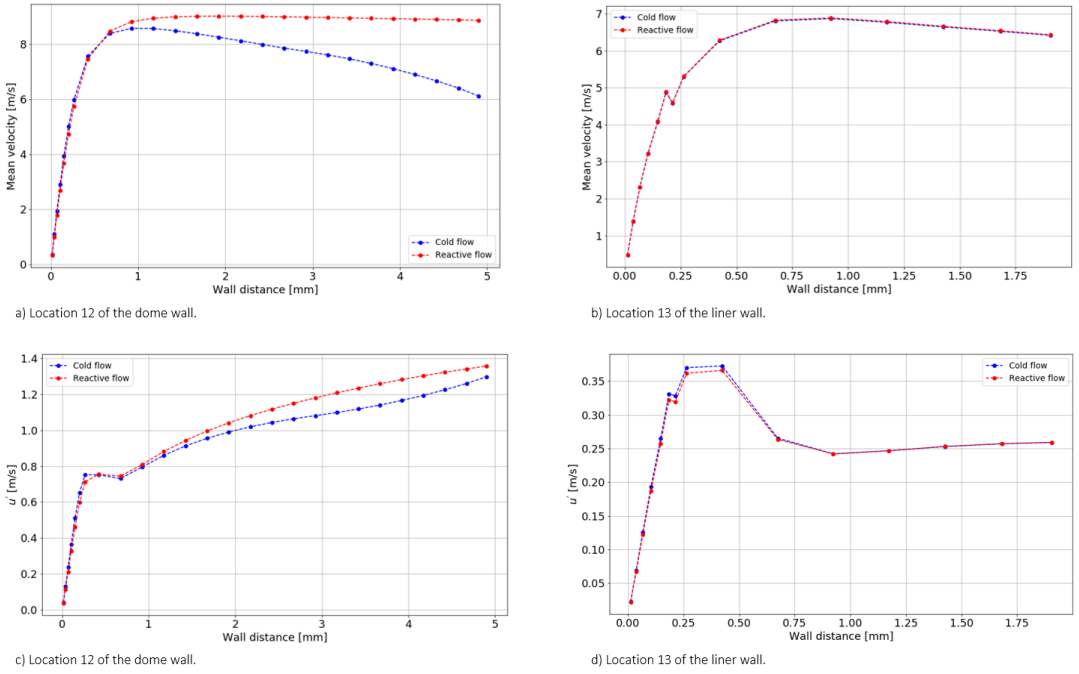

Figure 4.22: Mean velocity profile of the cold and the reactive flow in point 12 (a) and point 13 (b) of the dome and liner wall, respectively. The equivalence ratio of the H_2-air was set 0.4, and the inlet u_{bulk}=5.5 m/s, according to the experiments in Figure 4.2.

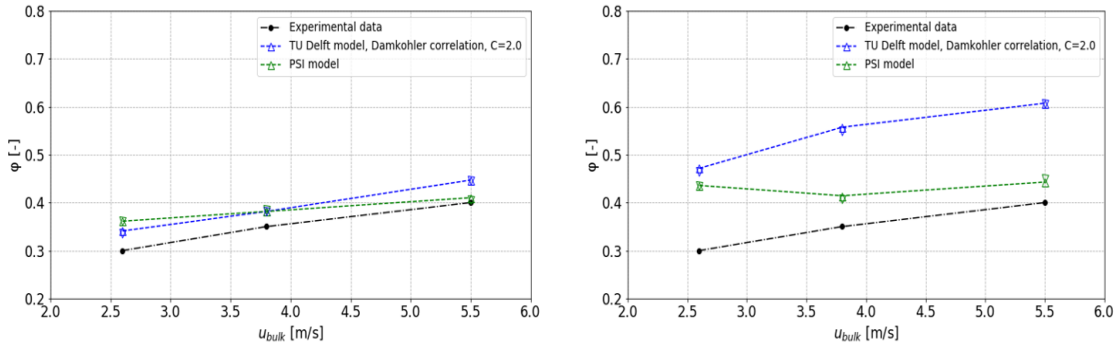

a) Location 12 of the dome wall.

b) Location 13 of the liner wall.

Figure 4.23: Flashback models applied to points 12 (a) and 13 (b) for different inlet bulk velocities. The up-pointing triangle (△) and down-pointing triangle (▽) refer to the cold and reactive flow simulations, respectively.

The negligible effect of the reactive flow on the velocity profile and turbulence intensity of points 12 (dome wall) and 13 (liner wall) is expected to have a minor effect on the flashback models at these locations. Figure 4.23 shows that both the TU Delft and PSI flashback models predict the same flashback equivalence ratio φ_{fb} using the turbulence properties from either cold or reactive flow CFD simulations. This is an important finding since it implies that the turbulence parameters adjacent to the burner head (point 12) and at the edge of the liner (point 13) are not affected by the flame's presence; thus, cold-flow simulation will suffice to model the turbulence parameters (i.e., mean velocity profile, *u'*) used in the flashback models.

4.1.8 **Summary**

The PSI and TU Delft flashback models were validated upon flashback experiments in the TU Delft FlameSheet™ combustor. It was shown that different locations along the burner's dome and liner wall show different flashback propensity. According to both models, the flashback propensity is the lowest at the burner's exit (i.e., the highest equivalence ratio φ was required to initiate flashback); thus, initiation of flashback at these locations would eventually lead to flame propagation further upstream.

The predicted equivalence ratio at flashback φ_{fb} for both the PSI and the TU Delft model compares well with the experiments for the 100% H_2 fuel mixture. Slight improvements were made in the Damköhler turbulent flame speed correlation based on a number of flashback experiments in the TU Delft FlameSheet™ burner.

For fuel mixtures less rich in H_2, the experimental data does not match adequately with the calculated equivalence ratio at flashback φ_{fb} for both the PSI and the TU Delft models. Both models predict a significantly higher maximum equivalence ratio φ_{fb} than the experimental data at lower H_2 concentrations. This was probably caused by the applied turbulent flame speeds, given that experiments with H_2-rich fuels were used to derive the turbulent flame speed correlations applied in both models. The Muppala's turbulent flame speed correlation in the TU Delft model was a promising option for fuel gases less rich in H_2. The application of the Muppala correlation to the TU Delft model yielded better agreement with the TU Delft's FlameSheet™ combustor flashback experiments for fuels with H_2 composition down to 50 % vol.

Finally, it was shown that cold flow CFD simulations could be used to calculate the flashback propensity, given that the impact of the flame's presence on the boundary layer flow and turbulence profile adjacent to the burner's exit and at the edge of the liner was negligible.

5. Conclusion and recommendations

Hydrogen combustion in modern combustion systems is a promising option to decarbonize the energy sector. The lean-premixed combustor technology has high potentials towards this path; however, methods of detecting and avoiding flame flashback have to be developed and applied in high-hydrogen fueled gas turbines. Towards this direction, state-of-the-art boundary layer flashback models were evaluated upon flashback experimental data in a number of academic burners at both atmospheric and elevated operating conditions.

In this chapter, important conclusions from the main part of the thesis are drawn in section 5.1, followed by recommendations for future research in section 5.2.

5.1 Conclusion

The key findings from the validation of the flashback models upon experimental flashback data in academic combustors are the following:

- The PSI flashback model shows overall good agreement with the flashback experiments in zero pressure gradient flows (0^o channel), whereas the predicted maximum equivalence ratio for flashback φ_{fb} is significantly overestimated for mild and strong diffusing flows (2^o-4^o diffusers).

- The current version of the TU Delft model did not capture the experimental flashback trend at elevated operating conditions. The turbulent flame speed correlation was identified as the main parameter influencing flashback at elevated operating conditions. Introducing a new turbulent flame speed correlation to the model, which includes an explicit term for pressure, allows a better prediction of the flashback limits. Considering the effect of the hot wall temperature on the fuel-air mixture at higher pressures and temperatures further improves the updated TU Delft model's accuracy.

- For the complex TU Delft FlameSheet™ combustor, the PSI and TU Delft flashback models showed that the flashback propensity varies with the different locations along the burner's dome and liner wall. According to both models, the flashback propensity is the lowest at the burner's exit (i.e., the highest equivalence ratio φ was required to initiate flashback); thus, initiation of flashback at these locations would eventually lead to flame propagation further upstream. The predicted equivalence ratios at flashback φ_{fb} for both the PSI and the TU Delft model (calculated at the TU Delft FlameSheet™ burner's exit) show good agreement with the 100% H_2 fuel experiments. Minor modifications have been made on the Damköhler turbulent flame speed correlation (tuning of the *C* constant) used in the TU Delft flashback model.

- The PSI and TU Delft flashback models' performance worsens for cases with fuel mixtures less rich in hydrogen. This was probably caused by the applied Damköhler turbulent flame speed correlation that was calibrated based on 100% H_2 fuel. A promising alternative is the Muppala turbulent flame speed correlation, resulting in a

better agreement with the flashback experiments in the TU Delft FlameSheet^{TM} combustor for fuels with H_2 composition down to 50 % vol.

The results from the evaluation of the flashback models against the experimental data of the academic burners examined in this thesis are summarized in Table 5.1. In the first columns, the fuel and flow properties (e.g., fuel composition, pressure, temperature, Reynolds number) of the experimental cases used to evaluate the flashback models are provided. Furthermore, the turbulent flame speed correlations applied to the TU Delft and PSI flashback models in each case are presented in a separate column. Finally, a brief description of each model's performance is provided in the last two columns of Table 5.1.

Table 5.1: Summary of the flashback models (TU Delft, PSI) results in academic burners.

Academic burners							
Geometry	*Fuel*	*Mixture temperature (K)*	*Static pressure (atm)*	*Reynolds number*	*Turbulent flame speed*	*TU Delft model*	*PSI model*
0° channel [11]	100% H_2	293	1	5×10^3 - 3×10^4	Damköhler: C=1.1 (TU Delft) Lin: H_2-rich fuel gases (PSI)	Overall good prediction. Slight overprediction[a] for $\phi<0.4$.	Overall good agreement. Overprediction for $\phi<0.5$.
2° diffuser [11]					Damköhler: C=1.1 (TU Delft) Lin: H_2-rich fuel gases (PSI)	Accurate prediction[c].	Significant overprediction.
4° diffuser [11]					Damköhler: C=1.3 (TU Delft) Lin: H_2-rich fuel gases (PSI)	Slight overprediction[c].	
Axial-dump (PSI) [44]	85% H_2 15% N_2	623	2.5-10	4×10^4 - 15×10^4	New correlation based on Damköhler.	Good prediction.	Good agreement for the PSI burner, deviation for the UCI burner [16].
Axial-dump (UCI) [47]	100% H_2	300-500	3-7	5×10^4 - 3×10^5	New correlation based on Damköhler.	Good prediction[d].	

Lab-scale combustor							
TU Delft FlameSheet™	100% H_2	293	1	2×10^3 - 5×10^3	Damköhler: C=2.0 (TU Delft) Lin: H_2-rich fuel gases (PSI)	Accurate prediction of the flashback limits (at the exit of the burner).	
	75% H_2 25% CH_4					Slight overprediction.	Slight underprediction[b].
	50% H_2 50% CH_4				Muppala (TU Delft) Lin: H_2-rich fuel gases (PSI)	Slight underprediction.	Significant underprediction.

a) Overprediction means that the predicted equivalence ratio at flashback φ_{fb} is higher than the experimental φ_{exp}.

b) Underprediction means that the predicted equivalence ratio at flashback φ_{fb} is lower than the experimental φ_{exp}.

c) The velocity fluctuations u' are corrected to the experimental values from Eichler's experiments in the 2^0 and 4^o diffuser [11].

d) The effect of the wall temperature on the fuel-air mixture's temperature is considered.

5.2 Recommendations

The TU Delft flashback model was updated (i.e., introduce a new turbulent flame speed correlation), allowing to efficiently investigate boundary layer flashback in H_2 fueled burners at elevated operating conditions. The updated version of the TU Delft model showed good agreement with both atmospheric and high-pressure academic burners operating at pressure up to 7 atm and temperature up to 500 K. However, the model has been only benchmarked against simple geometries (axial-dump combustors), so further validation of the updated TU Delft model with flashback experiments at complex confined geometries and gas turbine relevant conditions is required.

Even though the adjustment of the turbulent flame speed correlation used in the TU Delft model enhanced its accuracy at elevated pressures, further modifications are required. Based on a recent research of Endres and Sattelmayer [66] in confined BLF at higher pressures, additional quantities such as the local separation zone's size upstream of the flame front and the decreasing quenching distance have to be investigated in flashback modeling.

The fuel composition effect on flashback propensity was adequately captured by the TU Delft model by adjusting the turbulent flame speed correlation. However, the model was validated with H_2-CH_4 fuel mixtures at low flow velocity and ambient pressure, and room temperature; thus, validation of the model with additional flashback cases at elevated operating conditions and different fuel compositions is recommended.

Bibliography

[1] A. I. Köne and T. Büke, “Forecasting of CO2 emissions from fuel combustion using trend analysis,” *Renew. Sustain. Energy Rev.*, vol. 14, no. 9, pp. 2906–2915, 2010.

[2] S. Dunn and C. Flavin, “Moving the climate change agenda forward,” *State of the World*, pp. 24–50, 2002.

[3] A. Khosravi, R. N. N. Koury, L. Machado, and J. J. G. Pabon, “Energy, exergy and economic analysis of a hybrid renewable energy with hydrogen storage system,” *Energy*, vol. 148, pp. 1087–1102, 2018.

[4] M. Rashid, M. Al Mesfer, and H Naseem, “Hydrogen production by water electrolysis: a review of alkaline water electrolysis, PEM water electrolysis and high temperature water electrolysis,” *Int. J. Eng.*, 2015.

[5] M. Bui *et al.*, “Carbon capture and storage (CCS): The way forward,” *Energy and Environmental Science*, vol. 11, no. 5. Royal Society of Chemistry, pp. 1062–1176, 01-May-2018.

[6] V. Hoferichter, “Boundary Layer Flashback in Premixed Combustion Systems,” 2017.

[7] P. J. Stuttaford *et al.*, “FlameSheet Combustor,” 6,935,116, 2005.

[8] P. Stuttaford *et al.*, “FlameSheet™ combustor engine and rig validation for operational and fuel flexibility with low emissions,” *Proc. ASME Turbo Expo*, vol. 4A-2016, 2016.

[9] “High hydrogen gas turbine retrofit to eliminate carbon emissions - Topsector Energie.” [Online]. Available: https://projecten.topsectorenergie.nl/projecten/high-hydrogen-gas-turbine-retrofit-to-eliminate-carbon-emissions-00031823.

[10] Georg Martin Baumgartner, “Flame Flashback in Premixed Hydrogen-Air Combustion Systems,” 2014.

[11] C. T. Eichler, “Flame Flashback in Wall Boundary Layers of Premixed Combustion Systems,” p. 229, 2011.

[12] A. Kalantari and V. McDonell, “Boundary layer flashback of non-swirling premixed flames: Mechanisms, fundamental research, and recent advances,” *Progress in Energy and Combustion Science*, vol. 61. Elsevier Ltd, pp. 249–292, 2017.

[13] G. Von Elbe and M. Mentser, “Further studies of the structure and stability of burner flames,” *J. Chem. Phys.*, vol. 13, no. 2, pp. 89–100, 1945.

[14] B. Lewis and G. von Elbe, “Stability and Structure of Burner Flames,” *J. Chem. Phys.*, vol. 11, no. 2, pp. 75–97, Feb. 1943.

[15] Y. C. Lin, S. Daniele, P. Jansohn, and K. Boulouchos, “Turbulent flame speed as an indicator for flashback propensity of hydrogen-rich fuel gases,” *J. Eng. Gas Turbines Power*, vol. 135, no. 11, Nov. 2013.

[16] A. Kalantari, N. Auwaijan, and V. McDonell, “Boundary layer flashback prediction for turbulent premixed jet flames: Comparison of two models,” *Proc. ASME Turbo Expo*, vol. 4A-2019, pp. 1–9, 2019.

[17] A. Gruber, J. H. Chen, D. Valiev, and C. K. Law, “Direct numerical simulation of premixed flame boundary layer flashback in turbulent channel flow,” *J. Fluid Mech.*, vol. 709, pp. 516–542, 2012.

[18] V. Hoferichter, C. Hirsch, T. Sattelmayer, A. Kalantari, E. Sullivan-Lewis, and V. McDonell, “Comparison of Two Methods to Predict Boundary Layer Flashback Limits of Turbulent Hydrogen-Air Jet Flames,” *Flow, Turbul. Combust.*, 2018.

[19] V. Hoferichter, C. Hirsch, and T. Sattelmayer, “Prediction of Confined Flame Flashback Limits Using Boundary Layer Separation Theory,” *J. Eng. Gas Turbines Power*, 2017.

[20] B. S. Stratford, “The prediction of separation of the turbulent boundary layer,” *J. Fluid Mech.*, 1959.

[21] J. Tober, “Boundary layer flashback prediction of a low emissions full hydrogen burner for gas turbine applications,” 2019.

[22] O. H. Björnsson, “Boundary layer flashback prediction for low emissions full hydrogen gas turbine burners using flow simulation,” 2019.

[23] N. Hall, “Boundry layer.” [Online]. Available: https://www.grc.nasa.gov/www/k-12/airplane/boundlay.html. [Accessed: 17-Sep-2019].

[24] P. K. Kundu, I. M. Cohen, and D. R. Dowling, *Fluid Mechanics 6th Edition*. 2016.

[25] J. Hinze, *Turbulence*. New York: McGraw-Hill Publishing Co, 1975.

[26] Fluent, “ANSYS Fluent 12.0 user’s guide.” ANSYS Inc, 2009.

[27] F. M. White, *Viscous fluid flow*. McGraw-Hill, 1991.

[28] “Targeting a Specific y+ Value for your Turbulent Flow CFD Simulation (Part 2) - SIMTEQ Engineering.” [Online]. Available: https://simteq.co.za/blog/targeting-a-specific-y-value-for-your-turbulent-flow-cfd-simulation-part-2/. [Accessed: 12-Nov-2020].

[29] G. Ciccarelli and S. Dorofeev, “Flame acceleration and transition to detonation in ducts,” *Progress in Energy and Combustion Science*. 2008.

[30] S. Turns, *An Introduction to Combustion*. 2000.

[31] “1-D Premixed flame with CANTERA.” Cantera tutorial, 2017.

[32] “GRI-Mech 3.0.” [Online]. Available: http://www.me.berkeley.edu/gri_mech/.

[33] M. O’ Conaire, H. J. Curran, J. M. Simmie, and J. William, “A comprehensive modeling study of hydrogen oxidation,” *Int. J. Chem. Kinet.*, 2004.

[34] N. Peters, “The turbulent burning velocity for large-scale and small-scale turbulence,” *J. Fluid Mech.*, vol. 384, pp. 107–132, 1999.

[35] N. Peters, “Laminar flamelet concepts in turbulent combustion,” *Symp. Combust.*, vol. 21, no. 1, pp. 1231–1250, 1988.

[36] G. Damköhler, “Der Einfluss der Turbulenz auf die Flammengeschwindigkeit in Gasgemischen,” *Zeitschrift für Elektrochemie und Angew. Phys. Chemie*, vol. 46, no. 11, pp. 601–626, Nov. 1940.

[37] E. M. Burke, F. Güthe, and R. F. D. Monaghan, “A Comparison of Turbulent Flame Speed Correlations for hydrocarbon fuels at elevated pressures,” *Proc. ASME Turbo Expo 2016 Turbomach. Tech. Conf. Expo.*, pp. 1–13, 2016.

[38] S. P. Reddy Muppala, N. K. Aluri, F. Dinkelacker, and A. Leipertz, “Development of an algebraic reaction rate closure for the numerical calculation of turbulent premixed methane, ethylene, and propane/air flames for pressures up to 1.0 MPa,” *Combust. Flame*, vol. 140, no. 4, pp. 257–266, 2005.

[39] S. P. R. Muppala, M. Nakahara, N. K. Aluri, H. Kido, J. X. Wen, and M. V Papalexandris, “Experimental and analytical investigation of the turbulent burning velocity of two-component fuel mixtures of hydrogen, methane and propane,” vol. 34, pp. 9258–9265, 2009.

[40] S. Daniele, P. Jansohn, J. Mantzaras, and K. Boulouchos, “Turbulent flame speed for syngas at gas turbine relevant conditions,” *Proc. Combust. Inst.*, vol. 33, no. 2, pp. 2937–2944, 2011.

[41] Y. Lin, P. Jansohn, and K. Boulouchos, “Turbulent flame speed for hydrogen-rich fuel gases at gas turbine relevant conditions,” *Int. J. Hydrogen Energy*, vol. 39, no. 35, pp. 20242–20254, 2014.

[42] S. Daniele, P. Jansohn, J. Mantzaras, and K. Boulouchos, “Turbulent flame speed for syngas at gas turbine relevant conditions,” *Proc. Combust. Inst.*, vol. 33, no. 2, pp. 2937–2944, Jan. 2011.

[43] A. Kalantari, E. Sullivan-Lewis, and V. McDonell, “Flashback Propensity of Turbulent Hydrogen-Air Jet Flames at Gas Turbine Premixer Conditions,” *J. Eng. Gas Turbines Power*, vol. 138, no. 6, Jun. 2016.

[44] Y. Lin and S. Daniele, “Turbulent Flame Speed as an Indicator for Flashback Propensity of Hydrogen-Rich Fuel Gases,” vol. 135, no. November, pp. 1–8, 2013.

[45] V. N. Kurdyumov, E. Fernández, and A. Liñán, “Flame flashback and propagation of premixed flames near a wall,” *Proc. Combust. Inst.*, 2000.

[46] V. Kurdyumov, E. Fernández-Tarrazo, J. M. Truffaut, J. Quinard, A. Wangher, and G. Searby, “Experimental and numerical study of premixed flame flashback,” *Proc. Combust. Inst.*, vol. 31 I, no. 1, pp. 1275–1282, 2007.

[47] Alireza Kalantari, “Boundary Layer Flashback of Turbulent Premixed Jet Flames at Elevated Pressures and Temperatures,” 2018.

[48] S. Daniele, P. Jansohn, and K. Boulouchos, “Flashback propensity of syngas flames at high pressure: Diagnostic and control,” in *Proceedings of the ASME Turbo Expo*, 2010, vol. 2, no. PARTS A AND B, pp. 1169–1175.

[49] D. V. Thierry Poinsot, “Theoretical and Numerical Combustion, Second Edition,” *Decis. Support Syst.*, 2005.

[50] O. H. Björnsson, S. A. Klein, and J. Tober, “GT2020-14164 BOUNDARY LAYER FLASHBACK MODEL FOR CONFINED HYDROGEN FLAMES INCLUDING THE EFFECT OF ADVERSE PRESSURE GRADIENT FLOW´Olafur.”

[51] A. J. Aspden, M. S. Day, and J. B. Bell, “Characterization of low Lewis number flames,” *Proc. Combust. Inst.*, 2011.

[52] S. Kadowaki, “Flame velocity of cellular flames at low Lewis numbers,” *Combust. Sci. Technol.*, 2001.

[53] A. Kalantari, E. Sullivan-Lewis, and V. McDonell, “Application of a Turbulent Jet Flame Flashback Propensity Model to a Commercial Gas Turbine Combustor,” *J. Eng. Gas Turbines Power*, vol. 139, no. 4, Apr. 2017.

[54] D. B. Spalding, “A single formula for the ‘law of the wall,’” *J. Appl. Mech. Trans. ASME*, 1960.

[55] ANSYS, “Introduction to ANSYS Fluent,” *ANSYS Cust. Train. Mater.*, no. December, pp. 1–59, 2010.

[56] Siewert Piotr, “Flame front characteristics of turbulent lean premixed methane / air flame at high-pressure,” Swiss Federal Institute of Technology Zurich, 2006.

[57] S. Menon, “A Numerical Investigation of Aerodynamically Trapped Vortex Combustor for Premixed Hydrogen Combustion in Gas Turbines Using Detailed Chemistry,” Delft University of Technology, 2019.

[58] Y. C. Lin, S. Daniele, P. Jansohn, and K. Boulouchos, “Combustion characteristics and nox emission of hydrogen-rich fuel gases at gas turbine relevant conditions,” in *Proceedings of the ASME Turbo Expo*, 2012, vol. 2, no. PARTS A AND B, pp. 829–835.

[59] A. Kalantari, E. Sullivan-Lewis, and V. McDonell, “Flashback Propensity of Turbulent Hydrogen-Air Jet Flames at Gas Turbine Premixer Conditions,” *J. Eng. Gas Turbines Power*, vol. 138, no. 6, pp. 1–8, 2016.

[60] S. B. Pope, *Turbulent Flows*. Cambridge University Press, 2000.

[61] P. J. Stuttaford, S. Jorgensen, T. Hui, Y. Chen, H. Rizkalla, and K. Oumejjoud, “FlameSheet Combustor Dome,” US 9,752,781 B2, 2017.

[62] T. H. Shih, W. W. Liou, A. Shabbir, Z. Yang, and J. Zhu, “A New K-epsilon Eddy Viscosity Model for High Reynolds Number Turbulent Flows: Model Development and Validation,” *Comput. \& Fluids*, 1995.

[63] M. Pourquie, “Simulation tips for CFD,” 2017.

[64] H. Kido and M. Nakahara, “Model of turbulent burning velocity taking the preferential diffusion effect into consideration.,” *JSME Int J*, vol. 41, no. 3, pp. 667–73, 1999.

[65] “Chapter 15. Combustion Modeling Premixed Combustion,” *Ansys - Fluent Man.*, pp.

1–18, 2001.

[66] A. Endres and T. Sattelmayer, “Numerical investigation of pressure influence on the confined turbulent boundary layer flashback process,” *Fluids*, vol. 4, no. 3, 2019.

[67] B. E. Launder, G. J. Reece, and W. Rodi, “Progress in the development of a Reynolds-stress turbulence closure,” *J. Fluid Mech.*, 1975.

[68] B. E. Launder, “Second-moment closure: present... and future?,” *International Journal of Heat and Fluid Flow*. 1989.

[69] LEAP CFD Team, “Convergence and mesh independence study,” 2012. [Online]. Available: https://goo.gl/%0AGzorPW.

A. **Appendix**

A.1 **Mesh analysis and CFD set-up of channel and 2^o-4^0 burner.**

The Eichler's [11] channel geometry is modeled in two dimensions, and a pressure-based Reynolds-averaged Navier-Stokes simulation is conducted using the Reynolds Stress Model (RSM) with enhanced wall treatment. The RSM is the most elaborate type of turbulence model that ANSYS Fluent provides [67] [68], and it could enhance the predictive capability of the TU Delft model. The RSM solves anisotropic turbulence, which is necessary if anisotropic flame stretch might be included in the TU Delft model [22] in the future. Finally, the boundary conditions are set as velocity-inlet at the air-fuel inlet section and pressure-outlet at the fluid domain outlet.

The mesh size of the fluid domain is selected based on the following mesh independence analysis: A coarse mesh is initially selected, and a value of interest (i.e., the average velocity at the outlet) is monitored [69] once the solution converged with 10^{-6} residuals. Figure A.1 shows that the average velocity at the fluid domain's outlet reaches an almost steady value for 27500 cells. This is the final selected grid, which is the smallest mesh that gives this independent solution [69]. The essential near the wall-flow is carefully resolved using 20 inflation layers with element size 9e-04 m, and the final mesh is displayed in Figure A.2.

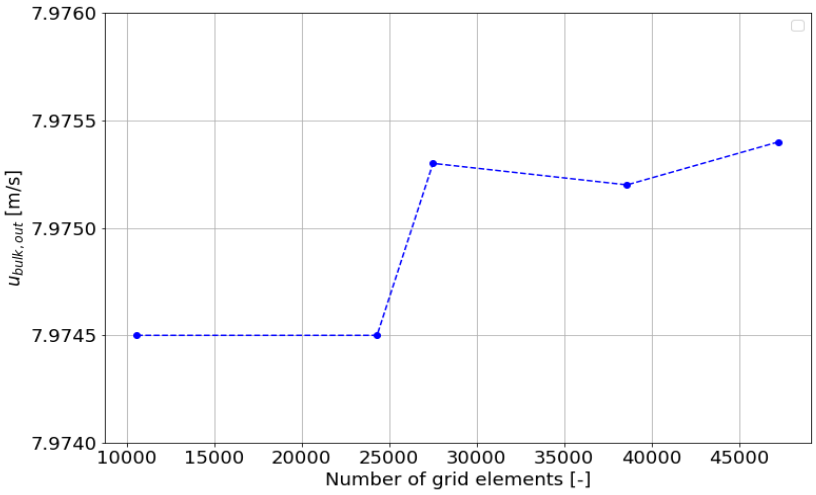

Figure A.1: Mesh independence analysis in the 0^o channel geometry.

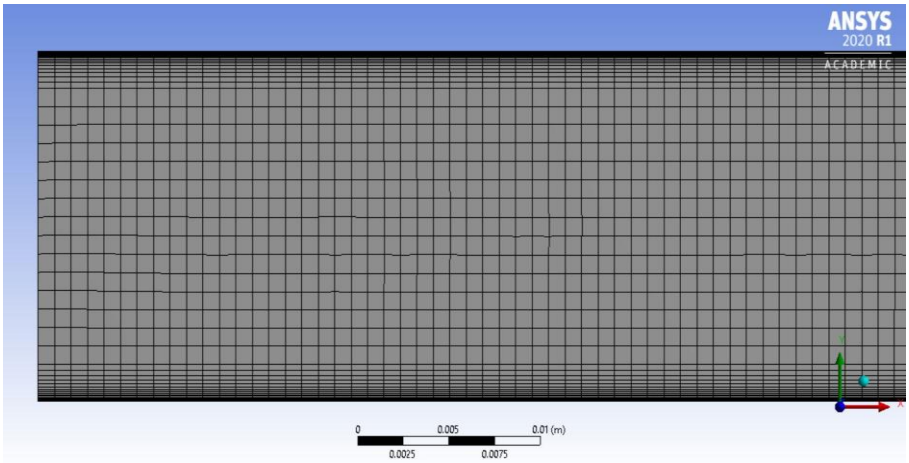

Figure A.2: Eichler's [11] channel geometry mesh and wall inflation layers.

A similar mesh independence analysis is performed for the 2° and 4° diffuser, and the resulting meshes have 167660 and 173600 quadrilateral elements, respectively. The important near-wall flow is fully resolved using the enhanced wall treatment option of ANSYS Fluent and 20 inflation layers on the wall, as can be seen in Figure A.3. Similar to the channel case, the two-dimension Reynolds-averaged Navier-Stokes (RANS) equations are solved using the Reynolds Stress Model as a turbulence model. The fluid properties are selected to those of atmospheric air; the boundary conditions are set as velocity-inlet at the air-fuel inlet section and pressure-outlet at the fluid domain outlet.

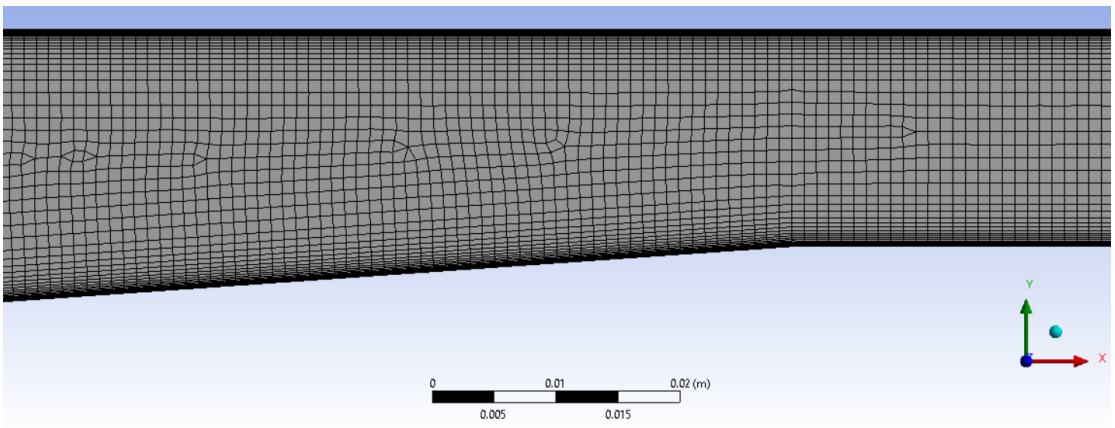

Figure A.3: Mesh and wall inflation layers of the Eichler's [11] 4° diffuser.

A.2 Codes

A.2.1 Laminar flame speed and flame thickness calculation

The unstretched laminar flame speed of H_2-fuel mixtures at atmospheric operating conditions is calculated based on Hoferichter's [6] polynomial (see Eq. (2.43)), similar to Björnsson's research [22]. The following python script developed by Tober [21] is used to the TU Delft flashback model:

```
import numpy as np
import math
A = np.ndarray(shape=(20,25,5))

file_name="LaminarFlameSpeed"
f=open(file_name+".txt",'r+')
lines=f.readlines()

for l in range(len(lines)):
    lines_split = lines[l].split()
    P = math.floor(l/20)
    L = l - P*20
    A[L,0:25,P] = lines_split

def inter(phi,T,p):
    i = math.floor((phi - 0.35)/0.05)
    if i > -1:
        j = math.floor((T - 273)/25.)
        if p>=7:
            k=3
        else:
            k=math.floor((p-1)/2.)
        p_list = [1,3,5,7,20]
        i = int(i)
        j = int(j)
        k = int(k)
        S_l0 = A[i,j,k] + (phi-(0.35+i*0.05))/(0.05) * (A[i+1,j,k]-A[i,j,k])\
        + (T-(273+j*25.))/(25.) * (A[i,j+1,k]-A[i,j,k]) + (p-p_list[k])/\
        (p_list[k+1]-p_list[k]) * (A[i,j,k+1]-A[i,j,k])
    else:
        j = math.floor((T - 273)/25.)
        i=0
        if p>=7:
            k=3
        else:
            k=math.floor((p-1)/2.)
        p_list = [1,3,5,7,20]
        i = int(i)
        j = int(j)
        k = int(k)
        S_l0 = A[i,j,k] + (phi-(0.35+i*0.05))/(0.05) * (A[i+1,j,k]-A[i,j,k])\
        + (T-(273+j*25.))/(25.) * (A[i,j+1,k]-A[i,j,k]) + (p-p_list[k])/\
        (p_list[k+1]-p_list[k]) * (A[i,j,k+1]-A[i,j,k])
        if S_l0 < 0:
            phi = 0.3
            S_l0 = A[i,j,k] + (phi-(0.35+i*0.05))/(0.05) * \
            (A[i+1,j,k]-A[i,j,k]) + (T-(273+j*25.))/(25.) * \
            (A[i,j+1,k]-A[i,j,k]) + (p-p_list[k])/(p_list[k+1]-p_list[k]) \
            * (A[i,j,k+1]-A[i,j,k])
            S_l0 = 0.5 * S_l0
    return(S_l0)
```

For H_2 fuel mixtures at elevated operating conditions and H_2-CH_4 fuel mixtures investigated in this thesis, the unstretched laminar flame speed and flame thickness are calculated based on 1-D steady-state free flame simulation using Cantera [31]. The python script used is the following:

```
import cantera as ct
import numpy as np
import re
def fspeed(T0,P0,fuel_species,air,phi,mechanism,transport_model):
    fuel=ct.Solution(mechanism)
    fuel.set_equivalence_ratio(phi,fuel_species,air)
    fuel.TP=T0,P0
```

```
    fuel.transport_model=transport_model
    # Laminar burning velocity and Le number
    n=fuel.n_species
    x=np.zeros(n)
    x_fuel=np.zeros(n) #mole fraction just of the fuel
    i_h2=fuel.species_index('H2')
    i_ch4=fuel.species_index('CH4')
    i_o2=fuel.species_index('O2')
    i_n2=fuel.species_index('N2')
    x[i_h2]=fuel.X[i_h2]
    x[i_ch4]=fuel.X[i_ch4]
    x[i_o2]=fuel.X[i_o2]
    x[i_n2]=fuel.X[i_n2]
    fuel_comp=re.findall('\d*\.?\d+',fuel_species)
    x_fuel[i_n2]=fuel_comp[-1]
    x_fuel[i_h2]=fuel_comp[1]
    x_fuel[i_ch4]=fuel_comp[3]
    # Initial grid chosen to be 0.02 m long
    initial_grid=np.linspace(0,0.02,100)

    # Set tolerance properties
    tol_ss=[1.0e-5,1.0e-14]
    tol_ts=[1.0e-5,1.0e-14]
    loglevel=1
    refine_grid=False
    # Create flame object
    f=ct.FreeFlame(fuel,initial_grid)
    f=ct.FreeFlame(fuel,initial_grid)
    f.flame.set_steady_tolerances(default=tol_ss)
    f.flame.set_transient_tolerances(default=tol_ts)
    f.inlet.X=x
    f.inlet.T=T0
    f.energy_enabled=False
    #First flame
    f.set_refine_criteria(ratio=5, slope=1, curve=1)
    f.set_max_jac_age(50,50)
    f.set_time_step(1e-05,[2,5,10,20,30,50,100,120,500])
    f.solve(loglevel,refine_grid)
    #Second flame
    f.energy_enabled=True
    refine_grid=True
    f.set_refine_criteria(ratio = 5.0, slope = 0.95, curve = 0.95)
    f.solve(loglevel, refine_grid)
    #Third flame
    f.set_refine_criteria(ratio = 3.0, slope = 0.3, curve = 0.2)
    f.solve(loglevel, refine_grid)
    #Fourth flame
    f.set_refine_criteria(ratio = 3.0, slope = 0.1, curve = 0.2)
    f.solve(loglevel, refine_grid)
    #Fifth flame
    f.set_refine_criteria(ratio = 2.0, slope = 0.025, curve = 0.05)
    f.solve(loglevel, refine_grid)
    sl0=f.u[0]
    #compute flame thickness
    z= f.flame.grid
    T = f.T
    size = np.size(z)-1
    grad = np.zeros(size)
    for i in range(size):
        grad[i] = (T[i+1]-T[i])/(z[i+1]-z[i])
    f_thick = (max(T) -min(T))/(max(grad))
    return sl0,f_thick
```

A.2.2 Flashback models (PSI, UCI, TU Delft)

The python scripts used for the application of the flashback models in the different burners are presented in this section. The velocity profiles coupled with the TU Delft model are exported from ANSYS Fluent at the desired locations using the profile export option. These files are saved in .csv format and then imported into python using the csv module.

A.2.2.1 Academic burner at atmospheric operating conditions

The python script used for the evaluation of the flashback models upon the flashback data in Eichler's channel and 2°-4° diffusers [11] is:

```
import sys
sys.path.insert(1,'D:/Program files/Documents/DELFT/EPT Track/Ept_thesis/Phases/Codes')
import numpy as np
import math
import os
import csv
import glob
import cantera as ct
import flame_1d_properties_H2
import LFS
import matplotlib.pyplot as plt
import re
burner=input('Enter name of the burner')
geometry=input('Enter geometry: channel or 2diffuser or 4 diffuser')
T,P=input('Enter temperature and pressure').split()  # Temperature 293 K, pressure 1 atm
directory='D:/Programm files/Documents/DELFT/EPT Track/Ept_thesis'\
'/Phases/Codes_ver2/'
mydir=directory+burner+'/'+geometry+'/profiles/'+'P_'+P+'/T_'+T  # Specify the path to the Codes folder
csv_file=glob.glob(os.path.join('*.csv'))
with open(str(csv_file[0]),'r') as csvfile:
    fieldnames=['channel_TUM_u','2diffuser_TUM_u','4diffuser_TUM_u','channel_TUM_sec','2diffuser_TUM_sec',\

                '4diffuser_TUM_sec','channel_TUM_phi','channel_TUM_ufb','2diffuser_TUM_phi','4diffuser_TUM_
phi','channel_TUM_gc',\
                '2diffuser_TUM_gc','4diffuser_TUM_gc','channel_TUM_x0','2diffuser_TUM_x0','4diffuser_TUM_x0
',\
                'channel_TUM_y0','2diffuser_TUM_y0','4diffuser_TUM_y0']
    csv_reader=csv.DictReader(csvfile,fieldnames)
    next(csv_reader)
    u_bulk_list=[]
    sec_list=[]
    phi_exp=[]
    gc_exp=[]
    x0=[]
    y0=[]
    u_channel_fb=[]
    for line in csv_reader:
        u_bulk_list.append(line[geometry+'_'+burner+'_u'])
        sec_list.append(line[geometry+'_'+burner+'_sec'])
        phi_exp.append(line[geometry+'_'+burner+'_phi'])
        gc_exp.append(line[geometry+'_'+burner+'_gc'])
        x0.append(line[geometry+'_'+burner+'_x0'])
        y0.append(line[geometry+'_'+burner+'_y0'])
        if geometry=='channel':
            u_channel_fb.append(line[geometry+'_'+burner+'_ufb'])
    sec_list=list(filter(None,sec_list))
    x0=list(filter(None,x0))
    y0=list(filter(None,y0))
    phi_exp=list(filter(None,phi_exp))
    phi_exp=np.asarray(phi_exp,dtype=np.float64,order='C')
    gc_exp=list(filter(None,gc_exp))
```

```
    gc_exp=np.asarray(gc_exp,dtype=np.float64,order='C')
    u_bulk_list=list(filter(None,u_bulk_list))
    u_bulk_list=np.asarray(u_bulk_list,dtype=np.float64,order='C')
    u_channel_fb=list(filter(None,u_channel_fb))
    u_channel_fb=np.asarray(u_channel_fb,dtype=np.float64,order='C')
# Tuning constants for turbulent flame speed
C=1.1  # For 2 diffuser, needs to be adjusted according to each case
n0=0.5
n_p=0
Re=0
T_w=300
w=0.157
phi_list=np.linspace(0.85,0.3,1)
phi_fl_psi=np.zeros((len(u_bulk_list),len(sec_list)))
phi_fl_uci=np.zeros((len(u_bulk_list),len(sec_list)))
phi_fl_pg=np.zeros((len(u_bulk_list),len(sec_list)))
da_pg=np.zeros((len(u_bulk_list),len(sec_list)))
da_uci=np.zeros((len(u_bulk_list),len(sec_list))) # channel hydraulic diameter
da_exp=np.zeros((len(u_bulk_list),len(sec_list)))
gf=np.zeros((len(u_bulk_list),len(sec_list)))
g_psi=np.zeros((len(u_bulk_list),len(sec_list))) # PSI critical wall velocity gradient
g_uci=np.zeros((len(u_bulk_list),len(sec_list)))
index_u=0
for u_bulk in u_bulk_list:
    pgrad_max=np.zeros(len(sec_list))
    index_sec=0
    for sec in sec_list:
         os.chdir(mydir+'/u_bulk_'+str(u_bulk)+'/x_'+sec)
         csv_file=glob.glob(os.path.join('*.csv'))
         with open(str(csv_file[0]),'r') as csvfile:
           fieldnames=['x','y','pressure','absolute-pressure','density', \
                   'velocity-magnitude','x-velocity',\
                   'y-velocity','turb-kinetic-energy', \
                   'uu-reynolds-stress','turb-diss-rate','y-plus',\
                   'viscocity-lam','wall-shear','x-wall-shear',\
                   'y-wall-shear','dx-velocity-dx',\
                   'dy-velocity-dx','dx-velocity-dy',\
                   'dy-velocity-dy','dp-dx','dp-dy']
           csv_reader=csv.DictReader(csvfile)
           x=[]
           y=[]
           p=[]
           pabs=[]
           rho=[]
           vel=[]
           vel_x=[]
           vel_y=[]
           k=[]
           turb_intensity=[]
           turb_dis=[]
           y_plus_wall=[]
           visc=[]
           tau=[]
           tau_x=[]
           tau_y=[]
           dx_veldx=[]
           dy_veldx=[]
           dx_veldy=[]
           dy_veldy=[]
           dp_dx=[]
           dp_dy=[]
           for line in csv_reader:
               x.append(float(line['x']))
               y.append(float(line['y']))
               p.append(float(line['pressure']))
               pabs.append(float(line['absolute-pressure']))
```

```
                rho.append(float(line['density']))
                vel.append(float(line['velocity-magnitude']))
                vel_x.append(float(line['x-velocity']))
                vel_y.append(float(line['y-velocity']))
                k.append(float(line['turb-kinetic-energy']))
                turb_intensity.append(float(line['uu-reynolds-stress'])**0.5)
                turb_dis.append(float(line['turb-diss-rate']))
                y_plus_wall.append(float(line['y-plus']))
                visc.append(float(line['viscosity-lam']))
                tau.append(float(line['wall-shear']))
                tau_x.append(float(line['x-wall-shear']))
                tau_y.append(float(line['y-wall-shear']))
                dx_veldx.append(float(line['dx-velocity-dx']))
                dy_veldx.append(float(line['dy-velocity-dx']))
                dx_veldy.append(float(line['dx-velocity-dy']))
                dy_veldy.append(float(line['dy-velocity-dy']))
                dp_dx.append(float(line['dp-dx']))
                dp_dy.append(float(line['dp-dy']))
    #Coordinate system transformation
        x0=[float(i) for i in x0]
        y0=[float(i) for i in y0]
        x0=np.array(x0)
        y0=np.array(y0)
        Y=y-y0[index_sec]
        X=x-x0[index_sec]
        r=np.sqrt(Y**2+X**2)
        h=r[-1]
        dh=4*w*h/(2*(w+h))
        #Velocity gradient at the wall
        vel=abs(np.array(vel))
        rho=np.array(rho)
        visc=np.array(visc)
    # Unit vector in the streamwise direction
        u0=np.divide(vel_x,vel)  #unit vector x
        v0=np.divide(vel_y,vel)  #unit vector y
        dp_ds=np.multiply(u0,dp_dx)+np.multiply(v0,dp_dy)
    # 1/n law
        u_fric=np.sqrt(tau[0]/rho[0])
        u_plus=vel/u_fric
        y_plus=u_fric*rho*r/visc
        upperb=50
        lowerb=30
        logic1=y_plus>lowerb
        logic2=y_plus<upperb
        logic=logic1*logic2
        y_nlaw=r[logic]
        y_plus_nlaw=y_plus[logic]
        vel_nlaw=vel[logic]
        delta=r[-1]/6  # according to Bjornsson suggestion
        n_list=np.linspace(2,15,121)
        sd_init=1e03
        u_0=vel[np.nanargmin(abs(r-delta))]
        sd=np.zeros(len(n_list))
        for j in range(len(n_list)):
           for kk in range(len(y_nlaw)):
            u_nlaw=u_0*(y_nlaw[kk]/(delta))**(1/n_list[j])
            sd[j]=(u_nlaw-vel_nlaw[kk])**2+sd[j]
           if sd[j]<sd_init:
            sd_init=sd[j]
            u0_opt=u_0
            n_opt=n_list[j]
        u_nlaw=u0_opt*(y_nlaw/(delta))**(1/n_opt)
        b=0.73 # for dp2/dx2 > 0
        rhs=((3*(0.41*0.73)**4)/((n_opt+1)*n_opt**2))\
                        **0.25*(1-(3/(n_opt+1)))**(0.25*(n_opt-2))
    # Maximum velocity fluctuations and pressure gradient within the BL
```

```
181.          ufluct=np.zeros(len(y_plus))
182.          vel_fb=np.zeros(len(y_plus))
183.          for i in range(len(y_plus)):
184.             if y_plus[i]<40:
185.                ufluct[i]=turb_intensity[i]
186.                vel_fb[i]=vel[i]
187.          jj=np.nanargmax(ufluct)
188.          if geometry=='channel':
189.                u_fluct_max=np.nanmax(ufluct)
190.          elif geometry=='2diffuser':
191.                u_fluct_max=1.33*np.nanmax(ufluct)
192.          else:
193.                u_fluct_max=1.43*np.nanmax(ufluct)
194.          p_fl_max=pabs[jj]
195.          pgrad_max[index_sec]=dp_ds[jj]
196.      # Plot 1/n law
197.          plt.figure(1)
198.          plt.figure(figsize=(10,5))
199.          plt.plot(r,vel,'r--',label=r'CFD')
200.          plt.plot(y_nlaw,u_nlaw,'k--',label=r'1/n law: n='+ \
201.                   str(round(n_opt,2))+', δ='+ str('{:.3e}'.format(delta))+' m')
202.          plt.legend(fontsize=14)
203.          plt.grid()
204.          plt.xlabel('y (m)',fontsize=18)
205.          plt.ylabel(r'u (m/s)',fontsize=18)
206.          plt.xticks(fontsize=18)
207.          plt.yticks(fontsize=18)
208.          plt.title(r'section:'+str(sec), fontsize=16)
209.      # lhs from TU Delft model and PSI model
210.          lhs_pg=np.zeros(len(phi_list))
211.          last_lhs_pg=0
212.          gf[index_u,index_sec]=tau[0]/visc[0] # Flow wall velocity gradient
213.          gpsi_test=np.zeros(len(phi_list))
214.          guci_test=np.zeros(len(phi_list))
215.          cond1=False
216.          cond2=False
217.          index_phi=0
218.          for phi in phi_list:
219.                fuel_species=('H2:1, CH4:0, N2:0')
220.                air=('O2:1.0, N2:3.76')
221.                mechanism='gri30.cti'   # Chemical kinetics mechanism
222.                transport_model='Multi'
223.                fuel=ct.Solution(mechanism)
224.                fuel.set_equivalence_ratio(phi,fuel_species,air)
225.                fuel.TP=float(T),float(P)*101325
226.                fuel.transport_model=transport_model
227.                rho_u=fuel.density_mass
228.                visc_u=fuel.viscosity
229.                therm_dif_u=fuel.thermal_conductivity/rho_u/fuel.cp_mass
230.                # Le number
231.                n=fuel.n_species
232.                x_fuel=np.zeros(n) #mole fraction just of the fuel
233.                i_h2=fuel.species_index('H2')
234.                i_ch4=fuel.species_index('CH4')
235.                i_o2=fuel.species_index('O2')
236.                i_n2=fuel.species_index('N2')
237.                fuel_comp=re.findall('\d*\.?\d+',fuel_species)
238.                x_fuel[i_n2]=fuel_comp[-1]
239.                x_fuel[i_h2]=fuel_comp[1]
240.                x_fuel[i_ch4]=fuel_comp[3]
241.                Le_eff=therm_dif_u*(x_fuel[i_h2]/fuel.binary_diff_coeffs[i_h2,i_n2]+x_fuel[i_ch4]/fuel.binar
    y_diff_coeffs[i_ch4,i_n2])
242.                fuel.equilibrate('HP')
243.                rho_b=fuel.density_mass
244.                aft=fuel.T
245.                R = 8.314
```

```
                Le_O2 = 2.32;
                Le_H2 = 0.33
                Ea = (8.4986*np.log(float(P)*1.01325)+30.1050)*4184 # J/mol
                sigma=rho_u/rho_b
                beta = Ea*(aft - float(T))/(R*aft**2)
                A = 1+ beta*(1/phi-1)
                Le = 1+ (Le_O2 - 1 + A*(Le_H2-1))/(1+A)
                sl0=LFS.inter(phi,int(T),p_fl_max*10**(-5))
                f_thick=2*therm_dif_u/sl0
                f_thick_1d,sl0_1d=flame_1d_properties_H2.f_1d_h2(int(P),int(T),phi)
                l_t=0.07*dh
                st_Lin=sl0_1d*10.5*Le_eff**-0.82*(u_fluct_max/sl0_1d)**0.45*(l_t/f_thick_1d)**-
0.41*(int(P)*101325/1e05)**0.75*(int(T)/298)**-1.33
                re_t=u_fluct_max*l_t*rho_u/visc_u
                st_damkohler=sl0*(1+C*re_t**Re*(u_fluct_max/sl0)**n0*(int(P)*101325/(10**5))**n_p)
                # Lewis correction
                if Le <1 and Le>=0.5:
                    st_damkohler=(0.6052*(1/Le)**2-1.1314*(1/Le)+1.5224)*st_damkohler
                if Le<0.5:
                    st_damkohler=1.678*st_damkohler

                dp_max =rho_u* st_damkohler**2*(sigma-1) #Rankin Huginot condition
                x_f=0.01 #maximum distance upstream the flame front pressure rise take place (flat plate ϕ=0
.55 DNS Eichler)
                P_sep_pg=dp_max*(x_f/x_f)**2+pabs[0]+pgrad_max[index_sec]*x_f
                dPdx_pg=2*dp_max/x_f**2*x_f+pgrad_max[index_sec]
                P_min=pabs[0]
                CP_pg=(P_sep_pg-P_min)/(0.5*rho_u*u0_opt**2)
                dCPdx_pg=dPdx_pg/(0.5*rho_u*u0_opt**2)
                lhs_pg[index_phi]=CP_pg**(0.25*(n_opt-2))*(delta*dCPdx_pg)**(0.5)
                if math.isnan(lhs_pg[0])==True:
                   phi_fl_pg[index_u,index_sec,]=phi_list[0]
                elif lhs_pg[index_phi] > rhs:
                   phi_fl_pg[index_u,index_sec,]=phi_list[-1]
                   cond1=True
                else :
                    if last_lhs_pg>rhs:
                      phi_fl_pg[index_u,index_sec,]=phi
                      cond1=False
                      cond2=True
                    elif cond2==False:
                      phi_fl_pg[index_u,index_sec,]=phi_list[0]
                last_lhs_pg=lhs_pg[index_phi]
                g_psi[index_u,index_sec]=st_Lin/Le_eff/f_thick_1d #PSI critical velocity gradient

                if  g_psi[index_u,index_sec] > gf[index_u,index_sec]:
                  phi_fl_psi[index_u,index_sec]=phi
                da_uci[index_u,index_sec]=5.79*10**-6*Le_eff**1.68*\
                                          (dh*sl0_1d/therm_dif_u)**1.91*\
                                          (int(T)/300)**2.57*(T_w/300)**-0.49*(int(P)/1)**-
2.1
                g_uci[index_u,index_sec]=sl0_1d**2/da_uci[index_u,index_sec]/therm_dif_u
                if g_uci[index_u,index_sec]> gf[index_u,index_sec]:
                   phi_fl_uci[index_u,index_sec]=phi
                gpsi_test[index_phi]=st_Lin/Le_eff/f_thick_1d
                guci_test[index_phi]=sl0_1d**2/da_uci[index_u,index_sec]/therm_dif_u
                index_phi=index_phi+1
            index_sec=index_sec+1
        index_u=index_u+1
```

A.2.2.2 **Academic burners at elevated operating conditions**

The python script used for the calibration of the TU Delft model according to flashback data at elevated operating pressure and temperature [43] is the following:

```
import csv
import glob
import os
import numpy as np
import cantera as ct
import matplotlib.pyplot as plt
import flame_1d_properties_H2
import re

burner='UCI' # or 'PSI'
directory='D:/Program files/Documents/DELFT/EPT Track/Ept_thesis/Phases/'\
'Codes/'+ burner
mydir=directory+'/profiles/'
section='1'
if burner=='UCI':
    d_h=0.0254
else:
    d_h=0.025
sd_init=1e02
C_list=np.linspace(0.2,0.6,1) #0.2 optimum
n0_list=np.linspace(0.6,0.9,1) #0.6 optimum
n_p_list=np.linspace(0.7,0.9,1) #0.7 optimum
re_list=np.linspace(0.25,0.7,1) #0.25 optimum
phi_exp=np.array([0.643,0.53,0.55,0.507,0.4,0.42,0.45,0.34,0.38]) #UCI flashback experiments
P_list=np.array([3,5,7]) # UCI
T_list=np.array([300,500]) #UCI
u_bulk_list=np.array([30,40]) #UCI
'''phi_exp=np.array([0.5,0.41,0.35]) #PSI flashback experiments
P_list=np.array([2.5,7.5,10]) # PSI
T_list=np.array([623,623,623]) # PSI
u_bulk_list=np.array([40]) '''  # PSI
for Re in re_list:
 for n0 in n0_list:
  for n_p in n_p_list:
   for C in C_list:
    sd_flash=0
    j=0
    phi_flash_apg=np.zeros(len(phi_exp))
    phi_flash_psi=np.zeros(len(phi_exp))
    phi_flash_uci=np.zeros(len(phi_exp))
    da_exp=np.zeros(len(phi_exp))
    da_uci=np.zeros(len(phi_exp))
    da_psi=np.zeros(len(phi_exp))
    for P in P_list:
        for u_bulk in u_bulk_list:
            for T in T_list:
              if T!=300 or u_bulk!=40:
               print(P,u_bulk,T)
               os.chdir(mydir+'x_'+section+'/p_'+str(P)+'/T_'+str(T)+ \
                        '/u_bulk_'+ str(u_bulk))
               csv_file=glob.glob(os.path.join('*.csv'))
               with open(str(csv_file[0]),'r') as csvfile: #read csv file with flow velocities
                fieldnames=['x','y','pressure','absolute-pressure','density', \
                'velocity-magnitude','axial-velocity','radial-velocity', \
                'turb-kinetic-energy','turb-intensity','turb-diss-rate',\
                'viscocity-lam','wall-shear','axial-wall-shear', \
                'radial-wall-shear','daxial-velocity-dx', \
                'dradial-velocity-dx','daxial-velocity-dy', \
                'dradial-velocity-dy','dp-dx','dp-dy']
                csv_reader=csv.DictReader(csvfile,fieldnames)
                next(csv_reader)
                x=[]
                y=[]
                p=[]
                pabs=[]
                rho=[]
```

```
                vel=[]
                axial_vel=[]
                rad_vel=[]
                k=[]
                u_fluct=[]
                omega=[]
                visc=[]
                tau=[]
                tau_ax=[]
                tau_rad=[]
                dax_veldx=[]
                drad_veldx=[]
                dax_veldy=[]
                drad_veldy=[]
                dpdx=[]
                dpdy=[]
                for line in csv_reader: #assign in a list the cfd data
                    x.append(float(line['x']))
                    y.append(float(line['y']))
                    p.append(float(line['pressure']))
                    pabs.append(float(line['absolute-pressure']))
                    rho.append(float(line['density']))
                    vel.append(float(line['velocity-magnitude']))
                    axial_vel.append(float(line['axial-velocity']))
                    rad_vel.append(float(line['radial-velocity']))
                    k.append(float(line['turb-kinetic-energy']))
                    u_fluct.append(float(line['turb-intensity']))
                    omega.append(float(line['turb-diss-rate']))
                    visc.append(float(line['viscocity-lam']))
                    tau.append(float(line['wall-shear']))
                    tau_ax.append(float(line['axial-wall-shear']))
                    tau_rad.append(float(line['radial-wall-shear']))
                    dax_veldx.append(float(line['daxial-velocity-dx']))
                    drad_veldx.append(float(line['dradial-velocity-dx']))
                    dax_veldy.append(float(line['daxial-velocity-dy']))
                    drad_veldy.append(float(line['dradial-velocity-dy']))
                    dpdx.append(float(line['dp-dx']))
                    dpdy.append(float(line['dp-dy']))
                if y[0]<y[-1]:
                 x.reverse()
                 y.reverse()
                 p.reverse()
                 pabs.reverse()
                 rho.reverse()
                 vel.reverse()
                 axial_vel.reverse()
                 rad_vel.reverse()
                 k.reverse()
                 u_fluct.reverse()
                 omega.reverse()
                 visc.reverse()
                 tau.reverse()
                 tau_ax.reverse()
                 tau_rad.reverse()
                 dax_veldx.reverse()
                 drad_veldx.reverse()
                 dax_veldy.reverse()
                 drad_veldy.reverse()
                 dpdx.reverse()
                 dpdy.reverse()
                vel=np.array(vel) #assign vel to a numpy array for easier manipulation
                y=abs(d_h/2-np.array(y))
# I want y to start from the wall and the y coordinate is at 0.0254 (this is how I defined the CFD model)
    # Thats why I have to subtract the pipe radius -> change of coordinate system
                rho=sum(rho)/len(rho)
                visc=sum(visc)/len(visc)
```

```
                u_fric=np.sqrt(tau[0]/rho) # 0 refer to the FIRST item of the list (refers to the Wall at r
    adius 0.0127) -> shear stress at the wall
                u_plus=vel/u_fric
                y_plus=rho*u_fric*y/visc
                u0=np.divide(axial_vel,vel)  #unit vector x
                v0=np.divide(rad_vel,vel)  #unit vector y
                dp_ds=np.multiply(u0,dpdx)+np.multiply(v0,dpdy)
                n_list=np.linspace(3,10,100)
                upperb=50
                lowerb=30
                logic1=y_plus>lowerb
                logic2=y_plus<upperb
                logic=logic1*logic2
                y_nlaw=y[logic]
                y_plus_nlaw=y_plus[logic]
                vel_nlaw=vel[logic]
                delta=y[-1]*np.linspace(1,2,1)
                n_list=np.linspace(2,15,121)
                sd_init_nlaw=1e03
                for i in range(len(delta)):
                   u_0=vel[np.nanargmin(abs(y-delta[i]))]
                   sd=np.zeros(len(n_list))
                   for jj in range(len(n_list)):
                    for kk in range(len(y_nlaw)):
                     u_nlaw=u_0*(y_nlaw[kk]/(delta[i]))**(1/n_list[jj])
                     sd[jj]=(u_nlaw-vel_nlaw[kk])**2+sd[jj]
                    if sd[jj]<sd_init_nlaw:
                     sd_init_nlaw=sd[jj]
                     delta_opt=delta[i]
                     u0_opt=u_0
                     n_opt=n_list[jj]
                u_nlaw=u0_opt*(y_nlaw/(delta_opt))**(1/n_opt)
                b=0.73 # for dp2/dx2 > 0
                rhs=((3*(0.41*0.73)**4)/((n_opt+1)*n_opt**2))\
                         **0.25*(1-(3/(n_opt+1)))**(0.25*(n_opt-2))
             # Set up mixture cantera
                phi_list=np.linspace(0.85,0.35,1)
                last_lhs=0
                # Find max u fluctuations (y+<40)
                ufluct=np.zeros(len(y_plus))
                for i in range(len(y_plus)):
                  if y_plus[i]<40:
                     ufluct[i]=u_fluct[i]
                ii=np.nanargmax(ufluct)
                u_fluct_max=np.nanmax(ufluct)
                pgrad_max=dp_ds[ii]
                count=0
                gc_psi=np.zeros(len(phi_list)) # critical velocity gradient PSI model
                gc_uci=np.zeros(len(phi_list)) #critical velocity gradient UCI model
                gc_blasius=np.zeros(len(phi_list))
                lhs=np.zeros(len(phi_list))
                for phi in phi_list:
                   fuel_species=('H2:1, CH4:0, N2:0')
                   air=('O2:1.0, N2:3.76')
                   mechanism='gri30.cti'   # Chemical kinetics mechanism
                   transport_model='Mix'
                   fuel=ct.Solution(mechanism)
                   fuel.set_equivalence_ratio(phi,fuel_species,air)
                   fuel.TP=float(T),float(P)*101325
                   fuel.transport_model=transport_model
                   rho_u=fuel.density_mass
                   visc_u=fuel.viscosity
                   therm_dif_u=fuel.thermal_conductivity/rho_u/fuel.cp_mass
                   # Le number
                   n=fuel.n_species
                   x_fuel=np.zeros(n) #mole fraction just of the fuel
```

```
                    i_h2=fuel.species_index('H2')
                    i_ch4=fuel.species_index('CH4')
                    i_o2=fuel.species_index('O2')
                    i_n2=fuel.species_index('N2')
                    fuel_comp=re.findall('\d*\.?\d+',fuel_species)
                    x_fuel[i_n2]=fuel_comp[-1]
                    x_fuel[i_h2]=fuel_comp[1]
                    x_fuel[i_ch4]=fuel_comp[3]
                    Le_eff=therm_dif_u*(x_fuel[i_h2]/fuel.binary_diff_coeffs[i_h2,i_n2]+x_fuel[i_ch4]/fuel.b
inary_diff_coeffs[i_ch4,i_n2])
                    fuel.equilibrate('HP')
                    rho_b=fuel.density_mass
                    aft=fuel.T
                    f_thick_1d,sl0_1d=flame_1d_properties_H2.f_1d_h2(P,T,phi)
                    sigma=rho_u/rho_b
                    #Turbulent flame speed closure
                    l_t = 0.07 * d_h
                    st_Lin=sl0_1d*10.5*Le_eff**-0.82*(u_fluct_max/sl0_1d)**0.45*(l_t/f_thick_1d)**-
0.41*(int(P)*101325/1e05)**0.75*(int(T)/298)**-1.33
                    re_t=u_fluct_max*l_t*rho_u/visc_u
                    st_damkohler=sl0_1d*(1+C*re_t**Re*(u_fluct_max/sl0_1d)**n0*(P*101325/(10**5))**n_p)
                      #Lewis correction
                    if Le_eff <=1 and Le_eff>=0.5:
                        st_damkohler=(0.6052*(1/Le_eff)**2-1.1314*(1/Le_eff)+1.5224)*st_damkohler
                    else:
                        st_damkohler=1.7*st_damkohler
                    # LHS from statford criteria
                    dp_max=rho_u* st_damkohler**2*(sigma-1)
                    x_f=0.01
                    P_sep=dp_max*(x_f/x_f)**2+pabs[0]+pgrad_max*x_f
                    dPdx=2*dp_max/x_f**2*x_f+pgrad_max
                    P_min=pabs[0]
                    CP=(P_sep-P_min)/(0.5*rho_u*u0_opt**2)
                    dCPdx=dPdx/(0.5*rho_u*u0_opt**2)
                    lhs[count]=CP**(0.25*(n_opt-2))*(delta_opt*dCPdx)**(0.5)
                    if rhs <= last_lhs and lhs[count] < rhs:
                        phi_flash_apg[j]=phi
                        break
                    last_lhs=lhs[count]
                    count=count+1
                sd_flash=sd_flash+(phi_flash_apg[j]-phi_exp[j])**2
                j=j+1
    if sd_flash<sd_init:
      C_opt=C
      n0_opt=n0
      n_p_opt=n_p
      phi_flash_apg_opt=phi_flash_apg
      sd_init=sd_flash
```

A.2.2.3 TU Delft FlameSheet™ burner

```
import sys
sys.path.insert(1,'D:/Program files/Documents/DELFT/EPT Track/Ept_thesis/Phases/Codes')
import numpy as np
import math
import os
import csv
import glob
import cantera as ct
import re
import flame_1d_properties_H2   #for cases with 100%H2
import flame_1d_properties_75H2 #for cases with 75%H2 25%CH4
import flame_1d_properties_50H2 #for cases with 50%H2 50%CH4
import LFS
import matplotlib.pyplot as plt
```

```
15.
16.  burner='TU_DELFT'
17.  T=293
18.  P=1
19.  directory='D:/Programm files/Documents/DELFT/EPT Track/Ept_thesis'\
20.  '/Phases/Codes_ver2/'+burner
21.  os.chdir(directory)
22.  csv_file=glob.glob(os.path.join('*.csv'))
23.  with open(str(csv_file[0]),'r') as csvfile:
24.     fieldnames=['TU_DELFT_u','TU_DELFT_sec','TU_DELFT_phi','TU_DELFT_x0',\
25.                 'TU_DELFT_y0']
26.     csv_reader=csv.DictReader(csvfile,fieldnames)
27.     next(csv_reader)
28.     u_bulk_list=[]
29.     sec_list=[]
30.     x0=[]
31.     y0=[]
32.     phi_exp=[]
33.     for line in csv_reader:
34.         u_bulk_list.append(line[burner+'_u'])
35.         sec_list.append(line[burner+'_sec'])
36.         x0.append(line[burner+'_x0'])
37.         y0.append(line[burner+'_y0'])
38.         phi_exp.append(line[burner+'_phi'])
39.     u_bulk_list=list(filter(None,u_bulk_list))
40.     u_bulk_list=np.asarray(u_bulk_list,dtype=np.float64,order='C')
41.     sec_list=list(filter(None,sec_list))
42.     x0=list(filter(None,x0))
43.     y0=list(filter(None,y0))
44.     phi_exp=list(filter(None,phi_exp))
45.     phi_exp=np.asarray(phi_exp,dtype=np.float64,order='C')
46.  C_list=[1.1,1.3,2.5] # Tuning constants for turbulent flame speed
47.  phi_list=np.linspace(0.85,0.3,5)
48.  sd_min=1e02
49.  phi_fl_pg=np.zeros((len(C_list),len(u_bulk_list)))
50.  phi_fl_psi=np.zeros(len(u_bulk_list))
51.  pmax=np.zeros((len(u_bulk_list),len(sec_list)))
52.  index_u=0
53.  for u_bulk in u_bulk_list:
54.      sd_opt_init=0
55.      lhs_pg=np.zeros((len(C_list),len(phi_list)))
56.      index_C=0
57.      for C in C_list:
58.          index_sec=0
59.          for sec in sec_list:
60.               os.chdir(directory+'/'+'profiles_combustion/'+'P_'+str(P)+'/T_'+str(T)+'/u_bulk_'+str(u_bulk)
     +'/x_'+sec)
61.               csv_file=glob.glob(os.path.join('*.csv'))
62.               with open(str(csv_file[0]),'r') as csvfile:
63.                     fieldnames=['x','y','pressure','absolute-pressure','density', \
64.                             'velocity-magnitude','axial-velocity',\
65.                             'radial-velocity','turb-kinetic-energy', \
66.                             'turb-intensity','turb-diss-rate','y-plus',\
67.                             'viscocity-lam','wall-shear','axial-wall-shear',\
68.                             'radial-wall-shear','daxial-velocity-dx',\
69.                             'dradial-velocity-dx','daxial-velocity-dy',\
70.                             'dradial-velocity-dy','dp-dx','dp-dy']
71.                     csv_reader=csv.DictReader(csvfile)
72.                     x=[]
73.                     y=[]
74.                     p=[]
75.                     pabs=[]
76.                     rho=[]
77.                     vel=[]
78.                     vel_ax=[]
79.                     vel_rad=[]
```

```
                    k=[]
                    turb_intensity=[]
                    turb_dis=[]
                    y_plus_wall=[]
                    visc=[]
                    tau=[]
                    tau_ax=[]
                    tau_rad=[]
                    dax_veldx=[]
                    drad_veldx=[]
                    dax_veldy=[]
                    drad_veldy=[]
                    dp_dx=[]
                    dp_dy=[]
                    for line in csv_reader:
                        x.append(float(line['x']))
                        y.append(float(line['y']))
                        p.append(float(line['pressure']))
                        pabs.append(float(line['absolute-pressure']))
                        rho.append(float(line['density']))
                        vel.append(float(line['velocity-magnitude']))
                        vel_ax.append(float(line['axial-velocity']))
                        vel_rad.append(float(line['radial-velocity']))
                        k.append(float(line['turb-kinetic-energy']))
                        turb_intensity.append(float(line['turb-intensity']))
                        turb_dis.append(float(line['turb-diss-rate']))
                        y_plus_wall.append(float(line['y-plus']))
                        visc.append(float(line['viscosity-lam']))
                        tau.append(float(line['wall-shear']))
                        tau_ax.append(float(line['axial-wall-shear']))
                        tau_rad.append(float(line['radial-wall-shear']))
                        dax_veldx.append(float(line['daxial-velocity-dx']))
                        drad_veldx.append(float(line['dradial-velocity-dx']))
                        dax_veldy.append(float(line['daxial-velocity-dy']))
                        drad_veldy.append(float(line['dradial-velocity-dy']))
                        dp_dx.append(float(line['dp-dx']))
                        dp_dy.append(float(line['dp-dy']))
                #Coordinate system transformation
                x0=[float(i) for i in x0]
                y0=[float(i) for i in y0]
                x0=np.array(x0)
                y0=np.array(y0)
                Y=y-y0[index_sec]
                X=x-x0[index_sec]
                r=np.sqrt(Y**2+X**2)
                #Velocity gradient at the wall
                vel=abs(np.array(vel))
                rho=np.array(rho)
                visc=np.array(visc)
                # Unit vector in the streamwise direction
                u0=np.divide(vel_ax,vel)  #unit vector x
                v0=np.divide(vel_rad,vel)  #unit vector y
                dp_ds=np.multiply(u0,dp_dx)+np.multiply(v0,dp_dy)
                # 1/n law
                u_fric=np.sqrt(tau[0]/rho[0])
                u_plus=vel/u_fric
                y_plus=u_fric*rho*r/visc
                upperb=50
                lowerb=25
                logic1=y_plus>lowerb
                logic2=y_plus<upperb
                logic=logic1*logic2
                y_nlaw=r[logic]
                y_plus_nlaw=y_plus[logic]
                vel_nlaw=vel[logic]
                delta=r[-1]*np.linspace(1E-03,1,1000)
```

```
            n_list=np.linspace(2,15,121)
            sd_init=1e03
            for i in range(len(delta)):
             u_0=vel[np.nanargmin(abs(r-delta[i]))]
             sd=np.zeros(len(n_list))
             for j in range(len(n_list)):
              for kk in range(len(y_nlaw)):
               u_nlaw=u_0*(y_nlaw[kk]/(delta[i]))**(1/n_list[j])
               sd[j]=(u_nlaw-vel_nlaw[kk])**2+sd[j]
              if sd[j]<sd_init:
               sd_init=sd[j]
               delta_opt=delta[i]
               u0_opt=u_0
               n_opt=n_list[j]
            u_nlaw=u0_opt*(y_nlaw/(delta_opt))**(1/n_opt)
            b=0.73 # for dp2/dx2 > 0
            rhs=((3*(0.41*0.73)**4)/((n_opt+1)*n_opt**2))\
                                **0.25*(1-(3/(n_opt+1)))**(0.25*(n_opt-2))

           # Maximum velocity fluctuations and pressure gradient within the Boundary layer
            ufluct=np.zeros(len(y_plus))
            vel_fb=np.zeros(len(y_plus))
            for i in range(len(y_plus)):
              if y_plus[i]<40:
                  ufluct[i]=turb_intensity[i]
                  vel_fb[i]=vel[i]
            jj=np.nanargmax(ufluct)
            u_fluct_max=np.nanmax(ufluct)
            vel_fb_max_fluct=np.nanmax(vel_fb) # velocity within the boundary layer at which the velocity
    fluctuation is max
            p_fl_max=pabs[jj]
            pgrad_max=dp_ds[jj]
            pmax[index_u,index_sec]=dp_ds[jj]
            # lhs from TU Delft model
            last_lhs_pg=0
            l_t=0.09**(3/4)*k[jj]**(3/2)/turb_dis[jj]
            gf=tau[0]/visc[0] # Flow wall velocity gradient
            cond1=False
            cond2=False
            g_psi=np.zeros(len(phi_list))
            index_phi=0
            for phi in phi_list:
             fuel_species=('H2:1, CH4:0, N2:0') # Composition of fuel mixture can be changed
             air=('O2:1.0, N2:3.76')
             mechanism='gri30.cti'   # Chemical kinetics mechanism
             transport_model='Mix'
             fuel=ct.Solution(mechanism)
             fuel.set_equivalence_ratio(phi,fuel_species,air)
             fuel.TP=float(T),float(P)*101325
             fuel.transport_model=transport_model
             rho_u=fuel.density_mass
             visc_u=fuel.viscosity
             therm_dif_u=fuel.thermal_conductivity/rho_u/fuel.cp_mass
             # Le number
             n=fuel.n_species
             x_fuel=np.zeros(n) #mole fraction just of the fuel
             i_h2=fuel.species_index('H2')
             i_ch4=fuel.species_index('CH4')
             i_o2=fuel.species_index('O2')
             i_n2=fuel.species_index('N2')
             fuel_comp=re.findall('\d*\.?\d+',fuel_species)
             x_fuel[i_n2]=fuel_comp[-1]
             x_fuel[i_h2]=fuel_comp[1]
             x_fuel[i_ch4]=fuel_comp[3]
             Le_eff=therm_dif_u*(x_fuel[i_h2]/fuel.binary_diff_coeffs[i_h2,i_n2]+x_fuel[i_ch4]/fuel.binar
    y_diff_coeffs[i_ch4,i_n2])
```

```
                fuel.equilibrate('HP')
                rho_b=fuel.density_mass
                aft=fuel.T
                sl0=LFS.inter(phi,int(T),p_fl_max*10**(-5))
                f_thick_1d,sl0_1d=flame_1d_properties_H2.f_1d_h2(P,T,phi)   #flame_1d_properties_75H2 or flame_1d_properties_50H2 should be used
for 75% H2 or 50% H2 fuel mixture
                st_Lin=sl0_1d*10.5*Le_eff**-0.82*(u_fluct_max/sl0_1d)**0.45*(l_t/f_thick_1d)**-0.41*(int(P)*101325/1e05)**0.75*(int(T)/298)**-1.33
                st_damkohler=sl0*(1+C*(u_fluct_max/sl0)**0.5)   # sl0 should be replaced with sl0_1d for fuel mixtures different than 100% H2
                ret=rho_u*u_fluct_max*l_t/visc_u
                st_mup=sl0_1d*(1+0.46/Le_eff*ret**0.25*(u_fluct_max/sl0_1d)**0.3) #Muppala flame speed correlation
                # Lewis correction
                if Le_eff <1 and Le_eff>=0.5:
                    st_damkohler=(0.6052*(1/Le_eff)**2-1.1314*(1/Le_eff)+1.5224)*st_damkohler
                if Le_eff<0.5:
                    st_damkohler=1.678*st_damkohler
                sigma=rho_u/rho_b
                dp_max =rho_u* st_damkohler**2*(sigma-1) #Rankin Huginot condition
                x_f=0.01 #maximum distance upstream the flame front pressure rise take place (flat plate ϕ=0.55 DNS Eichler)
                P_sep_pg=dp_max*(x_f/x_f)**2+pabs[0]+pgrad_max*x_f
                dPdx_pg=2*dp_max/x_f**2*x_f+pgrad_max
                P_min=pabs[0]
                CP_pg=(P_sep_pg-P_min)/(0.5*rho_u*u0_opt**2)
                dCPdx_pg=dPdx_pg/(0.5*rho_u*u0_opt**2)
                lhs_pg[index_C,index_phi]=CP_pg**(0.25*(n_opt-2))*(delta_opt*dCPdx_pg)**(0.5)
                if math.isnan(lhs_pg[index_C,0])==True:
                   phi_fl_pg[index_C,index_u]=phi_list[0]
                elif lhs_pg[index_C,index_phi] > rhs:
                   phi_fl_pg[index_C,index_u]=phi_list[-1]
                   cond1=True
                else :
                    if last_lhs_pg>rhs:
                      phi_fl_pg[index_C,index_u]=phi
                      cond1=False
                      cond2=True
                    elif cond2==False:
                      phi_fl_pg[index_C,index_u]=phi_list[0]
                last_lhs_pg=lhs_pg[index_C,index_phi]
                g_psi[index_phi]=st_Lin/Le_eff/f_thick_1d #PSI critical velocity gradient
                if  g_psi[index_phi] > gf:
                   phi_fl_psi[index_u]=phi
                index_phi=index_phi+1
               index_sec=index_sec+1
        index_C=index_C+1
    index_u=index_u+1
plt.figure(1)
plt.figure(figsize=(14,8))
plt.plot(u_bulk_list,phi_fl_pg[0,:],'b^-.',label='$ϕ_{fb}$: TU Delft model, C=1.1')
plt.plot(u_bulk_list,phi_fl_pg[1,:],'g^-.',label='$ϕ_{fb}$: TU Delft model, C=1.3')
plt.plot(u_bulk_list,phi_fl_pg[2,:],'r^-.',label='$ϕ_{fb}$: TU Delft model, C=2.5')
plt.plot(u_bulk_list,phi_fl_psi,'y^-.',label='$ϕ_{fb}$: PSI model')
plt.plot(u_bulk_list,phi_exp,'ko',label='$ϕ_{exp}$: Experimental data')
plt.legend(fontsize=14)
plt.grid()
plt.xlabel('$U_{bulk}$ [m/s]',fontsize=18)
plt.ylabel('$ϕ_{fb}$ or $ϕ_{exp}$ [-]',fontsize=18)
plt.xticks(fontsize=18)
plt.yticks(np.arange(0.2,0.9,0.1),fontsize=18)
plt.savefig('fl_limits_tudelft')
```